FACULTY OF SCIENCE & TECHNOLOGY

DEPARTMENT OF CHEMISTRY

SYNTHESIS OF CLAY DERIVED NANOSILICATES IMPREGNATED WITH *PROSOPIS JULIFLORA* BIOCHAR FOR REMOVAL OF SELECTED HEAVY METALS IN WATER

BY

MOHAMED HUSSEIN OMAR

REG. NO: I80/50030/2015

A THESIS SUBMITTED IN FULFILLMENT OF THE REQUIREMENTS FOR THE AWARD OF THE DEGREE OF DOCTOR OF PHILOSOPHY IN CHEMISTRY OF THE UNIVERSITY OF NAIROBI

AUGUST 2023

DECLARATION

I hereby declare that this thesis is my original work and has not been submitted elsewhere for the award of degree, examination, or publication. Where the work of another person was used, appropriate acknowledgment and referencing were done according to University of Nairobi requirements.

MOHAMED HUSSEIN OMAR

REG. NO: I80/50030/2015

Sign:  Date: 05-08-2023

This proposal has been submitted with our approval as university supervisors

Dr. Njagi Njomo Signature. 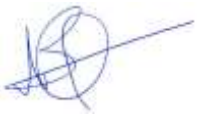 . Date: 05-08-2023

Department of Chemistry, University of Nairobi

Prof. Amir. Yusuf Signature:  . Date: 05-08-2023

Department of Chemistry, University of Nairobi

Dr. Immaculate N. Michira Signature 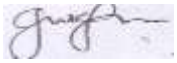 Date: 05-08-2023

Department of Chemistry, University of Nairobi

Dr. Fanelwa Ajayi Signature…  . Date: 05-08-2023

Department of Chemistry, University of the W outh Africa

DEDICATION

This work is dedicated to my sick mother and pray for her quick recovery. Also my dedication to my wife, children and siblings.

ACKNOWLEDGEMENTS

I have my heartfelt gratitude to all the staff members of the Department Chemistry, the University of Nairobi for their guidance and help. Special thanks to my supervisors, Dr. Njagi Njomo, Prof. Amir Yusuf and Dr. Immaculate N. Michira of the Department of Chemistry (University of Nairobi) and Dr. Fanelwa Ajayi of the Faculty of Chemistry, University of the Western Cape-South Africa for being there for me whenever I needed their guidance and help. Additional thanks to the University of Nairobi through the Department of Chemistry for allowing me to study at the University of Nairobi. Also thanks to the Government Chemist (Kenya) and Geology and Mines Department for allowing me to use their inductively coupled plasma mass spectrometry (ICP-MS) and X-ray fluorescence (XRF) Instruments for the analysis of the samples. Also, King Fahd University-Research Institute (Saudi Arabia) who helped me in the characterization of my materials. Special appreciation goes to National Research Fund for funding my research and Higher Education Loans Board for paying my tuition fees. Special thanks to Mr. Farah Dagane, Mr. Rashid Warsame and Abdullahi Musa of Garissa University for helping me in the laboratory work as research assistants.

ABSTRACT

Due to growing urbanization, population growth, and industrial activity, heavy metals are now entering water bodies at a faster pace. The current treatment methods are ineffective, and this has detrimental effects for both human health and the environment. The research reports the synthesis of clay-derived nanosilicates that has been fused with biochar from *Prosopis Juliflora*. The effectiveness of the synthesized materials in removing heavy metals from water was then evaluated. Elemental analysis and characterization of the nanosilicates revealed the composition of silicates at 83.6% in the extract with 20% (w/v %) NaOH as extracting media gave the best with the best result. The FTIR characterization depicted a typical structure for sodium silicates with IR bands of 1000, 1500, 1700, and 3500 cm^{-1} describing silicate bands. Nanosilicates with an average diameter of 85 nm that are agglomerated and round in shape were successfully synthesized, as demonstrated by the morphological analysis performed using SEM and TEM. Phase analysis with XRD displayed broadband at $2\theta=30^{o}$ depicting the presence of silicate nanoparticles with intense peaks from 25.26^{o} to 65.93^{o} which is usually related to silicate nanoparticles. The characterization of biochar biomaterial prepared through pyrolysis showed elemental composition mainly of carbon and oxygen atoms when characterized by XRF and EDX. The FTIR spectra showed O-H stretching at 3500 cm^{-1} and a peak at 1600 cm^{-1} ascribed to carboxylate (COO^{-1}) which is consistent with bands of most biochars. The XRD pattern of *Prosopis* biochar material showed a rise in the background level of between 11^{o} and 13^{o} absorption bands which is consistent with the existence of cellulose and other related organic compounds. A narrow sharp peak seen at 30^{o} was attributed to amorphous carbon. The SEM analysis revealed key morphological patterns of fibrous structure and pith. The biochar sample depicted uneven particles of different dimensions with vascular features filled in rolls with a comparatively uniform surface as observed in the literature for most biochars. Elemental analysis of nanocomposite material of biochar and clay silicates using EDX revealed the main composition of carbon, oxygen, silica, aluminum, and iron. The FTIR spectra revealed a broad peak at 3500 cm-1 suggesting O-H stretching, a second peak at 2350 cm^{-1} relating to CO_2 absorption, and a peak at 1063 cm^{-1} denoting C-O stretching vibration. XRD phase analysis of nanocomposite showed mineral crystal existence with peaks at 19.9^{o}, 25^{o}, and 35^{o} identified as phyllosilicates which means successful impregnation of silicates on carbon surfaces of biochar. The SEM images and EDX revealed high peaks of silicon, aluminum, titanium, and iron a typical composition of clay minerals. The efficiency of each synthesized substance in the elimination of heavy metals from water was evaluated using batch adsorption. Clay silicates (99.2 %), Biochar (99.5 %) and composite material (99.4 %) had very good effectiveness of removal of the selected heavy metals but biochar material had the highest efficacy level. The kinetic experiments using Langmuir and Freundlich isotherms indicated a second-order kinetic model fit with data giving a straight line and better correlation r^2 correlation of coefficient of 0.999.

TABLE OF CONTENTS

DECLARATION II
DEDICATION III
ACKNOWLEDGEMENTS IV
ABSTRACT V
TABLE OF CONTENTS VI
LIST OF TABLES X
LIST OF FIGURES XI
LIST OF ABBREVIATION /ACRONYMS AND SYMBOLS XIV
CHAPTER ONE 1
INTRODUCTION 1
1.1 BACKGROUND INFORMATION 1
1.2 STATEMENT OF THE PROBLEM 4
1.3 OBJECTIVES 5
1.3.1 Overall objective *5*
1.3.2 Specific objectives *6*
1.4 JUSTIFICATION AND SIGNIFICANCE OF THE STUDY 6
CHAPTER TWO 8
LITERATURE REVIEW 8
2.1 ENVIRONMENTAL POLLUTION 8
2.2.1 Growth in population 9
2.2.2 Modern technology and development 10
2.2.3 Deforestation and agricultural development 11
2.2.4 Industrial development and urbanization 12
2.3 WATER POLLUTION 13
2.4 HEAVY METAL POLLUTION 15
2.5 TOXICITY OF SELECTED HEAVY METALS 18
2.5.1 Lead (Pb) 18
2.5.2 Cadmium (Cd) 20
2.5.3 Copper (Cu) 21
2.5.4 Zinc (Zn) 22
2.6 TECHNIQUES FOR HEAVY METAL REMEDIATION 23
2.6.1 Chemical precipitation 23
2.6.2 Ion-exchange 24
2.6.3 Electrodialysis 24
2.6.4 Reverse osmosis 25
2.6.5 Adsorption 25

2.6.6 Clay adsorbent for heavy metal remediation 26
2.6.7 Plants biomaterial for heavy metal remediation 28
2.6.8 Biochar for heavy metal remediation 29
2.6.9 Composite adsorbent for heavy metal remediation 30
2.7 *PROSOPIS JULIFLORA* 31
2.8 ANALYSIS AND CHARACTERIZATION TECHNIQUES 33
2.8.1 High-resolution transmission electron microscopy (HRTEM) 34
2.8.2 High-resolution scanning electron microscopy (HRSEM) 35
2.8.3 X-ray diffraction (XRD) and X-ray fluorescence (XRF) 37
2.8.4 Energy-dispersive x-ray spectroscopy (EDX) 39
2.8.5 Inductively coupled plasma (ICP) and Inductively coupled plasma-Mass spectrometry (ICP-MS) 40
2.8.6 Fourier transform infrared spectroscopy (FTIR) 42

CHAPTER THREE 45

MATERIALS AND METHODS 45

3.1 STUDY AREA 45
3.2 SAMPLING 46
3.3 MATERIALS AND PIECES OF EQUIPMENT 47
3.4 QUALITY ASSURANCE AND QUALITY CONTROL 47
3.4.1 Sample blanks 47
3.4.2 Calibration standards 47
3.5 TREATMENT OF CLAY TO FORM NANOSILICATES, ANALYSIS AND CHARACTERIZATION 49
3.6 PROCEDURE OF BIOCHAR PREPARATION 49
3.7 NANOCOMPOSITE MATERIAL PREPARATION AND CHARACTERIZATION 50
3.8 CHARACTERIZATION OF THE SYNTHESIZED MATERIALS 50
3.9 METHOD OF BATCH ADSORPTION FOR HEAVY METAL REMEDIATION 52
3.9.1 Effect of pH 53
3.9.2 Effect of contact time 53
3.9.3 Effect of agitation speed of the shaker 54
3.9.4 Effect of np's dosage -calcined clay 54
3.9.5 Effect of np's dosage -biochar 55
3.9.6 Effect of np's dosage -nanocomposite material 55
3.10 ADSORPTION ISOTHERMS AND KINETIC MODELS 56
3.10.1 Freundlich Isotherm 56
3.10.2 Langmuir Isotherm 57
3.10.3 Pseudo first order and second order 58

CHAPTER FOUR 60

RESULTS AND DISCUSSION 60

4.1 INTRODUCTION 60
4.2 ELEMENTAL ANALYSIS AND CHARACTERIZATION OF CLAY NANOSILICATES 60

4.3 CHARACTERIZATION AND ANALYSIS OF BIOCHAR BIOMATERIAL OF *PROSOPIS JULIFLORA* 64
4.4 CHARACTERIZATION AND ANALYSIS OF NANOCOMPOSITE MATERIAL 68
4.5 ADSORPTION AND EFFICACY OF THE SYNTHESIZED MATERIALS 72
4.5.1 Effect of contact time 73
4.5.2 Effect of pH 74
4.5.3 Effect of agitation speed of the shaker 76
4.5.4 Removal efficiencies of calcined clay silicates 78
4.5.5 Removal efficiencies of biochar material 80
4.5.6 Removal efficiencies of the nanocomposite material 83
4.6 FREUNDLICH AND LANGMUIR ISOTHERMS 85
4.6.1 Freundlich isotherms for calcined clay, biochar, and composite material for zn, cu, cd and pb 86
4.6.2 Langmuir isotherms for calcined clay, biochar, and composite material for zn, cu, cd, and pb 92
4.7 KINETIC MODELS AND ORDER OF REACTIONS 98
CHAPTER FIVE 101
CONCLUSION AND RECOMMENDATIONS 101
5.1 CONCLUSIONS 101
5.2 RECOMMENDATIONS 103
REFERENCES 104
APPENDICES 120
APPENDIX A: RAW DATA OF THE EFFECT OF CONTACT TIME ON SELECTED HEAVY METALS ADSORPTION 120
APPENDIX B: RAW DATA OF THE EFFECT OF PH ON THE SELECTED HEAVY METALS ADSORPTION .. 121
APPENDIX C: RAW DATA OF THE EFFECT OF AGITATION SPEED OF SHAKER ON THE SELECTED HEAVY METAL ADSORPTION 122
APPENDIX D: RAW DATA OF THE REMOVAL EFFICIENCY OF CALCINED CLAY DOSAGE ON SELECTED HEAVY METAL ADSORPTION 123
APPENDIX E: RAW DATA OF THE REMOVAL EFFICIENCY OF BIOCHAR DOSAGE ON SELECTED HEAVY METAL ADSORPTION 124
APPENDIX F: RAW DATA OF THE REMOVAL EFFICIENCY OF COMPOSITE DOSAGE ON SELECTED HEAVY METAL ADSORPTION 125
APPENDIX G-1: RAW DATA OF FREUNDLICH ISOTHERM FOR CALCINED CLAY FOR ZINC METAL..... 126
APPENDIX G-2: RAW DATA OF FREUNDLICH ISOTHERM FOR CALCINED CLAY FOR COPPER METAL 126
APPENDIX G-3: RAW DATA OF FREUNDLICH ISOTHERM FOR CALCINED CLAY FOR CADMIUM METAL 127
APPENDIX G-4: RAW DATA OF FREUNDLICH ISOTHERMS FOR CALCINED CLAY FOR LEAD METAL.. 127
APPENDIX H-1: RAW DATA OF FREUNDLICH ISOTHERM FOR BIOCHAR FOR ZINC METAL 128
APPENDIX H-2: RAW DATA OF FREUNDLICH ISOTHERM FOR BIOCHAR FOR COPPER METAL 128
APPENDIX H-3: RAW DATA OF FREUNDLICH ISOTHERM FOR BIOCHAR FOR CADMIUM METAL 129

APPENDIX H-4: RAW DATA OF FREUNDLICH ISOTHERM FOR BIOCHAR FOR LEAD METAL 129
APPENDIX I-1: RAW DATA OF FREUNDLICH ISOTHERM FOR COMPOSITE MATERIAL FOR ZINC METAL 130
APPENDIX I-2: RAW DATA OF FREUNDLICH ISOTHERM FOR COMPOSITE MATERIAL FOR COPPER METAL 130
APPENDIX I-3: RAW DATA OF FREUNDLICH ISOTHERM FOR COMPOSITE MATERIAL FOR CADMIUM METAL 131
APPENDIX I-4: RAW DATA OF FREUNDLICH ISOTHERM FOR COMPOSITE MATERIAL FOR LEAD METAL 131
APPENDIX J-1: RAW DATA OF LANGMUIR ISOTHERM FOR CALCINED CLAY FOR ZINC METAL..... 132
APPENDIX J-2: RAW DATA OF LANGMUIR ISOTHERM FOR CALCINED CLAY FOR COPPER METAL 132
APPENDIX J-3: RAW DATA OF LANGMUIR ISOTHERM FOR CALCINED CLAY FOR CADMIUM METAL 133
APPENDIX J-4: RAW DATA OF LANGMUIR ISOTHERM FOR CALCINED CLAY FOR LEAD METAL..... 133
APPENDIX K-1: RAW DATA OF LANGMUIR ISOTHERM FOR BIOCHAR FOR ZINC METAL 134
APPENDIX K-2: RAW DATA OF LANGMUIR ISOTHERM FOR BIOCHAR FOR COPPER METAL 134
APPENDIX K-3: RAW DATA OF LANGMUIR ISOTHERM FOR BIOCHAR FOR CADMIUM METAL 135
APPENDIX K-4: RAW DATA OF LANGMUIR ISOTHERM FOR BIOCHAR FOR LEAD METAL..... 135
APPENDIX L-1: RAW DATA OF LANGMUIR ISOTHERM FOR COMPOSITE MATERIAL FOR ZINC METAL 136
APPENDIX L-2: RAW DATA OF LANGMUIR ISOTHERM FOR COMPOSITE MATERIAL FOR COPPER METAL 136
APPENDIX L-3: RAW DATA OF LANGMUIR ISOTHERM FOR COMPOSITE MATERIAL FOR CADMIUM METAL 137
APPENDIX L-4: RAW DATA OF LANGMUIR ISOTHERM FOR COMPOSITE MATERIAL FOR LEAD METAL 137
APPENDIX M-1: KINETIC MODEL OF PSEUDO SECOND-ORDER RAW DATA OF ZINC METAL ADSORPTION. 138
APPENDIX M-2: KINETIC MODEL OF PSEUDO SECOND-ORDER RAW DATA OF COPPER METAL ADSORPTION 138
APPENDIX M-2: KINETIC MODEL OF PSEUDO SECOND-ORDER RAW DATA OF CADMIUM METAL ADSORPTION 138
APPENDIX M-4: KINETIC MODEL OF PSEUDO SECOND-ORDER RAW DATA OF LEAD METAL ADSORPTION 139
APPENDIX N: RAW DATA FOR THE CALIBRATION OF THE HEAVY METALS ON ICP-MS 140
APPENDIX O: CALIBRATION CURVE OF HEAVY METALS 143

LIST OF TABLES

Table 1: Allowed maximum limits in Drinking water for heavy metals by different local and international organizations 17

Table 2: Biochar samples Identity and different temperatures of pyrolysis 50

Table 3: Study of pH effect on adsorption of heavy metals 53

Table 4: Study of contact time effect on adsorption of heavy metals 53

Table 5: Study of Shaker speed on adsorption of heavy metals 54

Table 6: Study of calcined clay dosage on adsorption of heavy metals 54

Table 7: Study of Biochar dosage on adsorption of heavy metals 55

Table 8: Study of composite material dosage on adsorption of heavy metals 56

Table 9: Percentage composition of calcined clay and silicate extract using XRF 60

Table 10: Percentage elemental composition of *Prosopis Juliflora* biochar at 500^{o}C 65

Table 11: Freundlich isotherms constant (n) for calcined clay, biochar and composite materials for selected heavy metals 91

Table 12: Freundlich isotherms constant (K) for calcined clay, biochar and composite materials for selected heavy metals 91

Table 13: Freundlich isotherms constant (q_m) for calcined clay, biochar and composite materials for selected heavy metals 97

Table 14: Langmuir isotherms constant (K_L) for calcined clay, biochar and composite materials for selected heavy metals 97

Table 15: Pseudo second order rate constants for zinc removal using calcined clay 99

Table 16: Pseudo second order rate constants for copper removal using calcined clay 100

Table 17: Pseudo second order rate constants for cadmium removal using calcined clay 100

Table 18 : Pseudo second order rate constants for lead removal using calcined clay 100

LIST OF FIGURES

Figure 1: Different types of clay mineral structures 27

Figure 2: A thicket of *Prosopis* coverage in front of Garissa University Road in Garissa town. 32

Figure 3:*Prosopis* coverage on the sides of a tarmacked road in Garissa town 33

Figure 4: *Prosopis* coverage on the sides of River Tana in Garissa town 33

Figure 5: High Resolution Transmission electron microscope Illustration (TEM) 35

Figure 6: Schematic details of SEM 37

Figure 7: High Resolution Scanning Electron Microscopy (HRSEM)..... 37

Figure 8: Schematic diagram of a diffractometer system 39

Figure 9: Construction of the EDX semiconductor detector 40

Figure 10: Schematic cross-section of an ICP 42

Figure 11: Inductively Coupled Plasma-Mass Spectrometry (ICP-MS) 42

Figure 12: Schematic detailed components of FTIR spectrometer..... 44

Figure 13: Sampling area in Mukurweini in Nyeri County 45

Figure 14: Sampling area in Garissa Township in Garissa County 46

Figure 15: EDX patterns of nanosilicates extract with (a) 20% NaOH and (b) 40% NaOH..... 61

Figure 16: FTIR spectrum of synthesized silicate nanoparticles 62

Figure 17: FESEM images of synthesized silicate nanoparticles using 20% NaOH (w/v%): (A) 2 μm, (B) 5 μm..... 62

Figure 18: FESEM images of synthesized silicate nanoparticles using 40% NaOH (w/v%) at 2 μm 63

Figure 19: FETEM images of synthesized silicate nanoparticles using (A): 20% NaOH (w/v%) and (B): 40% NaOH (w/v %)..... 63

Figure 20: XRD pattern of synthesized silicate nanoparticles using 20% NaOH (w/v %) 64

Figure 21: XRD pattern of synthesized silicate nanoparticles using 40% NaOH (w/v %) 64

Figure 22: EDX patterns of *Prosopis Juliflora* biochar @ 500 ^{o}C. 66

Figure 23: FTIR spectrum of *Prosopis Juliflora* biochar at 500 ^{o}C..... 66

Figure 24: XRD pattern of *Prosopis Juliflora* biochar at 500 ^{o}C. 67

Figure 25: SEM images of the *Prosopis Juliflora* biochar duplicates (A & B) at : 100 μm, and (C): 20 μm 68

Figure 26: EDX patterns of the nanocomposite material of clay nanosilicates and biochar material duplicate (A) and (B) 69

Figure 27: FTIR spectrum of nanocomposite material 70

Figure 28: XRD pattern of clay-biochar nanocomposite 70

Figure 29 (A).: SEM images of nanocomposite at 100 μm 71

Figure 30: EDX spectrum of the nanocomposite 72

Figure 31: Effect of contact time on heavy metals (A): Zn (B): Cu (C): Cd and (D): Pb adsorption 74

Figure 32: Effect of pH on adsorption of (A): Zn, (B): Cu, (C): Cd and (D): Pb metals 75

Figure 33: Effect of pH on adsorption of heavy metals 76

Figure 34: Effect of agitation speed of the shaker on adsorption of (A): Zn, (B): Cu, (C): Cd and (D): Pb metals 77

Figure 35: Effect of shaker speed on adsorption of heavy metals 78

Figure 36: Removal efficacy of calcined clay on: (A): Zn, (B): Cu, (C): Cd, and (D): Pb metals 80

Figure 37: Removal efficiency of calcined clay for selected heavy metals 80

Figure 38: Removal efficacy of biochar clay on: (A): Zn, (B): Cu, (C): Cd, and (D): Pb metals 82

Figure 39: Removal efficiency of biochar for selected Heavy metals 82

Figure 40: Removal efficacy of composite material on: (A): Zn, (B): Cu, (C): Cd, and (D): Pb metals 84

Figure 41: Removal efficiency of composite material for selected heavy metals 84

Figure 42: Removal efficiency of the synthesized materials for heavy metals 85

Figure 43: Freundlich isotherms for calcined clay demonstrating trends in zinc adsorption 87

Figure 44: Freundlich isotherms for calcined clay demonstrating trends in copper adsorption .. 87

Figure 45: Freundlich isotherms for calcined clay demonstrating trends in cadmium adsorption 87

Figure 46: Freundlich isotherms for calcined clay demonstrating trends in lead adsorption 88

Figure 47: Freundlich isotherms for biochar demonstrating trends in zinc adsorption 88

Figure 48: Freundlich isotherms for biochar demonstrating trends in copper adsorption 88
Figure 49: Freundlich isotherms for biochar demonstrating trends in cadmium adsorption..... 89
Figure 50: Freundlich isotherms for biochar demonstrating trends in lead adsorption 89
Figure 51: Composite material's Freundlich isotherm showing zinc adsorption trends 89
Figure 52: Composite material's Freundlich isotherm showing copper adsorption trends 90
Figure 53: Composite material's Freundlich isotherm showing cadmium adsorption trends 90
Figure 54: Composite material's Freundlich isotherm showing lead adsorption trends 90
Figure 55: Langmuir isotherms for biochar demonstrating trends in zinc adsorption..... 92
Figure 56: Langmuir isotherms for biochar demonstrating trends in copper adsorption 93
Figure 57: Langmuir isotherms for Biochar demonstrating trends in cadmium adsorption..... 93
Figure 58: Langmuir isotherms for Biochar demonstrating trends in lead adsorption 94
Figure 59: Langmuir isotherms for calcined clay demonstrating trends in zinc adsorption..... 94
Figure 60: Langmuir isotherms for calcined clay demonstrating trends in copper adsorption ... 94
Figure 61: Langmuir isotherms for calcined clay demonstrating trends in cadmium adsorption 94
Figure 62: Langmuir isotherms for calcined clay demonstrating trends in lead adsorption.....93
Figure 63: Composite material's Langmuir isotherm showing zinc adsorption trends ……..…94
Figure 64: Composite material's Langmuir isotherm showing copper adsorption trends ……...94
Figure 65: Composite material's Langmuir isotherm showing cadmium adsorption trends ……...94
Figure 66: Composite material's Langmuir isotherm showing lead adsorption trends ……...95
Figure 67 (A-D): Pseudo second order plot of Zinc (A), copper (B), cadmium (C), and lead(D) metals……..…97

LIST OF ABBREVIATION /ACRONYMS AND SYMBOLS

ACS: Activated carbons

BET: Branauer-Emmett-Toller

CNT-GAC: Carbon nanotubes-Granular activated carbon

CV: Capacitance–voltage

EDS: Energy dispersive spectroscopy

FTIR: Fourier transform infrared spectroscopy

g: gram

HREM: High-resolution Scanning electron microscopy

HRTEM: High-resolution transmission electron microscopy

FESEM: Field emission scanning electron microscopy

FETEM: Field Emission Transmission Electron Microscope

H_2O: Hydrogen peroxide

NaOH: Sodium Hydroxide

pH: Potential of Hydrogen

UN: United Nations

UV: Ultraviolet

XRD: X-ray diffraction

USEPA: United States Environmental Protection Agency ·

EU: European Union

WHO: World Health Organization

KEBS: Kenya Bureau of Standards

NEMA: National Environment management authority

WASREB: Water Services Regulatory Board

BIS: Bureau of Indian Standards

CCD: charge-coupled device

KIRDI: Kenya Industrial research and development institute

CHAPTER ONE

INTRODUCTION

1.1 BACKGROUND INFORMATION

Environmental pollution can be termed as introduction of matter or any form of energy to the environment at a proportion that makes the environment unclean and not safe or appropriate for use. The main categories of pollution are air, water, and soil pollution. Today's society is also disturbed about certain types of pollutants such as noise, light and plastic pollution. All types of pollution have a negative effect on flora and fauna and often affect the health and well-being of people. Pollution can be the result of natural disasters such as wildfires and volcanic eruptions, but the use of the term pollution generally means that the pollutant has an anthropogenic source (a source generated by human action) (Appannagari, 2017). The most conspicuous reason for environmental dilapidation and henceforth worldwide environmental pollution is the reality of the connection between humans and the environment. The rapid exploitation of natural resources, the advancement of technology, and the expansion of industry had an effect on the environment.

Water quality is affected by the climatic and geochemical position of the water bodies, temperature, precipitation, leaking, and overflow of elements from the earth's crust. Nevertheless, water quality is affected by the effects of human activity particularly in the discharge of domestic and municipal waste that contains pathogens, organic matter, and chemicals. Land-based activities in agriculture has resulted to pollution of water resources which subsequently resulted in degrading water quality as a result of runoff containing fertilizers and pesticides (Schindler, 2006). Wastes from numerous land-based sources, including agricultural, industrial, and sewage from domestic sources, transport dissolved salts and minerals into surface waters. Manufacturing activities and emergent pollutants such as heavy metals (e.g. mercury, lead, arsenic, and cadmium) and almost all artificial organic

compounds (e.g. PCBs, pesticides) are poisonous to existing faunas, comprising humans. This problem has been partially addressed through the establishment of recommended standards intended for metals and compounds in the World Health Organization (WHO) drinking water quality guidelines (WHO, 2011). The accessibility of such data at the global level is consequently sparse, although widely available for some countries (Hughes *et al.,* 2013). Heavy metal pollution in Africa is caused by processes of nature including rock weathering and shifts in tectonic plates. Additionally, human activity spreads environmental toxins, resulting in hazardous pollutants in major towns. The primary cause of river and lake contamination is agricultural pollution. Pesticides and fertilizers release chemicals into the groundwater, which is then used to produce drinking water (Mateo-Sagasta et al., 2017). Fast growth of population and high rates of urbanization have led to urban expansion without proper planning and a lack of waste disposal facilities. As a result, waste management has developed to be a major test in many African countries as waste production surpasses the collection and disposal abilities of local governments (Yabe *et al.,* 2010). The United Nations Center for Human Residents (UNCHS) reports that only one-third of the solid waste generated in urban areas of Africa is collected, of which 2% only is collected and reprocessed (UNCHS, 2002).

Humans and other living things depend on water as a vital commodity. Approximately seventy percent of the earth is covered by water, and seventy-five percent of the human body consists of water. In the body, it regulates the activities of fluids, cells, tissues, lymph, and glandular secretions. Clean drinking water is a requisite for a healthy human population. On 28th July 2010, the UN General assembly documented the right of an animal to water and hygiene, through resolution 64/292 recognizing that uncontaminated drinking water is important to the realization of human rights calling for states and international organizations to provide clean, safe, affordable and accessible water for drinking and sanitation to all

(Assembly, 2010). In Kenya, the right to clean and safe water is granted in the Water Act 2016 (Government of Kenya, 2016).

All types of pollution have an impact on the living environment, ranging from mild discomfort to severe diseases. The environmental management and coordination (water quality) regulations of 2006, protect and prevent pollution of water for all domestic use, highlighting the required quality standards for drinking, irrigation, and recreational purposes (Government of Kenya, 2006). In Kenya there are several environmental pollution reports compiled by different agencies highlighting incidences of various pollution to different matrices of the environment (Kimani, 2007; Kithiia, 2012; Kwak & Nguta, 1994). Of particular interest is a study done in Wajir County on water quality. That study showed that microbial and lead levels were beyond the international recommendations both for aesthetic and domestic use (Osman *et al.*, 2011). Heavy metal pollution of the vegetables with Zn and Cd in Machakos Municipality has been reported by Tomno *et al*., (2020). In Nairobi County, the use of untreated sewage water for irrigation revealed harmful levels of pollution with heavy metals like lead and cadmium (Kaluli *et al.*, 2014). Nairobi dam water study also revealed higher levels of heavy metal accumulation above the WHO, EU and KEBS recommended standards for drinking water (Ndeda & Manohar, 2014). A study conducted recently on the topsoil of suburban areas of Nyeri, Kapsabet, Ngong, and Voi towns of Kenya indicated heavy metal pollution (Mungai & Wang, 2019). In the analysis of fish collected from Fourteen falls in Kenya accumulation of heavy metals was also reported (Budambula & Mwachiro, 2006). This necessitated immediate action by relevant authorities. It is very difficult to reverse the effects of water pollution. Natural methods take years, decades, or even centuries to cleanse the effects. General water decontamination methods include conventional physical procedures such as percolation, sedimentation, biochemical procedures (flocculation, chlorination), biological methods (slow sand filters, stimulated/activated

sludge), and radiation by use of ultraviolet light. Conventional water pollution treatment techniques include air stripping, bioremediation, carbon activated filtration, phytoremediation, and chemical oxidation. Algae are used in wastewater treatment for a variety of purposes, including the removal of coliform bacteria, lowering chemical and biological oxygen demand, removing N and/or P, and removing heavy metals (Abdel-Raouf *et al*., 2012). Mining, industrial production, untreated sewage sludge, petrochemical facilities, pesticide manufacturing, the chemical industry, metal pipelines, traffic, and combustion by-products from coal-burning power plants are all heavy metals sources. (Briffa *et al*., 2020). Every organ in the body suffers severe harm from excessive amounts of heavy metals, which are also known to cause cancer, GI blockage, osteoporosis, neurological abnormalities, and other conditions (Briffa *et al.*, 2020). In general, a variety of techniques are used to remove heavy metals from aquatic and marine systems. Some of these techniques include filtration, adsorption, precipitation, electrodeposition, ion exchange, and reverse osmosis (Kumar *et al*., 2000). Some of the most frequently produced adsorbents are carbon materials (such as activated carbon, nanotubes, and graphene), polymers, metal compounds (such as nanoparticles, MXenes, metal-organic frameworks, and magnetic materials), boron and carbon nitrides, and zeolites. (Fei & Hu, 2022).

This research developed a nanocomposite for the elimination of heavy metals from water by synthesizing biochar from *Prosopis Juliflora* and then impregnating it with nanosilicates prepared of clay.

1.2 Statement of the Problem

The rate of ecological transformation and consequent environmental destruction due to human activity remains very rapid and extensive. Increase in population and limited resources has led to overcrowding which has brought about waste disposal in water bodies

like dams, and rivers. Metals and metalloids vary from many organic contaminants in that they occur naturally. However, in certain environments, anthropogenic actions related to mining and use in various industries can naturally surpass water quality and guidelines of safe drinking water. The destiny and harmfulness of metals greatly rely on their speciation or the form in which they occur in a particular water system. The Environmental Protection Agency (EPA) has a list of selected water contaminants that consist of organics, metalloids, and metals. The metals include silver, antimony, cadmium, arsenic, beryllium, chromium, copper, mercury, nickel, lead, zinc, and thallium. The contamination of water with heavy metals poses specific threats to humans and animals due to the bioaccumulation in the food web. Environmental pollution of water poses a huge threat and has attracted the interest of researchers in developing a cost operative and effective technique for the elimination of heavy metals from different environmental matrices. Numerous methods among them ion exchange, chemical electro precipitation (Lalia & Hashaikeh, 2021), reverse osmosis, and solvent extraction just to name a few are cost-intensive and unaffordable to the majority of the population for the treatment of drinking water in sub-Saharan Africa. Due to fast population growth, urbanization, and industrial activity, there is an increased discharge of heavy metals into water bodies. This has negative consequences on human health and the environment, and present remediation techniques are inefficient. This study aimed at developing a cost-effective method for the elimination of heavy metals from water.

1.3 OBJECTIVES

1.3.1 General Objective

The over-all objective of this study was to synthesize a binary nanocomposite of biochar from *Prosopis Juliflora* and clay-derived nanosilicates for the elimination of selected heavy metals from water.

1.3.2 Specific Objectives

Specific objectives of this study were to:

i. Develop nanosilicates from a natural Kenyan local clay sampled from a rural site in Mukurweini in Nyeri County, Kenya.
ii. Synthesize and characterize nonporous biochar from *Prosopis Juliflora* tree bark.
iii. Synthesize and characterize binary nanoporous biochar from *Prosopis Juliflora* impregnated with nanosilicates.
iv. Determine removal efficiencies of selected heavy metals by the synthesized nanocomposite from water.

1.4 Justification and significance of the study

The significance of having safe and clean water for living organisms cannot be overstated. Heavy metals present a great danger to the human health and environment. Owing to their high toxicity, cadmium, lead, zinc, and copper are among the metals with health implications. Even at low levels of interaction, these systemic poisons known as heavy metals can disrupt and destroy a variety of organs in the body. The health and environmental impacts of *Prosopis Juliflora* due to its invasive nature of the grassland also justifies the preparation of biochar from it. An alternative use of *Prosopis* will be a blessing for communities that it has affected for many years. The availability of the raw clay material in the proposed method justifies its potential application. Composite materials made from natural sources such as clay and biomaterial are environmentally friendly and the best solution for heavy metals elimination. A multiphase material is said to be a "nanocomposite" if one of the phases has one, two, or three dimensions that are less than 100 nm, or if the spaces that exist between the composite phases are nanoscale (Teixeira *et al.,* 2017). Nanocomposites are hybrid organic-inorganic materials that are effective for adsorption and decontamination of water. The low cost and availability of clay nanosilicates and biochar material in nature justifies their use.

Hence, the need to develop a cheap, simple nanocomposite material with improved surface capacity and robust heavy metal adsorptive abilities since removal of heavy metals through a variety of techniques has shown to be expensive and inefficient.

CHAPTER TWO

LITERATURE REVIEW

2.1 Environmental pollution

The understanding of the environment as an idea is as ancient as Mother Nature. It is a word that denotes to conditions under which air, water, food, and sunlight flourish and turn into sources of life for any organism as well as non-living things, such as plants. Life for all living and non-living beings, plants included. Environmental pollution is defined as "the introduction by man into the environment of substances or energy liable to cause hazards to human health, harm to living resources and ecological systems, damage to structure or amenity, or interference with legitimate uses of the environment" in the Royal Commission on Environmental Pollution's third report. (Owens, 1989). Pollution develops whenever there is a danger of harm. Human damage includes harm to one of his senses or the damage of his belongings and extends beyond physical injury (Appannagari, 2017).Pollution can be categorized as air, land, water and noise. Air pollution is as a result of particulate matter. Gases such as sulfur dioxide, nitrogen dioxide, carbon monoxide, and carbon dioxide emissions are emitted into the atmosphere above the acceptable limits leading to harmful effects. Water pollution is caused by foreign introduction of substances into water such as chemicals, sewage, pesticides and fertilizers. Land pollution is the pollution that result from household garbage and industrial waste. These wastes include wastes from paper and paperboard, food, plastics, solid waste, rubber, leather, textiles, metals, wood, glass among others. Noise pollution happens when sound exceeds the allowable limits from planes, industries, and other sources reaching harmful levels.

Natural pollution and man-made pollution are the two main categories of pollution. Natural pollution can result from disasters like floods, cyclones, earthquakes, and drought, whereas man-made pollution is caused by human actions that harm the ecosystem. Pollution of the

environment can also be categorized further as water, air, land, noise, food, and radioactive pollutions. Environmental pollution is caused by environmental and ecological variations as an end result of the changing practices of the 'economic and technological man' of the contemporary century. In reality, if the current century is categorized on one hand by socio-economic, scientific, and technological development, on the other hand, it suffers from serious environmental problems (Appannagari, 2017). The lives of ordinary people are being widely affected by man-made environmental degradation so fast and widespread that there has been a clear increase in interest in the standard of the environment, the distraction of the Earth's flora and fauna, and the exhaustion of natural resources over the previous decade. Among the most important environmental factors that make a major environmental impact on public health deterioration is air, water, and soil pollution causing likely contact to chemical or biological compounds in the form such as toxic heavy metals, carcinogens, or particulate matter in the air. These pollutants cause or exacerbate various ailments such as upper and lower respiratory tract diseases, cardiopulmonary infections, asthma, numerous types of cancer, chronic obstructive pulmonary disease (COPD) to mental and developmental delays (Prüss-Üstün & Corvalän, 2007).

2.2 Main causes of environmental pollution

The following grounds could be reported out as the general fundamental reasons for increased environmental pollution, although these too can all act concurrently and their strength may differ from one place to another over time:

2.2.1 Growth in population

Population growth is viewed as the primary cause of a number of human problems (Robinson, 1964).This thought is also applicable to environmental pollution. Population growth has a multiplier effect, and all the necessities necessary for human existence need to

be proportionally increased. Population growth entails abnormal utilization of resources to meet the basic daily provisions of life. It leads to the movement of people and the emergence of cities and municipalities, giving rise to new challenges of health, human environment, and sustenance (Walker, 2016). Population growth plays a vital role in decreasing agricultural land, forests, and water resources. Population growth has been reported to contribute to land degradation, soil erosion, energy production, and consumption, consequently affecting the industrious resource base of the economy (Aditya, 2011). One of the biggest impact on the environment by the population growth is the issue of global warming. The average sea level has risen by more than 8 inches since 1880, of which approximately 3 inches have risen over the last 25 years. Each year, the ocean level increases by an additional 0.32 cm (3.2 mm). According to a recent report that was released in 2020, sea level rise is accelerating and is expected to reach one foot by 2050 (Palm & Bolsen, 2020). Scientists have raised alarm that global warming will cause increase in sea levels and dangerous climate patterns in the future. To cater to the rising inhabitants, woodlands are being damaged at an worrying level (Mittal & Mittal, 2013).

2.2.2 Modern technology and development

The approach of modern production tools in latest years is narrowly linked to environmental degradation. Since World War II, sweeping transformations in production technology have displaced productive technologies with intense environmental impacts from less destructive ones (Leaning, 2000). Global warming, soil pollution, depletion of ozone, unsafe waste, acid rain, radioactive exposures, change in climate, deforestation, desertification, and declining biodiversity are cases of modern environmental concerns that are related with the modern development of technology (Jones *et al*., 1999). Plastic bottles, batteries, glass, artificial textiles, metals, and petrochemicals are only a few examples of the synthetic, non-biodegradable materials that are produced and are attributed to polluting

industries.(Appannagari, 2017). The direct effects of the production of these items are most often made possible by recent technologies created by the production of completely new materials (heavy metals, pesticides, DDT, chlorofluorocarbons (CFCs)). Several of these new materials have new environmental impacts.

Technology is vital for development and increased production to meet human desires, but uncontrolled technology negatively influences the environment. International Telecommunication Unions recounted that 781 million cellular phones were manufactured in 2015 and the figure has risen to more than 900 million gadgets by 2020. Cell phone waste should be categorized as hazardous because too much levels of lead, copper and chromium pose significant eco-toxicity risks, associated with cancerous and non-cancerous diseases (Chen *et al.,* 2018).

2.2.3 Deforestation and agricultural development

Forests are an important part of the biological element of the natural environment system, and environmental stability and ecological balance mainly depend on the state of forests in each region (Laksmi Hendrati, 2019). The main causes of deforestation on an international and regional scale are transformation of forest to agricultural use, conversion of forest to pasture, overgrazing, forest burning, logging, multiuse river projects just to name a few. Deforestation creates numerous problems, including environmental ruin via speedy soil erosion, rise in sediment loading of rivers, siltation of water pans/basins and riverbeds, surge in frequency and size of hoods and famines, changes in precipitation patterns, amplification of the greenhouse effect and increase in the destructiveness of the atmospheric storms (Zeraatpishe *et al*., 2013). This has led to economic losses due to damage to agricultural yields due to a surge in floods and droughts, decline in farming production, loss of productive topsoil, and the decline in the provision of raw materials for industry and construction. Therefore,

deforestation has led to an adverse shackle effect affecting the natural environment (Singh & Singh, 2017). Modern burn and slash techniques are a source of carbon emissions, especially when used to initiate permanent logging.

Agricultural development means expanding land for agriculture, increasing agricultural and net agricultural productivity. Converting forest land into farms on sloppy soil fast-tracks soil erosion. As farmland agriculture grew at the expense of deforestation and subsequent soil erosion, soil productivity increased significantly. This was through rigorous cultivation, better use of machinery and current scientific methods, use of chemical composts, insecticides and herbicides, growth in the frequency and area of agricultural land under irrigation. All these actions lead to increase agricultural development causing numerous and grave environmental challenges. It seems that the original source of all these environmental difficulties as a result of development in agriculture is the alarming growth in the human population (Mateo-Sagasta *et al.*, 2017).This activities have resulted into soil erosion and subsequently polluted the water bodies.

2.2.4 Industrial development and urbanization

Natural resource development and industrial production have increased as a result of rapid industrialization. Constituents of industrial development and industrial production have produced deadly environmental difficulties and instigated significant environmental complications and ecological disparities at international, national, and local levels in diverse ways (F. Ahmed *et al.*, 2022). The utilisation of natural resources to satisfy the industrial necessity for basic materials of production has led to; the decrease of cover of forest through the irresponsible cutting of trees, digging of land for mining, decrease of farming land through manufacturing growth, dropping of the groundwater level owing to disproportionate groundwater abstraction and breakdown of the earth's surface owing to the extraction of

water and oil from the ground (Nair, 1994). Besides the preferred production, there are numerous non-preferred productions from the industries like factory effluents, polluted water, poisonous gases, precipitation of chemicals, vapors/aerosols and smoke which pollute the air, water, soil, and habitat and as a result pollute the environment. These adverse impacts of industrialization can alter the general character of the accepted natural system, and the shackle effects occasionally become dangerous to humanity (Patnaik, 2018).

As a result of industrial growth and development, people move from rural to urban areas, and new urban centres are created and developed. They are responsible for the quick exhaustion of resources, several types of environmental deterioration, and contamination in both industrialized and developing nations. Growing metropolis and municipalities require land to construct the infrastructure anticipated to sustain growing populations that is accomplished by cutting woodlands. The construction of infrastructure, such as roads, railways, bridges, and airports, enables a nation to expand and attracts more and more people to the border of the forest. The city hurt from these predicaments of infrastructure development through slum settlements, absence of hygiene and water provision, overpopulation, overcrowding and pollution. Urban and industrial growth has led to rapid air quality decline due to severe air pollution from gases and aerosols released by vehicles, factories, and household usages. The amount of metropolitans solid waste is quickly growing with urban development and population rise (Chakravarty *et al.*, 2012).

2.3 Water pollution

Water is a precious natural resource that is fundamental for human civilization and agricultural sustainability. Water is essential for all life on earth to exist in its ecosystem. After the air we breathe, water is the second most vital element that humans need to survive (Obinnaa & Ebere, 2019). Water pollution is the adulteration of water by foreign substances

that degrade water quality (Verma & Dwivedi, 2013). Globally, human-made activities, especially the callous exploitation of natural water resources, have had a negative impact on water quality. Although the United Nations considers the supply clean drinking water as a fundamental human right, many people nevertheless experience a lack of it.. The World Water Council assessments estimates that by 2030, about 4 billion people will be living in water-strained areas (Obinnaa & Ebere, 2019). Water pollution remains one of the key environmental difficulties in modern times. The pollution of water is defined as when it undergoes modifications in composition or quality either naturally or by human activity so that it is less appropriate for consumption, agronomic, domestic, leisure or other use for which it would have been suitable (Haldar *et al*., 2014). Urbanization, industrialization, and population growth are progressing rapidly. As a result, the demand for water resources is rising day by day, leading to serious pollution of surface water and groundwater. In contrast to nutrient pollution, marine pollution refers to the introduction of harmful compounds (such as toxic metals, drugs, dyes, pesticides, and surfactants), whereas nutrient pollution is caused by the addition of excessive nutrients that primarily lead to eutrophication of surface waters.. Harmful chemicals that are released into wastewater can destroy marine life, rendering regular water sources unfit for human consumption. Studies show that it is a key cause of death and illness around the world killing 1.8 million people in 2015 (Kelland, 2017). This makes water pollution an international issue and necessitates continuous evaluation and revision of water guidelines and policies at all levels.

Both surface water and groundwater are created as a result of soil permeability. As a result, similar sources of pollution can pollute both surface and groundwater sources. Sewage is a major pollutant when discharged into freshwater and dumping raw sewage into rivers is extremely unhealthy. The notable result is a significant and instant reduction in dissolved oxygen in the water. This transpires because organic matter accelerates the breakdown of

bacteria that decompose suspended solids in wastewater. When breathing, the decomposer runs out of dissolved oxygen (O_2) and reduces biochemical oxygen demand (BOD). The plants and fauna of rivers and their numbers decrease due to lack of oxygen. Another cause of water pollution is the release of hot water from industries. This raises the water temperature and reduces the metabolism rate of the organisms by subsequently raising their demand for oxygen. The impact of pollution are greater in shallow depth, confined, or sluggish streams. Excessive fertilizers, herbicides, and pesticides can be life-threatening if washed into the river by rain. Excessive phosphorus in fertilizer leads to serious eutrophication. (Owa, 2014).

2.4 Heavy metal pollution

Natural elements known as heavy metals have an atomic weight greater than five times that of water and a density greater than that of air. (Duffus, 2002). With the assumption of a link between heaviness and toxicity, they also comprise metalloids such as arsenic, which can cause toxicity at low levels of exposure. Although heavy metals are present in every stratum of the Earth, the majority of pollution is caused by human activities including mining and smelting, manufacturing and consumption, and the use of metals and compounds that contain metals in buildings and agriculture. Metal weathering, atmospheric deposition, soil ion erosion, discharge of heavy metal, resuspension of sediment, and vaporization of metal from water bodies into groundwater and soil are other sources of pollution (Arruti *et al.,* 2010). The different pollution of water forms as a result of heavy metals toxicity is called heavy metal pollution (Hemantaranjan *et al.,* 2005). They are described as toxic in high concentrations but some are crucial for ordinary growth and reproduction in plants at small but acute level concentrations. Some of the essential heavy metals include Zn, Mo, Fe, Co, and Cu for plants and Sn, Cr, and Ni for animals. Some heavy metals such as Pb, Hg and Cd have not yet been shown to be essential for both plants and animals (Misra *et al.,* 2009). Cobalt (Co), copper (Cu), chromium (Cr), iron (Fe), magnesium (Mg), manganese (Mn),

molybdenum (Mo), nickel (Ni), selenium (Se), and zinc (Zn) are important nutrients required for various biological and physiological purposes. A scarce supply of these micronutrients leads to numerous deficiencies or syndromes (WHO *et al.*, 1996).

These metals are regarded as trace since they are present in various environmental matrices at trace concentrations. Their biological presence is affected through physical parameters such as temperature, phase relationship, adsorption, and isolation. They are also affected by thermodynamic equilibrium spacing, complexing kinetics, lipid solubility, and chemical factors that affect the octanol-water equilibrium partition coefficient. Biological influences such as metal type characteristics, nutritional interactions, and biochemical and physiological adaptation also are important characters (Tchounwou *et al.*, 2012). In biological systems, they have been cited to affect mechanism of workings of organelles such as mitochondria, lysosomes, endoplasmic reticulum, nuclei, membranes and metabolism and detoxification in the cell, and constitute several enzymes that are involved in damage and repair function in the cell (Beyersmann & Hartwig, 2008)

The health effect of heavy metal existence in the environs is enormous and hence has attracted high interest among scientists in its removal and eradication. Most of these metals are poisonous besides being carcinogenic in the environment and are harmful to living organisms. It is well-established that heavy metal ions like Pb^{2+}, Hg^{2+}, Cd^{2+}, Ni^{2+} and Cu^{2+} can result in severe toxicological complications, particularly in humans and livestock (Raikwa*r et al.,* 2008). Pollution of water happens in many ways including pollution by effluents from chemical industries (Tarzia *et al.*, 2002). Among the chemicals that pollute the water are heavy metals which are poisonous to the human body. They differ from organic contaminants because they are non-biodegradable (Vasanthy *et al*., 2004). However, unlike herbicides, pesticides, and other potential toxins that decompose very slowly, these metals

cannot be eliminated from the water bodies, so they remain in sediments and are slowly released into the water. The presence of these substances in surface and groundwater bodies has been classified as the most significant inorganic pollution in the environment due to their movement in water bodies and increased harm to living things. (Gautam *et al.*, 2016).

A study of open sewers in Nairobi, Kenya, showed that samples from open sewers in the Nairobi industrial area contained heavy metals more than the maximum acceptable levels (Kinuthia *et al.,* 2020). Based on WHO, EU and KEBS standards for water for drinking, Nairobi Dam water is heavily contaminated with Pb, Cd, Cu, and Ni. Therefore, water is not suitable for human or animal drinking or agricultural activities (Ndeda & Manohar, 2014). Overall, these metals are a danger to the ecological sustainability and well-being of different types of living organisms, including humans. Major aspects of the surroundings, namely air, water, and soil are experiencing the devastating effects of heavy metal pollution. Table 1 shows the allowable limits of some of the heavy metals in drinking water by different local and international organizations.

Table 1: Allowed maximum limits in Drinking water for heavy metals by different local and international organizations

Organization	Cd (**ppm**)	Pb (ppm)	Hg (**ppm**)	Cu (**ppm**)	Zn (**ppm**)
USEPA	0.005	0.01	0.002	1.3	5.0
EU	0.005	0.01	0.001	2.0	NM
WHO	0.003	0.01	0.002	2.0	NGL
KEBS/NEMA/WASREB	0.005	0.05	0.001	0.1	5.0
BIS	0.003	0.01	0.002	1.5	5.0

NM- Not mentioned NGL – No guideline

(U.S.EPA, 2009; WHO, 2011; EU, 2018; BIS, 2012; WASREB-Kenyan Government-, 2006)

2.5 Toxicity of selected heavy metals

Heavy metals are risky since they have a habit of accumulating in the body. Bioaccumulation means that the level of chemicals in an organism increases over a period compared to the level of chemicals in the environment. At low level concentrations amounts, some heavy metals fuel some biological processes, but at onset of allowable maximum limits, they become poisonous (Sharma *et al.,* 2021). Their toxicity can cause brain damage or diminished mental processes and central nervous system function, diminished vigour levels, damage to muscle and DNA, altered expression of gene, diseases of the skin, disorders of composition of blood, lungs, kidneys, liver and heart damage, and other important organs of human and living organisms (Fernández-Luqueño *et al.,* 2013). The pH, solubility, and bioavailability of these metals determine how harmful they are to aquatic organisms, including plants, animals, and humans. Metals are a complex mixture of distinct minerals that exist in water. Nevertheless, the effect of the metal on human health is governed by its bioavailability, which is established by metal speciation. Water-mediated exposure routes have been investigated in several studies, the most direct exposure routes, include skin contact and ingestion (Charity *et al.,* 2018).

2.5.1 Lead (Pb)

Lead is a heavy metal that falls in group fourteen (14) and period six (6) of the P block of the periodic table. It has an atomic number of 82 with an electronic configuration of $(Xe)4f^{14}5d^{10}6S^{2}6P^{2}$ and is solid at 20 ^{o}C. It can occur in various valence states of 0, I, II, and IV. Lead has historically been used to cover as paint and this is due to its covering power. Romans used it for making water pipes, coffins, and tableware. It is the main component of lead-acid batteries used expansively in car batteries. It is also a colouring agent in ceramic glazes as projectiles and as electrodes in electrolysis processes.

Generally, lead is rare in nature. It is usually found in the same ores as copper, silver and zinc and its extraction is with these metals. Lead is mainly introduced into the environment by human activity. The use of lead in gasoline has resulted to lead-cycle emergence, through the entrance of lead salts to the environment by the exhaust of cars. Leaded gasoline use is still one of the most significant human activities that contribute to lead pollution, even though it has been illegal or drastically reduced in many parts of the world (Pragst *et al.,* 2017). Lead can come into the drinking water through pipe corrosion and is expected to happen when the water is marginally acidic. The fate of this metal water depends on the condition of the water, including its acidity (pH), ionic strength, redox potential, flow rate, and amount and composition of suspended solids. Small particles of inorganic lead are taken up from the airways, and large particles are detached from the mucosal cells and carried to the oropharynx where they are ingested. Lead is spread throughout the body and is not dependent on any pathways. It is mainly spread to the skeletal bones (Abadin *et al.,* 2020). Prenatal period, menopause, breastfeeding, and osteoporosis are situations that can increase bone resorption and thus escalate lead in the blood. Lead is mainly contained in red blood cells. Lead transmission occurs from mother to unborn child and through mothers breast milk during breastfeeding (Abadin *et al.,* 2020). The urinary and fecal pathways are the main excretion pathways for inorganic lead. Additional routes include sweat, hair, nails, saliva, semen, and breast milk (Briffa *et al.,* 2020). Some of the health effects of lead include damage to the brain, kidney, sperm damage, increase in blood pressure, abortion and miscarriages, reduced learning abilities in children, nervous system disruptions, disruption in the synthesis of hemoglobin, and anemia In water bodies and soil organisms, lead bioaccumulates among others (Halim *et al.,* 2003). Lead bioaccumulates in the bodies of water and soil organisms. The USEPA, EU, WHO, and BIS regulations all state that 0.01 mg/L of lead is the maximum level that is allowed for drinking water..

2.5.2 Cadmium (Cd)

Cadmium is a naturally available metal with an abundance of 0.1 parts per million (ppm) in nature (Hans Wedepohl, 1995). Cadmium about three-quarters, is mostly used as an electrode constituent in the manufacture of batteries. Cadmium sources in the environment include excavating and producing of metal ores, burning of fossil fuels, nickel-cadmium batteries and is contained in phosphate fertilizers (Kumar *et al.,* 2009). Cadmium is discharged from manufacturing processes and cadmium smelters, fertilizers, and groundwater, remains in sediments and soils for decades and can be absorbed by plants (Engwa *et al.*, 2019). The acceptable maximum level for cadmium in drinking water is 0.005 mg/L according to USEPA, EU, and KEBS and 0.01 mg/L NEMA standards.

The main path of contact to this metal for non-smokers is through food. Even without environmental pollution, cadmium is in small component in most diets. High inhalation contact with cadmium oxide vapours can lead to acute pneumonitis with pulmonary edema, which in severe cases can lead to death (Sharma & Sohn, 2009). Long-lasting occupational interaction with this metal has resulted in prolonged effects, particularly in the kidneys and lungs. In the case of long-term parenteral or oral administration, the kidneys, the liver, skeletal, and cardiovascular systems have been affected (Basta *et al.*, 2001). The severe disease from Cd (II) in humans is "Itai- itai", which is associated with unbearable pain in the bone (Loganathan *et al.,* 2008). Epidemiological reports have shown that Cd^{2+} can lead to some cancers in humans and low exposure can result to kidney damage (Kolakowski, 1984). Cadmium is involved in supporting apoptosis, oxidative anxiety, methylation and damage of DNA. The main targets organs of the body to which this metal is toxic to are the lungs, kidneys and bones (Engwa *et al.,* 2019).

2.5.3 Copper (Cu)

Copper as a trace element in food, copper is indispensable for all living organisms and is classified as an important element because numerous enzymes require it for normal functioning. In humans, copper is found primarily in the liver, muscles, and bones. The body of an adult contains between 1.4 and 2.1 mg of Copper per kilogram of weight of the body. Copper is found in a variety of minerals, including native copper, copper sulphides, copper salts, copper carbonates, and copper(I) or copper(II) oxides such as cuprite and tenorite, respectively (Hammond, 2000). Copper is manufactured commercially largely by smelting or leaching, generally followed by electrodeposition from solutions of sulphate. In terms of thermal and electrical conductivity, pure copper metal is in second place after silver. Copper is a combination of two established isotopes: copper-63 (69.15 %) and copper-65 (30.85 %). Pollution of copper is triggered by extraction of copper through mining, circuit boards, metallurgy, production of fiber, pipe corrosion, and plating of metal (Briffa *et al.,* 2020). Copper is used in the production of several alloys, ceramics, and pesticides. It is also used in the manufacture of wires for industries such as automotive, electrical, and electrical appliances (Shrivastava, 2009). Copper ions are involved in the construction of reactive oxygen species (ROS) as copper (Cu^{2+}) and copper (Cu^{1+}), which may be involved in reactions of oxidation and reduction (Engwa *et al.*, 2019). The acceptable maximum limit for copper in drinking water is 2.0 mg/L according to EU, and WHO standards, while USEPA, KEBS/NEMA, and BIS recommend 1.3 mg/L, 0.05 mg/L, and 1.5 mg/L respectively.

Copper beyond permissible limit in air, water, and food cause diseases such as ‘Wilson’s Disease. It is a reason for detrimental biochemical effects, toxicity, and hazards in plants, animals, and human beings (Shrivastava, 2009). The toxicity of copper leads to irritation of the mucous membranes, capillary damage, chemical burns, kidney and liver damage, and irritation of the nervous system, followed by depression (Krishnamurti *et al.,* 1991).

2.5.4 Zinc (Zn)

Zinc is a vital element for floras, faunas and humans, which occurs in the form of salts or organic complexes in almost all foods and drinking water (Swaminathan *et al*., 2011). Even though drinking water hardly has zinc above 0.1 mg/L, the concentration levels in tap water can be significantly higher due to the its use in the sanitary substances (Swaminathan *et al*., 2011). The normal adult holds between 2-3 g of zinc in his/her body and it is used in the formation of connective tissues such as tendons and ligaments (Liao *et al.,* 2006). The main anthropogenic sources of zinc in the environment include rubber industry, paints, exhaust fumes, electrified parts of metal and railings, dust of tire, motor oil and hydraulic fluid, linings of brake, and production of cement (Selinus *et al.,* 2013). The metallic element occurs in the body as a divalent cation. Consequently, it is not subject to any breakdown. It relates electrostatically with anions such as hydroxide, carbonate, phytic acid, oxalate, and negatively charged entities on biomolecules such as proteins (Stahl & James, 1991). It is categorised as an essential element required by more than 300 enzymes. The function of zinc in these metal enzymes is to be involved in catalytic and regulatory functions and to maintain structural firmness. Zinc is involved in the synthesis of DNA and RNA and cell multiplying. Zinc iron-related transport protein (ZIP) is a transmembrane protein that transports Zn^{2+} ion in eukaryotes. These proteins are usually in the plasma membrane and have been found to form eight transmembrane domain channels tangled in the directing of intracellular zinc levels (Briffa *et al.,* 2020). Zinc is tangled in cell proliferation as a protein structural element and is also involved in regulation of growth. When deprived of zinc the cell dies, where apoptosis occurs in a variety of cell types. Apoptosis also occurs when it is in high extracellular concentrations and surpasses the capacity of its homeostasis, which induces elevated intracellular levels leading to cytotoxicity. Cell necrosis happens at elevated high zinc concentrations (Valko, 2005). Zinc is important for sustaining good health, but elevated

levels can be a source of skin irritation, vomiting, stomach cramps, and nausea (McBrid*e et al.*, 2009). Higher concentrations cause respiratory diseases, liver failure, and it interrupts protein metabolism (Beesley & Marmiroli, 2011). The acceptable maximum level for zinc in drinking water is 5 mg/L according to USEPA, BIS, and KEBS and 1.5 mg/L NEMA standards.

2.6 Techniques for heavy metal remediation

Typically, numerous techniques have been utilized in the removal of various heavy metals namely; ion-exchange, reverse osmosis, ultra-filtration, electrodialysis, precipitation and adsorption procedure (Jiang *et al.*, 2009). Adsorption is separation process that is effective owing to its low cost of operation and energy consumption. Activated carbon has gained prominence of late but due to its high cost, it has led to research into other methods (Yang & Al-Duri, 2001; Alyüz, & Veli, 2005; Mohan & Pittman, 2007).

2.6.1 Chemical precipitation

Chemical precipitation is mostly used to remove heavy metals from wastewater. Equation 1 depicts the hypothesized process of heavy metal removal through chemical precipitation.

$$M^{2+} + 2(OH) \rightarrow M(OH)_2 \text{ ----------(1)}$$

By adding precipitants like alum, lime, iron salts, and polymerized organic molecules, one can precipitate the metal. The main drawback is the substantial volume of sludge that is produced throughout the process that contains harmful substances. Lime precipitates can be used to efficiently treat inorganic wastewater with levels of metal above 1000 ppm. The simplicity of the process, the need for less expensive equipment, as well as the convenience and safety of operation, are additional advantages of using lime precipitates. Nevertheless, this method needs huge amounts of chemicals to moderate the metal to allowable level for

discharge. Other disadvantages include too much sludge formation that needs further treatment, slow, inadequate and accumulation of metal sediment, and the long term effects on the environment (Barakat, 2011).

2.6.2 Ion-exchange

Ion exchange is a chemical reaction that is reversible in which ions are replaced from solution to similar charged ions coated to immovable solid particles. The solid ion exchangers units are either naturally occurring inorganic zeolites or artificially organic resins. Ion exchange resins are divided into cation and anion exchangers. Anion exchange resins have mobile ions that are positively charged which are used for exchange. The same organic base polymer is used to create both cationic and anionic resins. Ionizable sets bound to the hydrocarbon complex are where they vary. Chemical behavior of the resin is controlled by this functional group. The majority of resins can be classified as either strong or weakly acidic cation exchangers or basic anion exchangers. (Kurniawan *et al.,* 2006). Another method used in the production industry to effectively remove heavy metals from wastewater is ion exchange. The disadvantage of this method is that the matrix is easily contaminated with organic and extra solids in the wastewater, making it impossible to process metal solutions that are concentrated. In addition, it is also nonselective and highly dependent on the pH of the solution (Parmar & Thakur, 2013).

2.6.3 Electrodialysis

When an electric potential is applied to a membrane during electrodialysis (ED), species that are ionized in solution pass through the membrane. These membranes typically consist of plastic sheets with cationic and anionic properties. The anions migrate to the anode and the cations move to the cathode, passing via the anion and cation exchange membranes, as the solution containing the various ionic type's flows through the cell compartment. The problem

is that metal hydroxides form and clog the membrane. An ion-selective membrane that is semipermeable is used in electrodialysis to separate the solution's ions. Problems related to the electrodialysis process for wastewater purification include the precipitation of chemicals of poorly soluble salts on the membrane surface (Chen, 2004).

2.6.4 Reverse osmosis

The reverse osmosis procedure relies on a semipermeable membrane which pressurized water is forced to pass through. Basically, reverse osmosis is the opposite of water's natural osmosis. The process of moving from a weakly alkaline solution to one with a strongly alkaline solution is known as osmosis. As the semipermeable membrane separates the two solutions, the salt concentration of each solution gradually equalizes. However, reverse osmosis forces the movement of water into the semipermeable membrane from a higher concentrated saline solution to a weaker concentrated saline solution. Membranes block the passage of salt particles because salt particles are physically larger than water molecules. The product is a desalinated solution on one side of the membrane and a high concentration of the saline solution on the other side (Barakat, 2011). The shortcoming of this method is that it is of high cost.

2.6.5 Adsorption

A process known as adsorption occurs when a dissolved gas or liquid gathers on the surface of a solid or liquid (an adsorbent) to form a clump of particles or molecules (an adsorbate). As opposed to desorption, which is the opposite process, sorption encompasses both processes (adsorption and absorption). Adsorption is widely used in sectors including the use of activated carbon, synthetic resins, and water filtration because it is effective in natural physical, biological, and chemical systems. The exact mode of connection is governed by the specifics of the type of species involved, but adsorbed materials are commonly categorized as

demonstrating physical or chemisorption. The intermolecular attractive interaction between the molecules of the adsorbent and adsorbate causes physiosorption. The van der Waals force, a physical attraction between molecules, is what keeps the adsorbate to the surface in this situation. This is a phenomenon that can be easily reversed. Chemisorption, on the other hand, is the result of a chemical interaction between a solid and an adsorbent. This is also termed activated adsorption (Matos & Arruda, 2003). It is permanent. It is especially significant in catalyzed processes. Therefore, the energy of chemisorption can be thought of as a chemical reaction.

2.6.6 Clay adsorbent for heavy metal remediation

Clay can be categorized into shapeless and crystalline based on the variance in the inner layer structure arrangement. Crystalline clay can be further categorized into several types, such as: 1:1 type layer (Kaolinite), type tube 1:1 (Halloysite), 2:1 type layer (Mt, Smectite, Illite, Vermiculite, Beidellite), Normal mixed layer (Chlorite group), Type 2: 1 chain structure type (playgorskite and sepiolite). Clay is wide-ranging and plenty mineral resource of great industrial significance for a wide variety of use and application. It is one of the world's prominent minerals in terms of both value and annual production. Clays are aluminosilicates described largely as those ores that constitute the portion of colloid of sediments, rocks, soils, and water and they contain combinations of fine soil minerals and clay-sized rocks of other raw materials like metal oxides, carbonate and quartz (Pinnavaia, 1983).

The term "bentonite" is vague. According to geologists, it is extremely colloidal, plastic clay rock primarily made up of montmorillonite, a mineral of clay from the smectite group that is created by the volcanic ash in-situ devitrification. Regardless of their geological origin, all plastics, colloids, and swelling clays are commercially referred to as bentonite. Such clays are usually made of primarily of montmorillonite minerals. The name "kaolin" comes from the word kaolin or "high ridge", which is the name of the hill near Jau Chau Fu in China where

kaolin was originally mined. Kaolin, commonly termed as China clay, is clay that contains 10-95% of the mineral kaolinite. It is usually composed primarily of kaolinite (85-95%). In addition to bentonite and kaolin, the most significant other types of commercial clay are ball clay, common clay and shale, and fire clay. Ball clay is mainly composed of kaolinite and small amounts of illite, chlorite, smectite minerals, quartz and organic matter. common clay and shale contain illite and chlorite as the main constituents, while fire clay mainly contains kaolinite, halloysite, and / or diaspore (UNEP, ILO, 2005). Figure 1 shows different types of clay mineral structure (Kumari and Mohan, 2021).

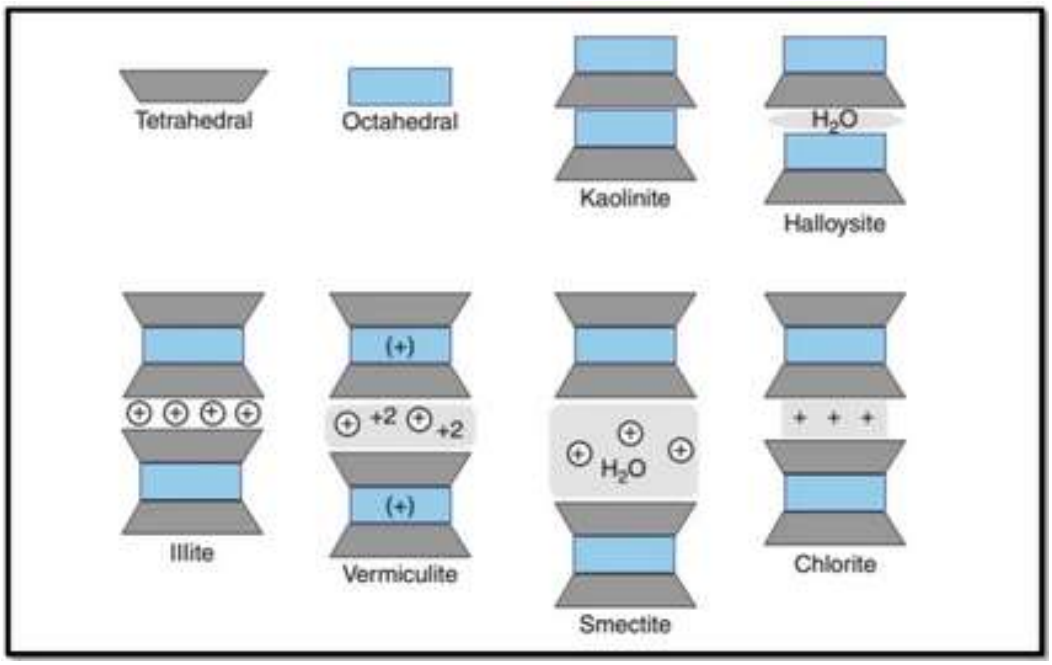

Figure 1: Different types of clay mineral structures-

The need for the development of pollution control technology has been widely recognized relatively recently. Perhaps the most environmentally relevant uses of clay identified over 40 years ago were for radioactive waste disposal, soil adsorbents, and water purification. Given the ubiquitous presence of clay in soils and sediments, it is remarkable that clay has long been used to control toxic substances, albeit only on a small scale or locally. For example, the "Earth of Lemnian", known only for its location, was used medically in ancient Greece and

Turkey to counteract the special effects of snake bites and venoms and to heal purulent injuries. Similarly, Sudanese villagers along the Nile have long used local clay (recently identified as bentonite) to distill the muddy waters of the river (Churchman *et al.*, 2006).

Clay has recently gained prominence as a remediation and clean-up tool for various environmental contaminants including heavy metals (Bhattacharyya, *et.al,* 2006). The usage of natural clay in the remediation of heavy metals has been employed because of its cost-effectiveness (Sdiri, *et.al*, 2012). Due to widespread accessibility and cheaper cost of naturally occurring clay it has become an attractive adsorbent in the remediation of heavy metals from contaminated sources.

2.6.7 Plants biomaterial for heavy metal remediation

There is growing attention to research into the use of unconventional low-cost adsorbents. Resources such as microbial biomass, dung, leaf soil, palm fiber, charcoal, sugar cane bagasse, straw, by-products of rice milling, wool fiber, soybean husks, and cotton seed husks, have all been researched in detail. Researchers have looked into low-cost agricultural waste by-products to remove heavy metals from wastewater, including sugar cane bagasse, paddy husks, coconut, oil palm, and sawdust. Neem bark has also been investigated. Adsorbent constituent material from agronomic wastes has been utilized for the active and accurate retrieval and elimination of lead ions from wastewater (Saka, *et.al*, 2012). Tea waste is the top most economical adsorbent owing to its higher accessibility and adsorption capacity than other ordinary available adsorbents. Traditional carbon-based adsorbents can be replaced with a noble and affordable alternative: tea waste biomass. Drumstick seed, also known as *Moringa oleifera*, is a cheap adsorbent. Sawdust is an adsorbent that results from the action of timber with a saw or other gear tools. It consists of small or fine particles of wood (Bryant *et.al*, 1992). The study by Bryant *et.al*, 1992 revealed successful adsorption of chromium (VI) by red sawdust which is mainly composed of material such as lignin. The capacity of

adsorption was very high in this material. Plants waste and extracts have also been used for the remediation of several heavy metals and have proved to be viable choices (Dhabab *et.al*, 2011). Plant-derived biomaterials generally have a very uneven and irregular surface and contain many cavities, holes, fissures, cracks, crevices and swirls. These features are good sites that aid to improve surface sorption especially of heavy metals (Ighalo & Adeniyi, 2020).

2.6.8 Biochar for heavy metal remediation

Under conditions of constrained oxygen content and low to medium temperatures (450-650°C), slow pyrolysis is used to create biochar, a small grain, permeable, and carbonaceous solid from biomass waste residues (Lehmann & Joseph, 2012). Olive-green waste and chicken manure are two examples of the renewable raw materials used to make biochar. It is a high carbon substance that is currently renowned for its agronomic advantages and capacity to reduce climate change through its capacity for carbon sequestration (Khan *et al.,* 2014). The characteristics of biochar include its porous structure, high pH value, abundance of surface functional groups, substantial surface area, cation exchange capacity (CEC), organic matter content, and high water-holding capacity. The adsorption capacity of biochar can be increased through activation. Comparatively to non-activated biochar, activating biochar improves nutrient retention and plant uptake (Borchard *et al.*, 2012). The theory behind the mechanism of heavy metal adsorption by biochar has not been determined. The mechanism is thought to go through adsorption of cationic π function, co-precipitation, complexation, and electrostatic absorption (Shuguang *et al.,* 2018). Future prospects for using biochar to remove these metals and other contaminants are bright. Because biochar has a low metal content, frequent use won't have a negative impact on agricultural soils. However, there exists some problems in its theoretical system and research direction. Research is currently in a laboratory phase and use of that in large contaminated areas is much limited. The uptake cycle of

biochar is not clear, the mechanisms of how its properties change over time and how the environment can be affected has yet to be studied. In addition, the different types of soils and matrices, use of different optimal pyrolytic temperatures for preparation possess challenges in achieving comparable results after remediation (Wang *et al.,* 2018). Pyrolysis conditions of the system (consisting of temperature, pH and response time) would have a greater impact on the biochar absorption rate and properties. Biochar for efficient removal of selected heavy metals from aqueous solution as an adsorbent has been reported using Scots pine (*Pinus sylvestris L*.) biochar and Silver birch (*Betula pendula*) biochar (Komkiene & Baltrenaite, 2016). Namgay *et al.,* (2010), have shown that after enriching polluted soil with biochar, heavy metals are reduced in availability, which in turn reduces heavy metal uptake by plants.

2.6.9 Composite adsorbent for heavy metal remediation

A composite is a natural or manufactured material composed of two or more than two materials with dissimilar physical and biochemical properties that are distinct at macroscopic and microscopic scales within the substance (Srinivasan, 2011). Various nanocomposites were used as adsorbents in the removal of heavy metals from various matrices in the environment. Kanchana *et al.,* (2012) concluded that the nanocomposite material of chitosan composed of methylcellulose and nanochitosan with kaolin clay in the existence of cross-linking agent performs as a noble adsorbent to remove Pb (II) ions from artificial wastewater. Sdiri and colleagues (2012) compared the single and binary composites for the removal of zinc and copper from wastewater (Sdiri *et.al,* 2012). They envisaged the usage of natural clay from the Aleg formation, Tunisia, as an initial material to improve clay-based economical adsorbents with improved surface capacity and robust capabilities of adsorption for numerous environmental contaminants in aqueous media (Kanchana *et al.,* 2012). Yao *et al.,* (2014) established a biochar-clay composite material in which clay particles were fused to the carbon surface on the pores of biochar. The subsequent composites had distinctive features

and functions acquired from both clay and biochar, and are abundant in starting materials and inexpensive, making them suitable for large-scale applications. Composites have recently gained prominence for the elimination of contaminants from water and waste water. Onundi *et.al*, (2011) explored the possibilities of nanotubes of carbon (CNT) on Granular Activated Carbon (GAC) to produce a composite material substance CNT-GAC and in remediating nickel, copper, and lead ions from aqueous solution.

2.7 *Prosopis Juliflora*

Prosopis Juliflora is an ever-green tree, approximately 15 m high and 3 m wide. *Prosopis* is a flexible tree used as timber, feed, shade, fences, and control of soil erosion. *Prosopis Juliflora* (Swahili: Mathenge) is a plant or small tree in the Fabaceae family. It is naturally found in Mexico, the Caribbean, and South America. It has become well established as an offensive weed in Africa, Asia, Australia, and most parts of the world. It has recently expanded dramatically and is now widespread. *Prosopis* is a main invader in arid and semi-arid areas. The invasion of *Prosopis* significantly reduces the density, basal area, wealth and diversity of native woody plants, and water bodies, and their strong and sharp thorns cause damage to both animals and humans (Wakie *et al.*, 2016).

While other invading tree plant species spread better in moist and sub-humid mid- and highland regions, *Prosopis* grows well in dry, hot, lowland areas, making it almost the only contender to local native species. It was declared a harmful weed in Kenya in 2008 through the Suppression of Noxious Weeds Act (CAP 325). It was introduced in Kenya first in the early 1970's to rehabilitate a quarry in Bamburi near Mombasa; then later in Baringo in 1980 (Shitanda, *et.al*, 2013). *Prosopis* has a few robust fantastic attributes. The pods of *Proso*pis are incredible feedstuff. Mature timber is tough and resistant to termite, excellent for poles, charcoal, carving, veneer and so on. The plant stays green, even in very dry situations and gives incredible color in warm dry areas as shown in Figures 2, 3 and 4.

Environmentally it has robust ability for carbon sequestration, controls sand dunes, and protects erosion of soil. It gives a supply of earnings to numerous families particularly via charcoal, poles and pods. Despite these very noble attributes, *Prosopis* has many disadvantages. It effectively competes with native species that offer livelihoods for locals (grass, herbs, leaves, pods). The effect of strong shades adversely affects biodiversity. It invades rangelands, farmlands and dwellings, compelling people to leave the region or incur/spend money, time and energy to manage it (Shiferaw *et al.*, 2021). Thorns cause physical and mental injury to the locals. While families live in anxiety for their children and animals, the cost of medicines and treatments is high and not affordable for many (Maundu, *et.al*, 2009). *Prosopis Juliflora* waste material cost very little and has also been established to be a commercially effective substitute to activated carbon for heavy metals remediation (Sivakumar & Dheenadayalan, 2012). *Prosopis Juliflora* tree is widely available in Kenya and especially in the Tana River and Garissa Counties where it has been a cause of problems for farmers and pastoralist in those two counties.

Figure 2: A thicket of *Prosopis* coverage in front of Garissa University Road in Garissa town

Figure 3: *Prosopis* coverage on the sides of a tarmacked road in Garissa town

Figure 4: *Prosopis* coverage on the sides of River Tana in Garissa town

2.8 Analysis and Characterization Techniques

The emergence of nanomaterial science has elicited the research activities on the invention of sophisticated nano characterization techniques for better understanding of size, morphology and dimension of materials at nano range. Characterization techniques that have been used include: High-Resolution Transmission Electron Microscopy (HRTEM), High Resolution Scanning Electron Microscopy (HRSEM), X-Ray Diffraction (XRD) and X-Ray

Fluorescence (XRF), Energy-dispersive X-ray spectroscopy (EDX), Inductively Coupled Plasma (ICP) and Inductively Coupled Plasma-Mass Spectrometry (ICP-MS), and Fourier Transform Infrared Spectroscopy (FTIR).

2.8.1 High-Resolution Transmission Electron Microscopy (HRTEM)

The transmission electron microscope (TEM) is formed from the notation nanospace of 10^{-6} m (1 micron) and 10^{-9} m (1 nanometer). A TEM comprises of an electron source called a gun or electron gun. This is ordinarily a V-shaped filament made of LaB_6 (lanthanum hexaboride) or tungsten. An electric potential to the anode is applied, thereby the cathode filament heats up until it produces a flow of electrons of the wavelength given by the De Broglie equation.

Before the electron beam reaches the sample, it is modified by a condenser and aperture lens to improve the coherence of the light. That is, waves with a constant phase difference stay in the same direction. The electron beam then hits the sample, causing some processes (elasticity) in which the electrons colliding with the sample scatter to avoid energy loss, and other processes (inelasticity) in which the electrons give part of their energy to internal electrons of the sample. Next is the objective lens. It has the ability to focus the scattered rays to form the first image, thanks to the diffraction process performed by the projection lens that magnifies the electron beam and reflects it off the emission screen (Carter & Williams, 2009). The worth of the image made by this lens actually defines the resolution of the entire microscope. The diffractive lens underneath the objective lens focuses on either the image or the diffractive pattern, thereby defining which of these is further magnified by the projection lens. The final image or diffraction pattern can be viewed directly on the display screen in the forecast chamber or on a TV or CCD (charged-coupled device) camera mounted under the microscope column (Hubbard, 1995) as shown in figure 5. TEM will be used to ascertain the structural and chemical nature of the nanomaterials and nanocomposites prepared.

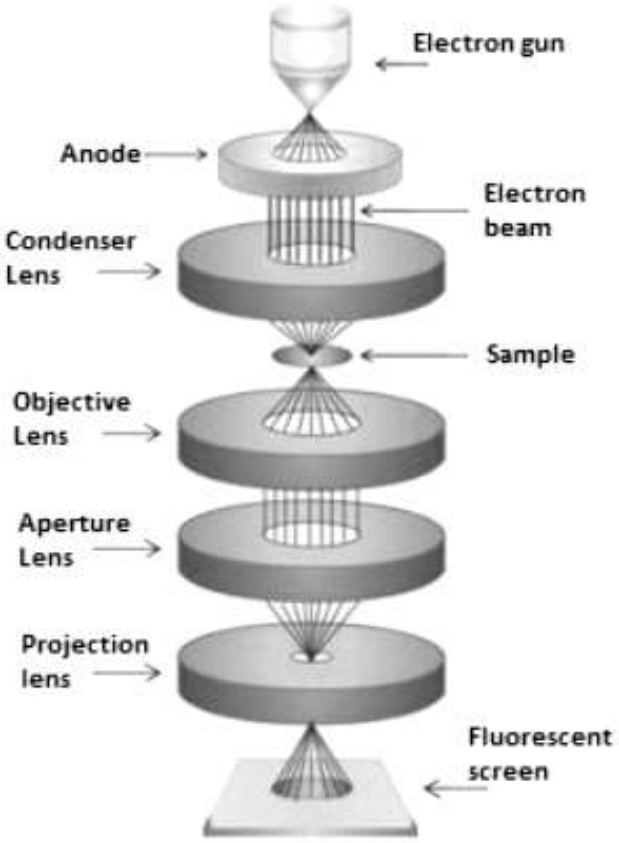

Figure 5: High Resolution Transmission electron microscope Illustration (TEM)

2.8.2 High-Resolution Scanning Electron Microscopy (HRSEM)

When examining a sample or a substance, a scanning electron microscope (SEM) is used to determine the surface morphology. Secondary electrons are emitted from a sample's surface after it has been exposed to a suitable electron beam (also known as an electron probe). When the electron probe is scanned across the surface in two dimensions and secondary electrons are found, a picture of the detected electrons can be taken to show the surface topography. The SEM has a sample holder for holding samples, a secondary electron detector for gathering secondary electrons, an image display device, and an operation system for performing various operations. It also has an electro-optical system for producing electron probes. An electron gun, a condenser lens, an objective lens for producing an electron probe, a scanning coil for scanning the electron probe, and other components make up the electron

optics system. Vacuum conditions are required for the operation of the electron optics system (located inside the microscope column) and the area around the sample.

The electron gun releases an electron beam. Electron microscopes commonly use magnetic lenses. The key attribute of magnetic lenses is that when the current flowing through the coil is changed, the power of the lens also changes. This cannot be achieved with optical lenses. By placing the lens under the electron gun adjustment to the diameter of the electron beam is possible. The electron beam from the electron gun is guided by the two-stage lenses (the condenser and objective lenses), and a small electron probe is released. The objective lens is meant for focusing and this lens is essential in defining the final diameter of the electron probe. Secondary electron detectors are used to identify secondary electrons emitted from a sample as shown in Figure 6 (Richard *et.al*, 1992) and 7. In High resolution Scanning Electron Microscopy (HRSEM), ray of electrons, fast-tracked by a relatively low power voltage of 1-20 kV, is examined on the sample/specimen surface. As the low power voltage ray of electron reaches the sample surface, huge signal figures are produced from the surface of the sample in the form of photons. The signals generated from the sample are brought together by sensors to give picture images and the images are presented on a cathode ray conduit display monitor (Brundle *et.al,* 1992). To understand the morphology and composition of the prepared nanomaterials and nanocomposites HRSEM was used for characterization.

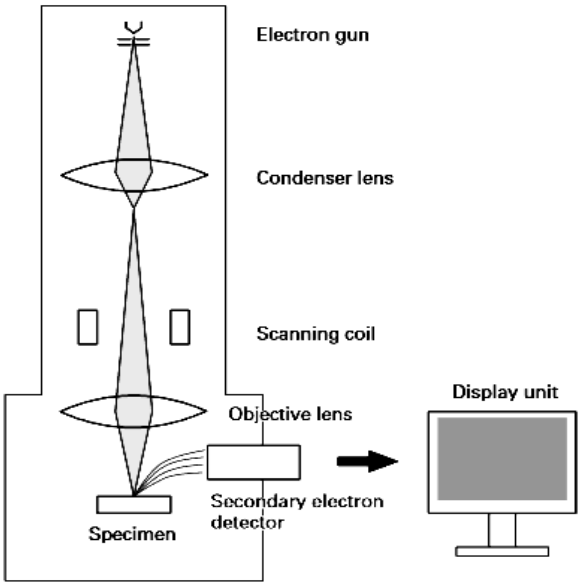

Figure 6: Schematic details of SEM

Figure 7: High Resolution Scanning Electron Microscopy (HRSEM)

2.8.3 X-Ray Diffraction (XRD) and X-Ray Fluorescence (XRF)

When a beam of incident X-rays diffracts in a different direction, it is called X-Ray Diffraction (XRD), and it is a method of investigation and analytical characterization for atomic identification and molecular crystal structure. Measuring the intensities and angles of the beams diffracted produces within the crystal a three-dimensional image of electron

density. XRD is now a common method for studying structures of crystal and interatomic distances. X-ray diffractometry (XRD) is grounded on the constructive interference of crystalline materials with monochromatic X-rays. A cathode ray tube generates these X-rays, which are then sieved to produce monochromatic radiation, collimated, and focussed at the sample. Equation 2 demonstrates how constructive interference (and diffracted beam) are produced when the incident beam makes contact with the sample under Bragg's law.

$$\eta\lambda = 2d\sin\theta \quad \text{.....(2)}$$

Where n is an number, λ is the X-ray wavelength, d is the space distance between the planes that generate the diffraction, and θ is the diffraction angle. This law associates the wavelength of electromagnetic radiation with the diffraction angle and grid spacing of a crystal sample. Then these diffracted X-rays are identified, handled, and calculated. Each compound posseses its own set of distances (*d*-spacing), so the compound can be identified by converting the diffraction peaks to distances (*d*-spacing). This is commonly achieved by associating the distance with a standard reference pattern (Bunaciu *et al.,* 2015). An X-ray diffractometer comprises of three basic elements: an X-ray tube, a sample holder, and an X-ray detector. The detector registers this X-ray signal, processes it, transforms the signal to a count rate, and then outputs it to devices such as printers and computer monitors. The shape of the X-ray diffractometer is such that the sample revolves the collimated X-ray path at an angle of **θ**, and an X-ray detector is attached to the arm to assemble the diffracted X-rays at an angle of 2θ as shown in figure 8. The equipment used to keep the angle and rotate the sample is called a goniometer. X-ray powder diffraction is most commonly used to identify unknown crystalline substances (minerals, and inorganic compounds).

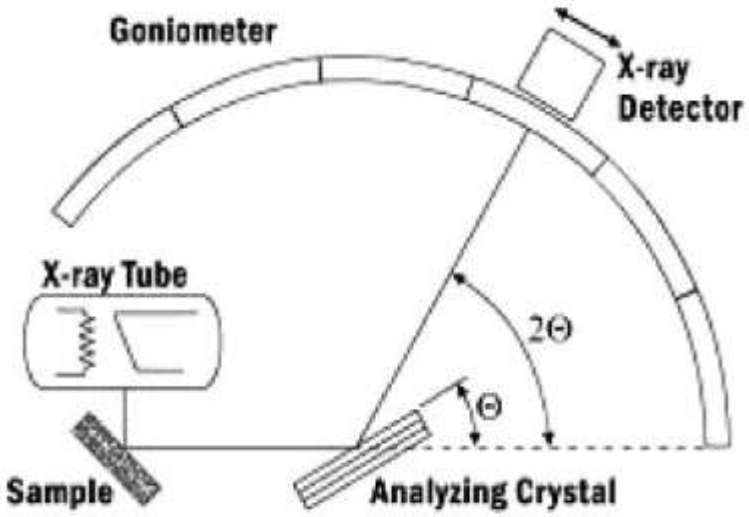

Figure 8: Schematic diagram of a diffractometer system

X-ray fluorescence (XRF) is a non-destructive technique for the elemental study of solids and liquids. The sample is exposed to a strong X-ray, thereby emitting fluorescent X-rays. The released X-rays can be sensed with either energy or wavelength dispersive detectors. XRF is a quick and easy analysis method. XRF is a method for the fast, concurrent analysis of many elements. When excited by a suitable source, a sample produces X-rays with energies typical of the elements that make up the sample. By measuring the energies of X-rays produced by an excited sample and counting the number of X-rays of each energy, XRF allows us to detect which elements are present in a sample and to also measure the relative composition levels of those elements in the sample. In probing the structure of synthesized nanomaterials and nanocomposites XRD and XRF were used.

2.8.4 Energy-dispersive X-ray spectroscopy (EDX)

By determining the energy of X-rays, the Energy Dispersive X-ray Spectrometer (EDX) is used to study common X-ray spectra. It is an instrument that detects the characteristic X-ray released by each element resulting from the bombardment of samples with electrons that are

high in energy in an electron microscope. As shown in figure 9, when the X-ray emitted from the sample enters the semiconductor detector, electron-hole pairs energy amount corresponds to the X-ray energy that is generated. By evaluating these quantities (currents), you can get the X-ray energy value. Recording of the X-rays produces information on the essential structural elemental conformation of the sample which is then superimposed on top of the enlarged sample image. The advantage of EDX is that X-rays of a widespread kind of elements from Boron (B) to Uranium (U) can be analyzed concurrently (Hodoroaba, 2019). For the elemental and chemical analysis and characterization of the nanomaterials and nanocomposites, EDX was used on the synthesized materials.

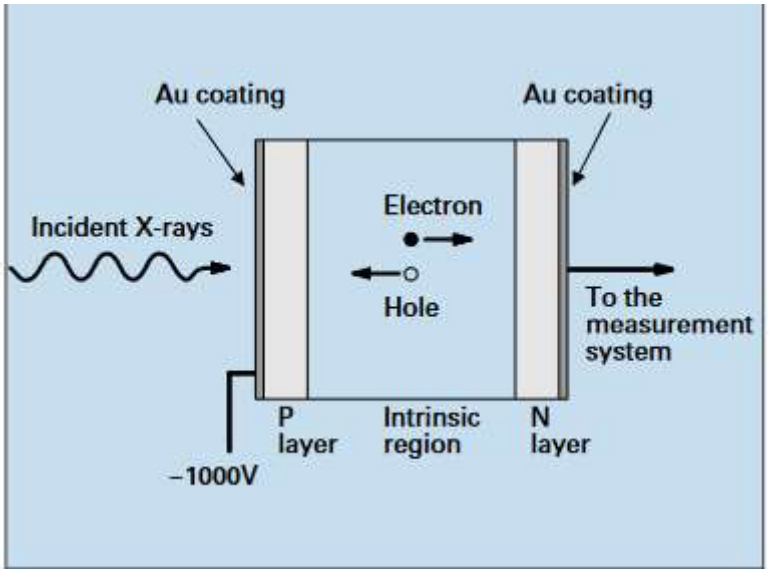

Figure 9: Construction of the EDX semiconductor detector

2.8.5 Inductively Coupled Plasma (ICP) and Inductively Coupled Plasma-Mass Spectrometry (ICP-MS)

Inductively coupled plasma (ICP) is an analytical method for the identification of trace metals in environmental matrices. The fundamental objective of ICP is to make elements release specific light with a distinctive wavelength, which can then be measured. The skill and knowledge for the ICP process was first used in the early 1960s with the objective of improving crystal growing techniques. Subsequently, ICP has been developed and applied in

conjunction with other techniques of quantitative analysis. An ICP is a high temperature (7000-8000k) excitation source that ably de-solvates, evaporates, excites, and ionizes atoms. Molecular disturbances are significantly lower with this excitation source, but not completely eradicated. In ICP elements to be analyzed should be in solution form. An aqueous solution is preferred over an organic solution because organic solutions entail exceptional handling prior to injection into the ICP. The sample is atomized and carried in the stream of plasma carrier gas, which is typically argon (Ar) (Voellkopf et al., 1992).

The plasma torch comprises of concentric quartz tubes, the inner tube having the sample aerosol and Ar carrier gas and the outer tube comprising a stream of Ar gas to cool the tubes. A high radiofrequency generator (RF) (typically 1-5 kW at 27 MHz or 41 MHz) creates a fluctuating current in an induction coil surrounding the tubes. The induction coil generates a fluctuating magnetic field which in turn creates an oscillating current in the ions and electrons of the carrier gas. These electrons and ions collide to transfer energy to other atoms in the carrier gas to generate a high temperature plasma. The light discharged by the ions of an element in the ICP must be transformed into a quantitatively quantifiable electrical signal, which is done by the photomultiplier in the spectrometer as shown in figure 10. A form of mass spectroscopy known as ICP-MS is extremely delicate, sensitive, and capable of identifying a variety of metals and various non-metals in concentrations as low as one in 10^{-12} (parts per trillion). Generally, it is used for sorting out and detecting the ions. Figure 11 shows typical ICP-MS.

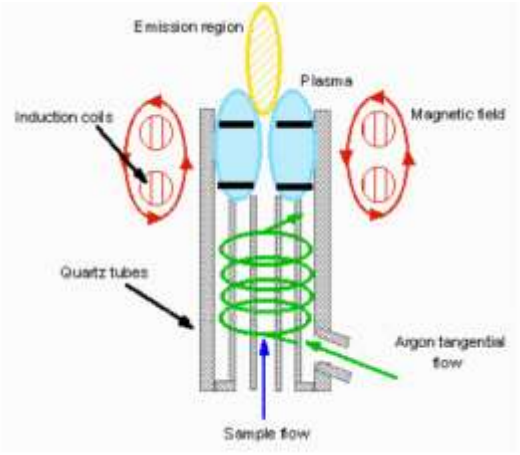

Figure 10: Schematic cross-section of an ICP

Figure 11: Inductively Coupled Plasma-Mass Spectrometry (ICP-MS)

- Picture taken by Mohamed from Government Chemist Laboratories-Kenya

2.8.6 Fourier Transform Infrared Spectroscopy (FTIR)

FTIR stands for Fourier Transform Infrared and is a method of infrared spectroscopy (IR). IR is a characterization technique where a specimen or sample is positioned in the track/path of an Infrared radiation source and measurement of different Infrared frequencies absorption are taken (Kendall, 1996). In infrared spectroscopy, IR radiation passes through the sample.

Some of the IR radiation is absorbed by the sample and partially transmitted. The resulting spectrum creates a molecular fingerprint of the sample by indicating the molecule's absorbance and transmittance. Two different molecular structures do not produce the same infrared spectrum, just like different fingerprints do not. As a result, various forms of analysis can benefit from using infrared spectroscopy (Shahid, *et.al* , 2018). As shown in Figure 12, the standard instrumental FTIR procedure for the sample analysis process entails the following steps:

Power Source: IR radiation is produced from a radiant blackbody source. The ray goes through a hole that regulates the quantity of energy delivered to the sample Interferometer: The ray goes into the interferometer, where "spectral coding" is done. The resulting interferogram leaves the interferometer. Sample: The ray arrives in the sample space, then it is absorbed, transmitted or reflected on the surface of the sample, subject on the type of analysis executed. This is where certain frequencies of energy-specific of the sample are absorbed. Detector: The beam is lastly sent to the detector for final quantification. The detector used is specially made for measuring special interferogram signals. Computer: The measured signal is decoded and guided to the computer where the Fourier transform is performed. The ultimate IR spectrum is then presented to the user for the elucidation and any extra management (Kendall, 1996). .

For the positive identification (qualitative analysis) and determination of the amount of the synthesized materials FTIR was used.

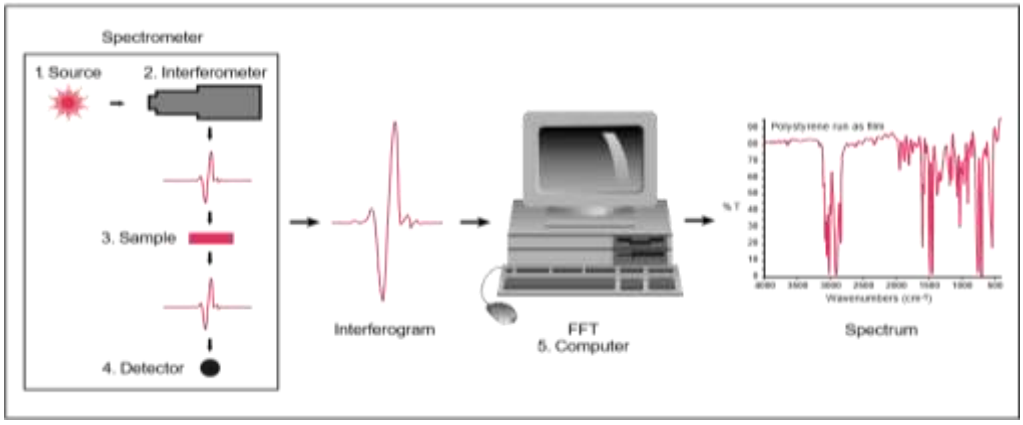

Figure 12: Schematic detailed components of FTIR spectrometer

CHAPTER THREE

MATERIALS AND METHODS

3.1 Study area

Ordinary clay was collected from Mukurweini in Nyeri County. Biochar was prepared from *Prosopis Juliflora* tree stem/bark collected from Garissa County. Figures 13 and 14 show the study area where the material samples were collected.

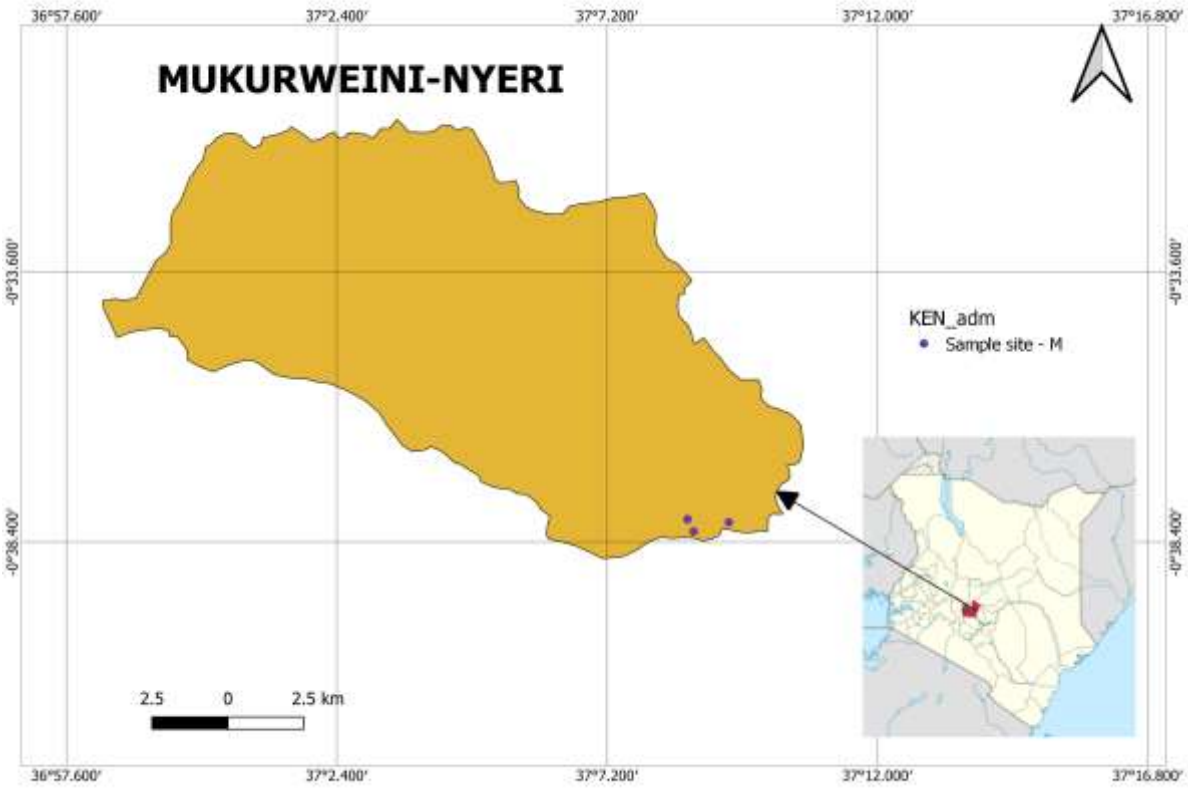

Figure 13: Sampling area in Mukurweini in Nyeri County

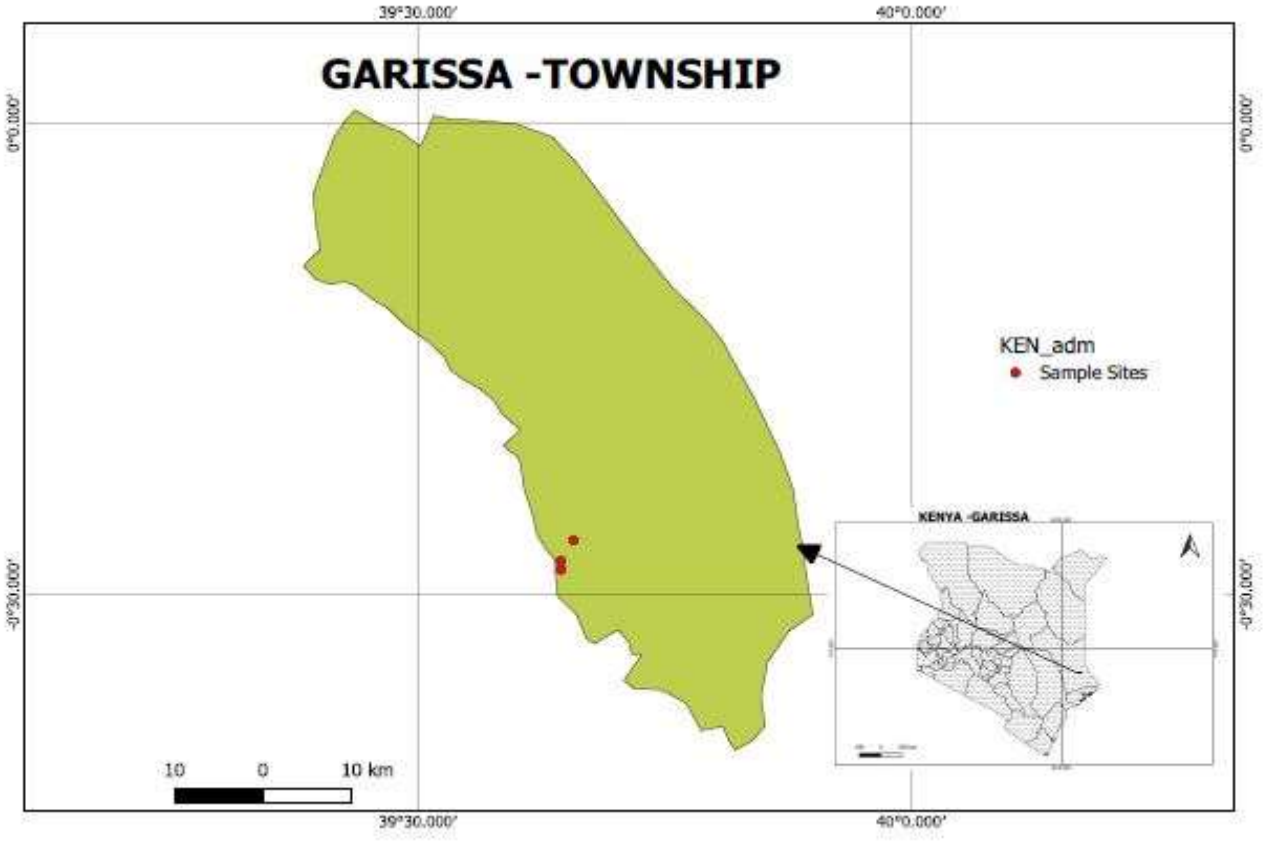

Figure 14: Sampling area in Garissa Township in Garissa County

3.2 Sampling

Ordinary kaolinite clay was collected from the Kimathe Valley in the Mukurweini sub-county, Nyeri County (latitude 0° 37' 55.9 "S, longitude 37° 9' 43.8' 'E). This area was chosen because of the interest of international companies in the area's clay mining. Random samples were taken from three locations in the Kimathe Valley. The collected samples of clay were taken at 500 m intervals along the same area where the clay mines were located. The depth of the samples taken from the surface was 0.45 m. The samples were packed in a plastic bags and then taken to the laboratory for analysis. The sampling of *Prosopis Juliflora* was done for trunk part on the banks of river Tana, in Garissa County (latitude 0° 27' 50" S, longitude 39° 38' 12" E). The types of *Prosopis* tree were carefully chosen from possibly clean zones as wood biomass supplies for charcoal production. In order to avoid possibility of pollution and inaccuracies in the trees types, *Prosopis Juliflora* trees were carefully selected for their

similar age (determined by the diameter of their stems). Sampling was done at a distance of approximately 100–150m from any road network and 2000 m from any industrial pollution source.

3.3 Materials and pieces of equipment

The analytical grade Sodium Hydroxide (NaOH) used was acquired from LOBA CHEMIE PVT LTD with percentage purity of 98%. Calcination was performed using a furnace (Daihan FHX, digital muffle furnace, standard type, 1200 ° C, FHX-03 / 05/12/14/27/63). Deionized water from a local vendor (Science lab limited (Kenya)) was utilized throughout the procedure of experiments.

3.4 Quality assurance and Quality control

Quality assurance and quality control (QA / QC) procedures were undertaken to minimize adulteration throughout research experimentation and analysis. Great precaution was in use in dismantling and cleaning the equipment with acid prior to each experiment, but there were possibility of contamination. To quality assure from these contamination sample triplicates and sample blanks were taken for each investigation.

3.4.1 Sample blanks

To assess the degree of laboratory contamination in the samples, experimental blanks were used. These blanks served as a tool to detect impurities that are leaked into the water as well as a way to test for heavy metals in deionized water. Laboratory reagent blanks were used to detect background contamination in the deionized water used to make experimental solutions. These blanks were run in the analysis to establish quality assurance and control.

3.4.2 Calibration standards

Standards of selected heavy metals were prepared as follows;

Zinc: 1.000g of zinc metal granules obtained from Kenya Industrial Research and Development Institute (KIRDI) of 99.99% purity was placed in a litre volumetric flask. 40 mL of HCl: H_2O (1:1) was added to the volumetric flask with swirling to dissolve the zinc. Then diluted this to 1 liter with deionized water to give 1000 mg/ L (1000 ppm).

Copper: 1.000g of copper metal strip/wire obtained from Kenya Industrial Research and Development Institute (KIRDI) of 99.99% purity was placed in a litre volumetric flask. 40 mL of HCl: H_2O (1:1) was added to the volumetric flask with swirling to dissolve the copper. Then diluted this to 1 liter with deionized water to give 1000 mg/ L (1000 ppm).

Cadmium: 1.000g of cadmium metal strip/granules obtained from Kenya Industrial Research and Development Institute (KIRDI) of 99.99% purity was placed in a litre volumetric flask. 40 mL of HCl: H_2O (1:1) was added to the volumetric flask with swirling to dissolve the cadmium. Then diluted this to 1 liter with deionized water to give 1000 mg/ L (1000 ppm).

Lead: 1.000g of lead metal strip/wire obtained from Kenya Industrial Research and Development Institute (KIRDI) of 99.99% purity was placed in a litre volumetric flask. 40 mL of HCl: H_2O (1:1) was added to the volumetric flask with swirling to dissolve the Lead. Then diluted this to 1 liter with deionized water to give 1000 mg/ L (1000 ppm).

The blank was deionized water which was 0.00 concentration of the target heavy metals while the multipoint calibration points concentration ranged from 200, 400,600,800 to 1000 Pbb (1ppm). The r^2 for each of the target heavy metal element on the calibration curve were as follows: Cu= 0.9661, Zn= 0.9865, Cd=0.9838 and Pb=0.9966.

The equipment were standardized using calibration standards prior to each sample run. The multipoint calibration curve produced by these calibration standards is as shown in appendix O. To establish its accurateness a reference standard was run on the calibration curve.

Attached in Appendix N is calibration curve of heavy metal standards used for analysis with ICP-MS.

3.5 Treatment of clay to form nanosilicates, analysis and characterization

Impurities were first removed from the clay by pretreatment. The clay was dried, crushed, divided, and pulverized in order to fully homogenize samples and produce the desired grain size. A sufficient amount of deionized water was used to wash the fresh clay, after which it was kept for 24 hours and decanted until the water was crystal clear. The clay was then allowed to air dry. The dry clay was then crushed and sieved (Abdullahi *et al.,* 2013). The clay was calcined at 1000 ° C for 1 hour. The silica component in the clay was converted to an amount that is soluble form by allowing a wait of one hour while maintaining the temperature at 1000 °C to avoid recrystallization of the clay.

To dissolve the silicate in the flask's contents, a 50 ml solution containing 20% excess NaOH (w/v %) was added after weighing a 25 g sample of clay. The flask was magnetically stirred while submerged in a water bath. After 20 minutes of extraction at room temperature, the extract was filtered. To dry the residue, it was placed in an oven set to 65 °C for 4 hoursThe dried sample was weighed to determine its weight. Optimal yields for extraction of NaOH solution were achieved using different concentrations of NaOH (10%, 20%, 40% (w / v%)) and duration. (Rayzman *et al.,* 2003).

3.6 Procedure of biochar preparation

The cut pieces of *Prosopis* were grounded and the powder was air-dried for 24 hours to decrease the moisture content. Using a Daihan FHX, Digital Muffle Furnace, Standard-type, 1200 °C, FHX-03/05/12/14/27/63 furnace, the pyrolysis process was carried out. 5g of the *Prosopis* feedstock was put in a ceramic crucible and heat pyrolyzed for two hours at various temperatures (200 ^{o}C, 400 ^{o}C, 500 ^{o}C, and 700 ^{o}C). After the process of pyrolysis was over,

the furnace was left for some time for the sample to cool to room temperature. The biochars obtained were marked as S-1-1, S-1-2, S-1-3, and S-1-4 for sample S-1, and S-2-1, S-2-2, S-2-3, and S-2-4 for sample S-2 representing 200 ^{o}C, 400 ^{o}C, 500 ^{o}C, and 700 ^{o}C temperatures respectively. The prepared samples were weighed after cooling down. Table 2 shows biochar Identity of samples at different temperatures.

Table 2: Biochar samples Identity and different temperatures of pyrolysis

Temperature / sample ID	**200 ^{o}C**	**400 ^{o}C**	**500 ^{o}C**	**700 ^{o}C**
S-1	**S-1-1**	**S-1-2**	**S-1-3**	**S-1-4**
S-2	**S-2-1**	**S-2-2**	**S-2-3**	**S-2-4**

3.7 Nanocomposite material preparation and characterization

The obtained modified clay silicate and biochar were fused by heat pyrolysis using a ratio of 1:1 to form a nanocomposite material at 500 ^{o}C temperature for 2 hours. Initially, equal amounts of each were used and subsequently varying ratios to achieve an optimum dispersion for impregnation. However, according to studies, the suggested dosage for combining the two materials is the same amount for equal dispersion of the two elements to be attained (Rallet *et al*., 2022). For the adsorption studies, an equal amount of the clay silicates and biochar (5g each) was used.

3.8 Characterization of the synthesized materials

The calcined clay, synthesized silicate and composite material were characterized using FTIR (Nicolet 6700 FTIR system, Model: 16F PC), TEM (JEM-2100F), SEM (Model; Quarto S), XRF, EDX, and XRD (Rigaku powder XRD-model ultima IV of wavelength of 1.54 A (Cu-anode) or 0.71 A (Mo-anode). The maximum power is 12 kW (60 kV and 200 mA); start

angle 5 and stop angle 70; scan speed 5. XRF and EDX were used to perform an elemental composition analysis on the clay and silicates produced. To determine the phase analysis, silicates underwent XRD analysis. Field Emission Scanning Electron Microscopy (FESEM) and Transmission Electron Microscopy (TEM) were used to examine particle shape and determine size. Tablets constructed of KBr were analyzed using FTIR to ascertain the chemical structure.

In SEM procedure of investigation of the synthesized materials for characterization, a dual adhesive was positioned on a sample holder stub. The sample was then spread on the stub and conveyed to a spatter coater using 5 nm gold. The sample was positioned in a charge reduction sample vessel and inserted into the column of the SEM instrument. It was initially observed by the navigation camera before being guided to SEM mode. The microscope acceleration voltage was fixed to 15 kV, enlargement of up to 1500 and under high vacuum.

Materials were basically distributed onto TEM lattices by means of appropriate solvents, and air-dried before TEM analysis. Materials of thin diameter of 3 mm (<50 microns) were set on a disc which was prepared to generate thinned-hole ends for TEM examination. This involved several steps of preparation for TEM such as cutting of multi-stage, machining (electro-discharge machining (EDM)), crushing, refining of materials and jet-electro refining. These were then fixed onto a TEM grid for analysis.

In the XRD analysis procedure qualitative assessment of the synthesized materials were done routinely; the samples were generally ground and sieved through a 325-mesh sieve (45 μm). Crushing was achieved through an automatic mechanical grinder incase the materials were not fine powder. For the type of mount, the ground particles on flat surface of 1–5 mm were filled onto a sample holder to adopt different positioning and guarantee reflections from numerous planes. They were then prepared by creation of a slurry of the sample with

deionized water. The water was then made to vaporize until the slurry is applied onto the glass slide, a sample holder and subsequently introduced into the XRD machine.

For the FTIR analysis the materials were ground with potassium bromide (KBr) salt in a ratio 1:100 and then hard-pressed at high pressure to yield KBr pellets. KBr is a hygroscopic which shows peaks of water in the spectrum and may hinder those peaks that originate from the materials. However, KBr plates were prepared judiciously by evading the absorption of moisture, thereby no peak appears in the spectrum. The other benefit was that KBr does not show any peaks below 400 cm^{-1} on FTIR.

3.9 Method of Batch adsorption for heavy metal remediation

Batch adsorption procedure was used to study the removal efficacy of the heavy metals by the clay nanosilicates, biochar material, and prepared nanocomposite materials. Mix standards of selected heavy metals (1000 ppm) were diluted in a 1L volumetric flask to achieve a concentration of 1ppm of each of the selected heavy metals. 25 mL or 50 mL volume of the diluted solution selected heavy metal ion was put in Erlenmeyer flask and appropriate dosage of the synthesized material was added. pH adjustment was carried out using dilute NaOH or HCl to achieve the desired pH. The degree of removal of various heavy metals (lead, cadmium, zinc, copper) was assessed by varying various parameters such as pH, contact time, and amount of adsorbent (R. Ahmed et al., 2006). The amounts of heavy metals were quantified by quadrupole inductively coupled plasma mass spectrometry (ICP-MS), Model: iCAP RQ ICP-MS from Thermo Fisher Scientific, with Qtegra Intelligent Scientific Data Solution (ISDS) software, a quartz spray chamber, a glass concentric nebulizer, an online Internal Standard (ISTD) addition kit, and replaceable skimmer cones. The optimization of different parameters was carried out as follows;

3.9.1 Effect of pH

By varying the pH from 4 to 9, while retaining the other parameters constant, the effect of the change of pH was investigated (dosage of nanomaterial, agitation speed, and time) (i.e. 10g/50ml, 150 rpm, and 120 min.) as given in Table 3.

Table 3: Study of pH effect on adsorption of heavy metals

No.	**pH**	**Dosage of calcined clay (solution of 1 ppm metal ions)**	**Agitation speed of shaker**	**Time** min	**Sample ID**
1)	4	10 g in 50 mL solution	150 rpm	120	P-2
2)	7	10 g in 50 mL solution	150 rpm	120	P-3
3)	8	10 g in 50 mL solution	150 rpm	120	P-4
4)	9	10 g in 50 mL solution	150 rpm	120	P-5

Initial concentration of the solution = 1 ppm (Zn, Cu, Cd & Pb) only

3.9.2 Effect of Contact time

The variation of contact time from 10 -120 min was conducted while keeping the rest of the parameters constant (dosage of nanomaterial, agitation speed, and pH) i.e. 5 g/25ml, 150 rpm, and pH-8 as given in Table 4.

Table 4: Study of contact time effect on adsorption of heavy metals

No.	**pH**	**Dosage of calcined clay (solution of 1 ppm metal ions)**	**Agitation speed of shaker** (rpm)	**Time min**	**Sample ID**
1)	8	5 g in 25 mL solution	150	30	C-2
2)	8	5 g in 25 mL solution	150	60	C-3
3)	8	5 g in 25 mL solution	150	90	C-4
4)	8	5 g in 25 mL solution	150	120	C-5

The initial concentration of the solution = 1 ppm (Zn, Cu, Cd & Pb) only

3.9.3 Effect of agitation speed of the shaker

With the other parameters (nanomaterial dosage, contact time, and pH) remaining constant (5 g/50 ml, 120 min, and pH-8 as shown in Table 5), the examination of the effects of shaker speed was carried out.

Table 5: Study of Shaker speed on adsorption of heavy metals

No.	**pH**	**Dosage of calcined clay (solution of 1 ppm metal ions)**	**Agitation speed of shaker** (rpm)	**Time** (min)	**Sample ID**
1)	8	5 g in 25 mL solution	50	120	AS-2
2)	8	5 g in 25 mL solution	100	120	AS-3
3)	8	5 g in 25 mL solution	150	120	AS-4
4)	8	5 g in 25 mL solution	200	120	AS-5

The initial concentration of the solution = 1 ppm (Zn, Cu, Cd & Pb) only

3.9.4 Effect of NP's dosage -Calcined clay

The batch procedure was carried out by changing the amounts of the synthesized materials (calcined clay) of 5, 10, 20, and 40 mg (considering the amount of the synthesized material) while keeping the rest of the parameters constant (contact time, agitation speed, and pH) i.e. 120 min, 150 rpm, and pH-8 respectively as given in Table 6.

Table 6: Study of calcined clay dosage on adsorption of heavy metals

No.	**pH**	**Dosage of calcined clay –- (solution of 1 ppm metal ions)**	**Agitation speed of shaker(**rpm**)**	**Time** (min)	**SAMPLE CODE**
1)	8	5 g in 25 mL solution	150	120	CC-2
2)	8	10 g in 25 mL solution	150	120	CC-3

3)	8	20 g in 25 mL solution	150	120	CC-4
4)	8	40 g in 25 mL solution	150	120	CC-5

The initial concentration of the solution = 1 ppm (Zn, Cu, Cd & Pb) only

3.9.5 Effect of Biochar dosage

The batch procedure was carried out by changing the amounts of the synthesized materials (biochar) to 0.5, 1, 2, and 1.2 mg (considering the amount of the synthesized material) while keeping the rest of the parameters constant (contact time, agitation speed, and pH) i.e. 120 min, 150 rpm, and pH-8 respectively as given in Table 7.

Table 7: Study of Biochar dosage on adsorption of heavy metals

No.	**pH**	**Dosage of biochar - (solution of 1 ppm metal ions)**	**Agitation speed of shaker** (rpm)	**Time** (min)	**Sample ID**
1)	8	0.5 mg in 25 mL solution	150	120	BC-2
2)	8	1 g in 25 mL solution	150	120	BC-3
3)	8	1.2 g in 25 mL solution	150	120	BC-4
4)	8	2 g in 25 mL solution	150	120	BC-5

The initial concentration of the solution = 1 ppm (Zn, Cu, Cd & Pb) only

3.9.6 Effect of NP's dosage -Nanocomposite material

The batch procedure was performed by changing the amounts of the synthesized nanocomposite material of 1, 2, 4, and 6 mg (considering the amount of the synthesized material) while keeping the rest of the parameters constant (contact time, agitation speed, and pH) i.e. 120 min, 150 rpm, and pH-8 respectively as given in Table 8.

Table 8: Study of composite material dosage on adsorption of heavy metals

No.	pH	Dosage of Nanocomposite material- (solution of 1 ppm metal ions)	Agitation speed of shaker (rpm)	Time (min)	Sample ID
1)	8	1 g/ in 25 mL solution	150	120	NC-2
2)	8	2 g in 25 mL solution	150	120	NC-3
3)	8	4 g in 25 mL solution	150	120	NC-4
4)	8	6 g in 25 mL solution	150	120	NC-5

The initial concentration of the solution = 1 ppm (Zn, Cu, Cd & Pb) only

Before the analysis using the ICP-MS instrument, the samples of adsorption study of different synthesized material for the removal of the selected heavy metals were subjected to filtration with Nylon syringe filters with a pore size of 0.22 μm and a diameter of 13 mm from the membrane solution. Inductively Coupled Plasma-Mass Spectrometry (ICP-MS) was employed to evaluate the concentration of the heavy metal before and after the adsorption procedure.

3.10 Adsorption Isotherms and kinetic models

3.10.1 Freundlich Isotherm

The premise of Freundlich isotherms is that the absorbable quantity of adsorbate is almost limitless and occurs as multilayer adsorption. The amount of metal taken up was calculated according to the relationship in Equation 3

$$q_e = \frac{(C_0 - C_e) \times V}{m} \quad \text{---------- (3)}$$

Where q_e is the adsorbed amount of adsorbent, where m = weight of adsorbent (g); and V = volume of the solution (L). C_o is the initial concentration of the Heavy Metal (mg/ L) and C_e is the final concentration of the heavy metal in water after the adsorption process (mg/ L).

The Freundlich isotherm model is the first recognized correlation that describes non-ideal and reversible adsorption that can be employed in multi-layer based adsorption on presumptions about energy surface heterogeneity. The equation of Freundlich isotherm model for non-linear situation can be expressed as shown in equation 4

$$q_e = K_F C_e^{1/n} \quad \text{---------- (4)}$$

Where C_e denotes the equilibrium concentration of the metal pollutant solution (mg/L). While K_F and n are constants that evaluate adsorption strength and capacity, respectively, q_e is equivalent to adsorption capacity (mg/g).

The application of the Freundlich adsorption isotherm in linear form is demonstrated by Equation 5.

$$\ln q_e = \ln K_F + \frac{1}{n} \ln C_e \quad \text{..... (5)}$$

Where K_F (mg/g) and n are the Freundlich adsorption constants that may be calculated from the slope and intercept of a plot of ln q_e vs ln C_e, and q_e and C_e are the amount of analyte adsorbed and the equilibrium concentration in (mg/mg) and (mg/L), respectively.

3.10.2 Langmuir Isotherm

The Langmuir isotherm model is an empirical model that assumes that adsorption can occur only at a finite number of distinctive localized sites and that the adsorption layer is a single molecule thick or single layer adsorption.

Equation 6 can be used to express the Langmuir isotherm model's nonlinear equation

$$q_e = q_m K_L \frac{C_e}{1 + K_L C_e} \quad \text{---------- (6)}$$

Where C_e denotes the equilibrium concentration of the metal pollutant solution (in mg/L). The appropriate adsorption capacity is denoted by q_e (mg/g). q_m (mg/g), K_L (mg/ L), and net adsorption enthalpy are the respective constants for adsorption volume, energy, and enthalpy.

In equation 7, the linear form of the Langmuir adsorption isotherm was employed

$$\frac{C_e}{q_e} = \frac{1}{q_m K_L} + \frac{C_e}{q_m} \quad \text{---------- (7)}$$

Where C_e/q_e = ratio of the equilibrium concentration (ug/L) to the amount of pollutants adsorbed in equilibrium (ug/L), q_m= Langmuir adsorption constant that describes the highest monolayer capacity, and K_L = Langmuir constant of adsorption energy. The values of Langmuir parameters q_m and K_L are Slopes and intercepts of a C_e / q_e vs. Ce linear plot.

The data obtained from experiments were used to test the applicability of various isotherms like Freundlich and Langmuir isotherm models.

3.10.3 Pseudo first order and second order

Because of the chemical reactions that occur, kinetic system design and reaction rate control steps require reaction rate prediction. The nature of the sorption process depends on the physicochemical properties of the adsorbent and system conditions such as temperature.

Lagrange's first-order pseudo-equations are commonly expressed as in equation 8:

$$\frac{dq_t}{dt} = K(q_e - q_t) \quad \text{---------- (8)}$$

After applying the integral and boundary conditions, t= 0 to t = t and q_t = 0 to q_t = q_t the equation becomes equation 9;

$$\log(q_e - q_t) = \log q_e - \frac{k_1}{2.303} t \quad \text{----------(9)}$$

The log (q_e -q_t) vs. t plot shows a straight line where K_1 and q_e can be found using slope and intercept.

The pseudo-secondary rate equation is based on the sorption capacity of the solid phase used in the analysis of the chemisorption rate equation. It is given by equation 10

$$\frac{dq_t}{dt} = k_2(q_e - q_t)^2$$ ----------(10)

Boundary condition $q_t = 0$ or $q_t = q_t$ and $t = 0$ to $t = t$. The integrated form of the equation is as shown in equation 11 as follows;

$$\frac{t}{q_t} = \frac{1}{k_2 q_e^2} + \frac{1}{q_e} t$$ ----------(11)

The t/q_t vs. t plot shows a straight line from which K_2 and q_e can be calculated.

To examine the kinetics of adsorption involved, pseudo-first-order and second-order kinetic equations were applied. (Sazali *et al.*, 2020).

CHAPTER FOUR

RESULTS AND DISCUSSION

4.1 Introduction

This chapter reports on the results and discussion of the characterization and analysis of the synthesized materials and their removal effectiveness of selected heavy metals.

4.2 Elemental analysis and characterization of clay nanosilicates

XRF and EDX were used to determine the compositional elements of the calcined clay and extracted silicates. Table 9 and Figure 15 shows the results of XRF and EDX respectively. The results of the XRF analysis demonstrated that the method of extraction significantly increased the amount of the percentage extracted silicates. Following extraction, the pattern shows that sodium silicates made up the majority of nanosilicates, and that silica content decreased as alkali (NaOH) concentration increased. The best outcome came with 20% NaOH. Equation 12 illustrates the chemical reaction of the process.

$$SiO_{2\ (Calcined\ clay)} + NaOH_{(aq)} \longrightarrow NaSiO_{3\ (aq)} + H_2O_{(l)} \quad \text{---------- (12)}$$

Table 9: Percentage composition of calcined clay and silicate extract using XRF

Composition	Calcined Clay	Silicate extract (20%)	Silicate extract (40%)
Al_2O_3	32.4	5.1	8.2
SiO_2	55.0	83.6	72.3
K_20	1.1	5.0	8.5
CaO	1.1	1.3	4.1
Fe	6.1	1.0	2.2
P_2O_5	0.5	0.6	0.5
Others	3.8	3.4	4.2

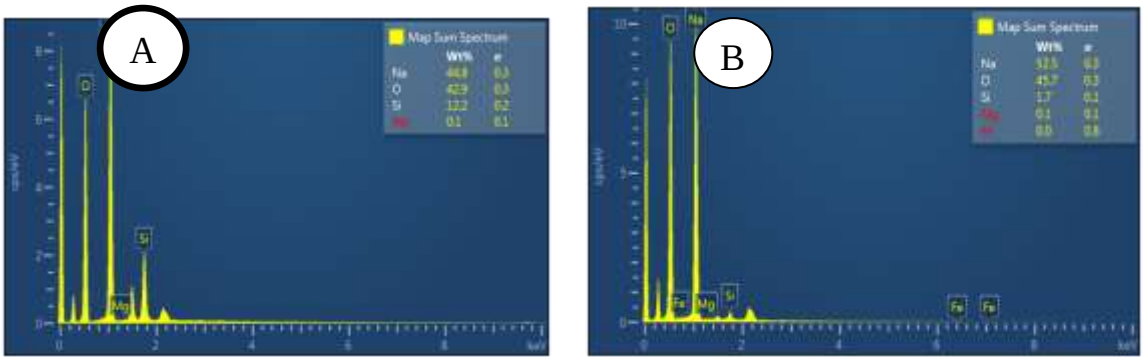

Figure 15: EDX patterns of nanosilicates extract with (a) 20% NaOH and (b) 40% NaOH

It is evident from Figure 15 that the synthesis of silicates was successful. A better yield was obtained with 20% NaOH concentration as opposed to 40% NaOH. This is consistent with literature-reported findings that the amount of silicates extracted decreases with increasing extracting media concentration. This is due to a complex formed when the extra extraction medium reacts with the available alumina (Abdullahi, *et al.*, 2013). Additionally, FTIR was used to characterize the synthesized nanosilicates. It closely represented the normal sodium silicate structure that is mentioned in the literature (Yang, *et al.*, 2008). The bands of silicates as depicted in Figure 16 were clearly defined by the infrared bands of 1000, 1500, 1700, and around 3500 cm-1.The Infrared bands of 1000, 1500, 1700, and approx. 3500 cm^{-1} clearly described the bands of silicates as shown in Figure 16.

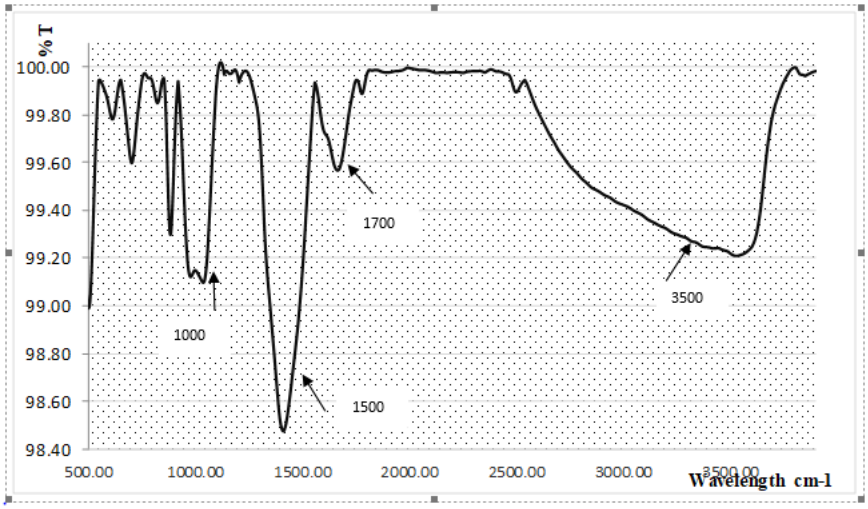

Figure 16: FTIR spectrum of synthesized silicate nanoparticles

Figures 17 and 18 are FESEM images of the nanosilicates while Figure 19 are FETEM images showing the surface morphologies respectively. FESEM study revealed aggregated, spherical-shaped nanosilicates that were produced using various molar concentrations of sodium hydroxide solution. It showed molar concentration of extracting media had effect on the morphology of the nanosilicates produced. Van der Waals forces or chemical bonding between the nanoparticles have been suggested as the primary mechanisms for the aggregation or agglomeration. Nanosilicates had spherical morphology, excellent disparity, and colloidal spheres of uniform size with diameters ranging from 80 to 90 nm. The synthesized nanosilicates' structure and shape are in good agreement with what is published in the literature and shown in the FESEM study (Szegedi *et al.*, 2004). The nanosilicates' average particle diameter was between 80 and 90 nm.

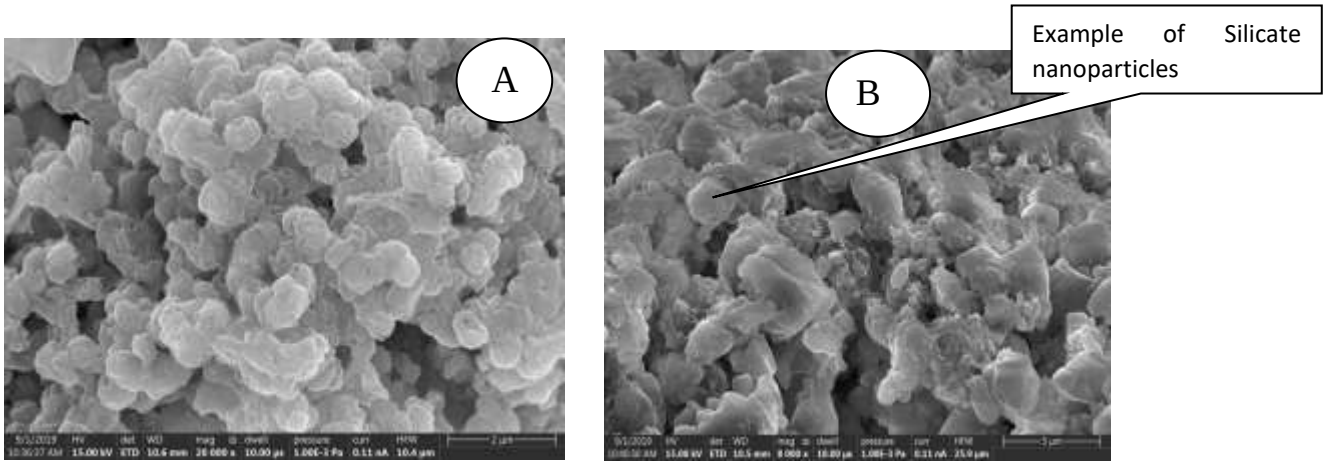

Figure 17: FESEM images of synthesized silicate nanoparticles using 20% NaOH (w/v%): (A) 2 µm, (B) 5 µm

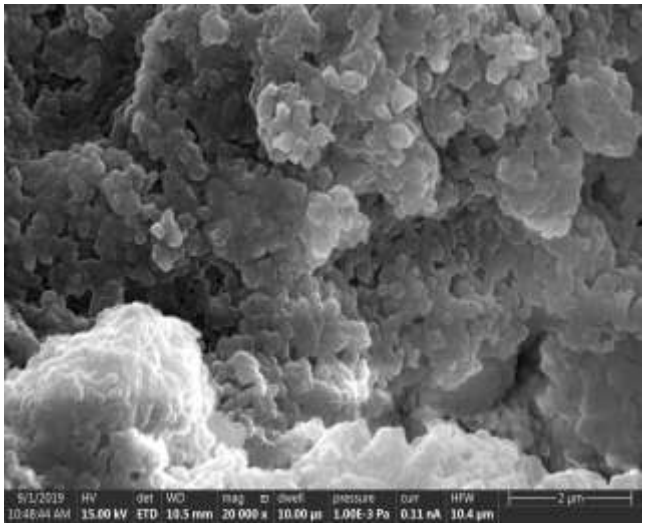

Figure 18: FESEM images of synthesized silicate nanoparticles using 40% NaOH (w/v%) at 2 µm

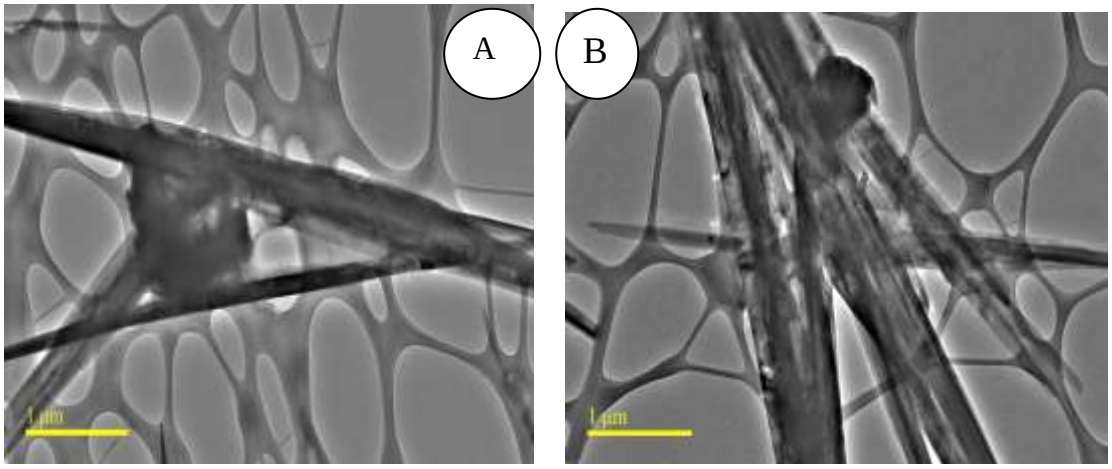

Figure 19: FETEM images of synthesized silicate nanoparticles using (A): 20% NaOH (w/v %) and (B): 40% NaOH (w/v %)

Since sodium hydroxide (NaOH) was used as the extraction medium, phase analysis with XRD demonstrated the creation of silicate nanoparticles that corresponded to sodium silicates. The spectra of the nanoparticles that were extracted using 20% and 40% NaOH, respectively, are shown in Figures 20 and 21. The silicate nanoparticles synthesized revealed a $2\theta=30^{o}$ that indicated their presence and showed that their peak positions agreed with the reference peaks (JCDPS, No. 29-1233). Sodium silicate is typically associated to the strong, intense diffraction peaks between 25.26° and 65.93°. When the two concentrations were

compared, the silicates were more intense at 40% NaOH solution as compared to 20% NaOH solution, with nearly identical peaks at the same 2θ degree level for nanosilicates.

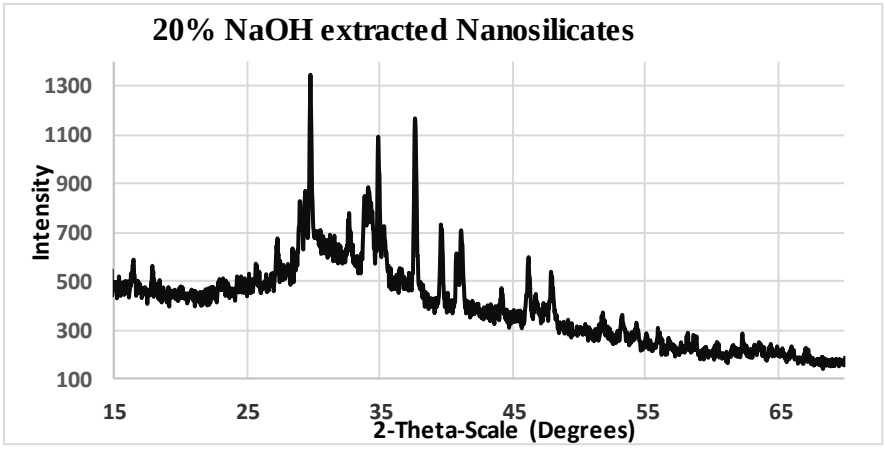

Figure 20: XRD pattern of synthesized silicate nanoparticles using 20% NaOH (w/v %)

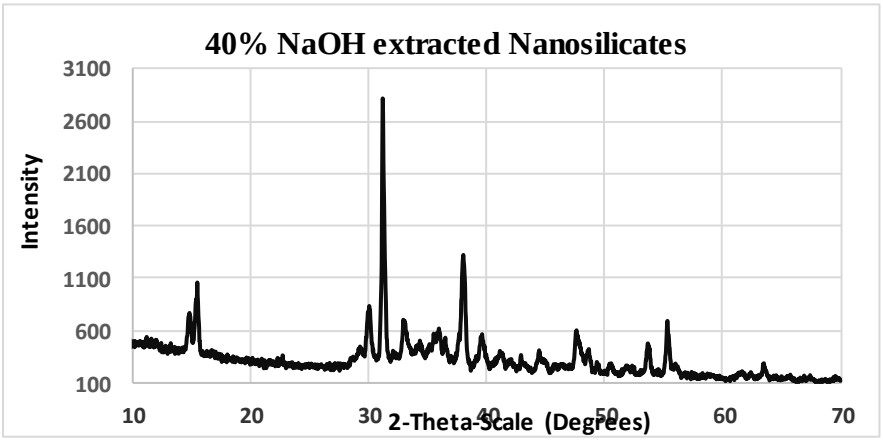

Figure 21: XRD pattern of synthesized silicate nanoparticles using 40% NaOH (w/v %)

4.3 Characterization and analysis of biochar biomaterial of *Prosopis Juliflora*

The elemental analysis of the prepared biochar was done by EDX. The pyrolysis parameters (such as temperature, pH, and duration) had a stronger impact on the adsorption rate and the properties of the biochar. However, as the temperature rose, carbon content and the surface area of majority of biochars rose but their performance generally decreased. By increasing the pyrolysis temperature, the yield of biochar and the hydrogen content decreased, while the ash and carbon content and the pH value increased. In our case, it was evident that low

temperatures reduced the performance of the biochar while high temperatures also reduced hydrogen content in the biochar material as reported in the literature by Chatterjee *et al.*, (2020). This is attributed to the general principle that visibility of functional groups on the FTIR of biochar samples often decreases with higher pyrolysis temperatures (Elnour *et al.*, 2019). Table 10 shows the EDX elemental analysis of the biochar which indicated that it is composed of carbon and oxygen which was consistent with what was reported in the literature on most biochars (Yaashikaa *et al.,* 2020). This information corresponded well with the EDX analysis as seen in figure 22. The presence of gold (Au) is attributed to the FESEM instrument used which was coupled with EDX and usually gold is used for sputter coating material in the initial stage of sample preparation. This metal is preferred due to its high conductivity and relatively small particle size, making it ideal for high-resolution imaging.

Table 10: Percentage elemental composition of *Prosopis Juliflora* biochar at 500 ^{o}C

Elements	Biochar composition Wt. %
Carbon (C)	62.5
Oxygen (O)	21.1
Potassium (K)	6.0
Calcium (Ca)	5.3
Chloride (Cl)	2.3
Sodium (Na)	1.0

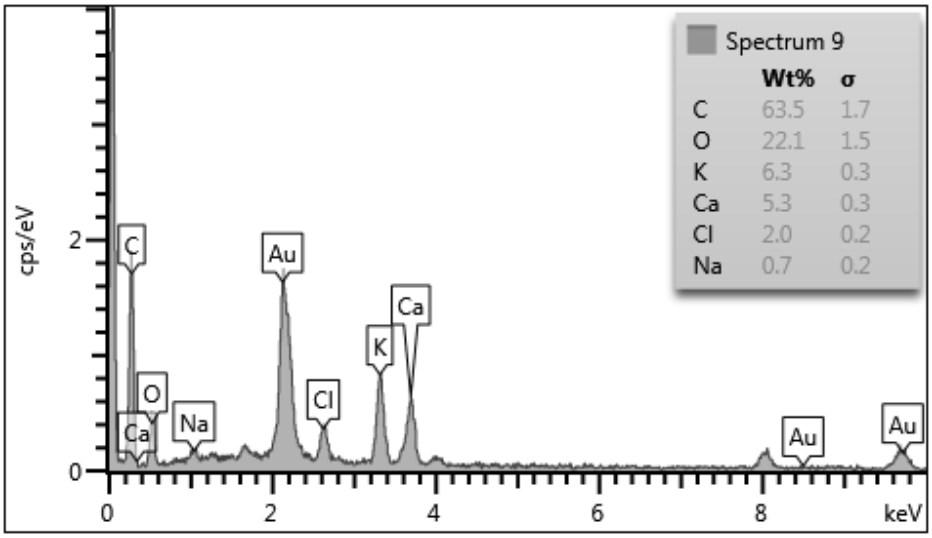

Figure 22: EDX patterns of *Prosopis Juliflora* biochar @ 500 ºC.

The spectrum shown in Figure 23 of the *Prosopis* Biochar's FTIR spectrum, additionally demonstrates the CO_2 absorption peak at 2,350 cm^{-1} and the stretching of the O-H band of hydroxyl-hydrogen bonded groups at 3500 cm^{-1}. The carboxylate (COO^-) and primary amine (1^o) N-H bending are assigned to the absorption band at 1,600 cm^{-1}, respectively. (Liu *et al.*, 2015), and ~1,405 cm^{-1} is ascribed to aromatic C=C stretch (Zhao *et al.*, 2017). The band at 1,099 cm^{-1} is attributed to C-O stretching bands or the C-N stretch of a straight chain primary amine.(Coates,2006).

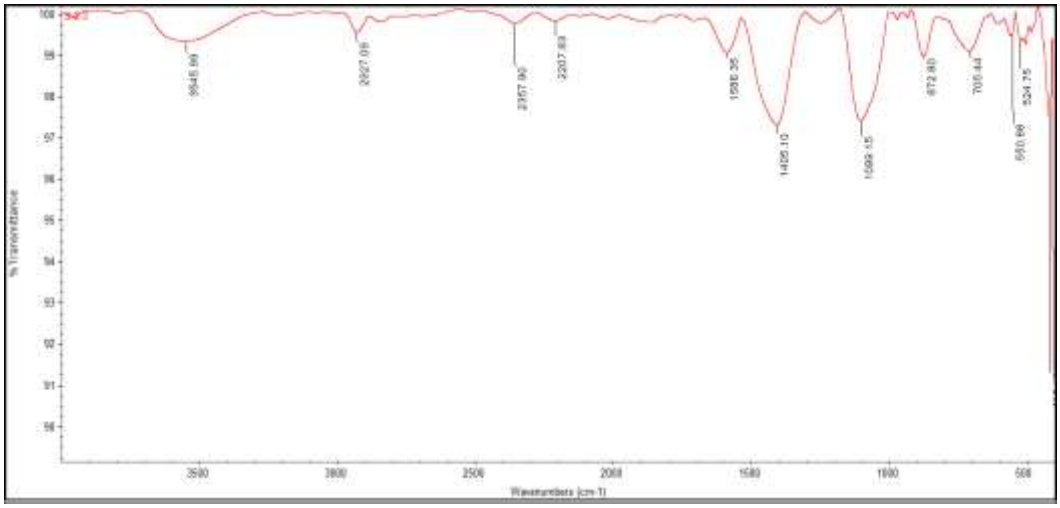

Figure 23: FTIR spectrum of *Prosopis Juliflora* biochar at 500 ºC

Figure 24 displays the *Prosopis* biochar's XRD pattern. The increase in background level and the significant hump between 11 and 13º suggests that cellulose or other comparable organic components are prevalent (Fancello *et al.,* 2019). The crystalline cellulose in the spectrum is associated to the broad peak at the 2θ values about 23º (Osman *et al.,* 2018). Amorphous carbon was identified as a thin, sharp peak at roughly 30º. (Fu *et al.,* 2016).

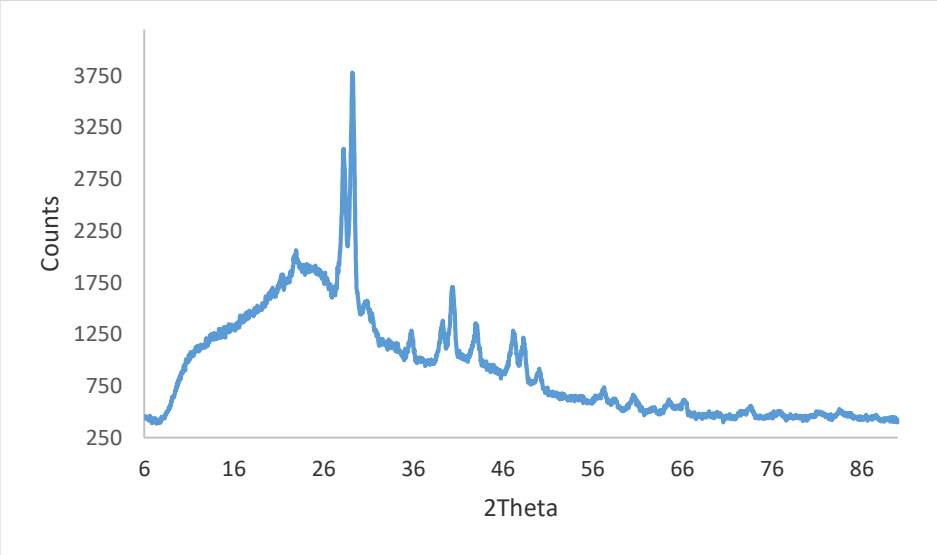

Figure 24: XRD Pattern of *Prosopis Juliflora* biochar at 500 ºC.

The SEM images of the biochar as seen in Figures 25 (a-c) depict particles varying in shape. The milling, sieving, and handling of the Prosopis material during sample preparation is what caused this variance. Fibrous structures and pith were two important morphological characteristics that the SEM pictures of the biochar samples revealed. The pith is a more fragile and fragmented structure, mostly made up of fissures linking adjacent cells on the surface of the walls, as opposed to the fibrous surface, which is composed of parallel shreds and is partially covered by residual material. Figures 25 (A, B, and C) show how the biochar sample is composed of rough particles of various sizes packed in rolls with vascular

characteristics and has a relatively flat surface; this has also been reported in the literature (Zhang *et al.,* 2014; Wang *et al.,* 2015). Due to the pyrolysis's release of volatile chemicals such acetic acid, carbon dioxide, and methanol, all *Prosopis* biochar samples exhibit fractures and cracks.

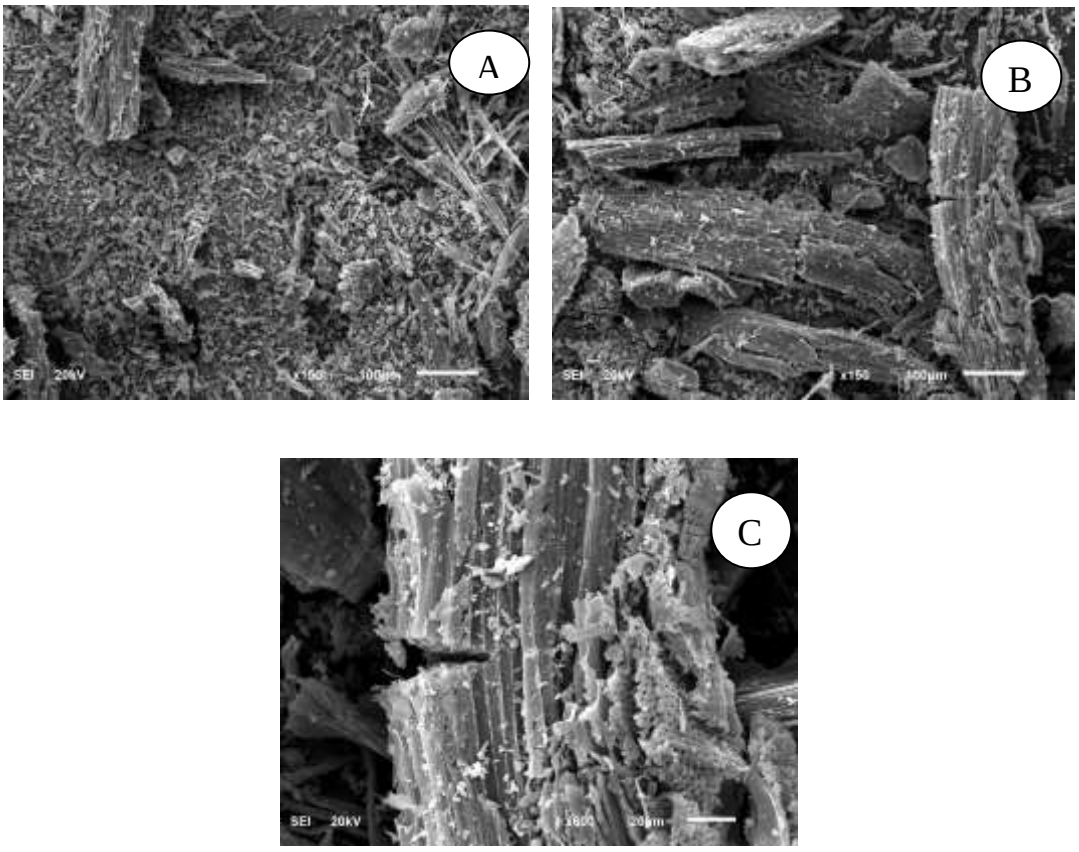

Figure 25: SEM images of the *Prosopis Juliflora* biochar duplicates (A & B) at : 100 μm, and (C): 20 μm

4.4 Characterization of nanoparticles materials

The elemental analysis of the nanocomposite material of clay and biochar was done with EDX. The results as shown in Figures 26 (a) and (b) showed the elemental composition of the nanocomposite to be high in carbon (C), oxygen (O), silica (Si), aluminium (Al), and iron (Fe). Mainly the carbon is coming from the biochar while the other elements originated from

clay material. The average composition was 49.05% C, 35.85% O, 5.7% Si, 5.2% Al and 2.05% Fe.

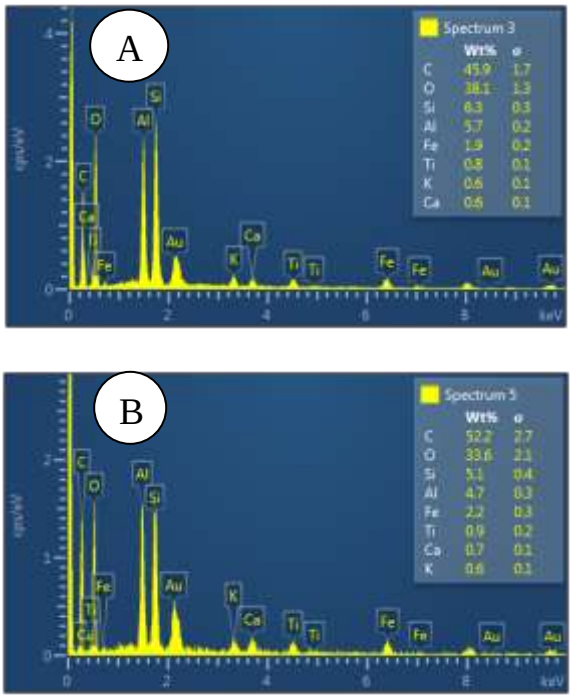

Figure 26: EDX patterns of the nanocomposite material of clay nanosilicates and biochar material duplicate (A) and (B)

Figure 27 shows the FTIR spectrum of the nanocomposite material. The pattern showed a broad weak peak at approximately 3645 cm^{-1} symbolic of O-H stretching as a result of the hydroxyl group and another peak at 2349 cm^{-1} associated with CO_2 absorption. Also, The band at 1,063 cm^{-1} was ascribed to C-O stretching vibrations. This was an indication that the biochar material composition is well contained in the nanocoposite material, therefore successful impregnation of clay silicates on the biochar surface.

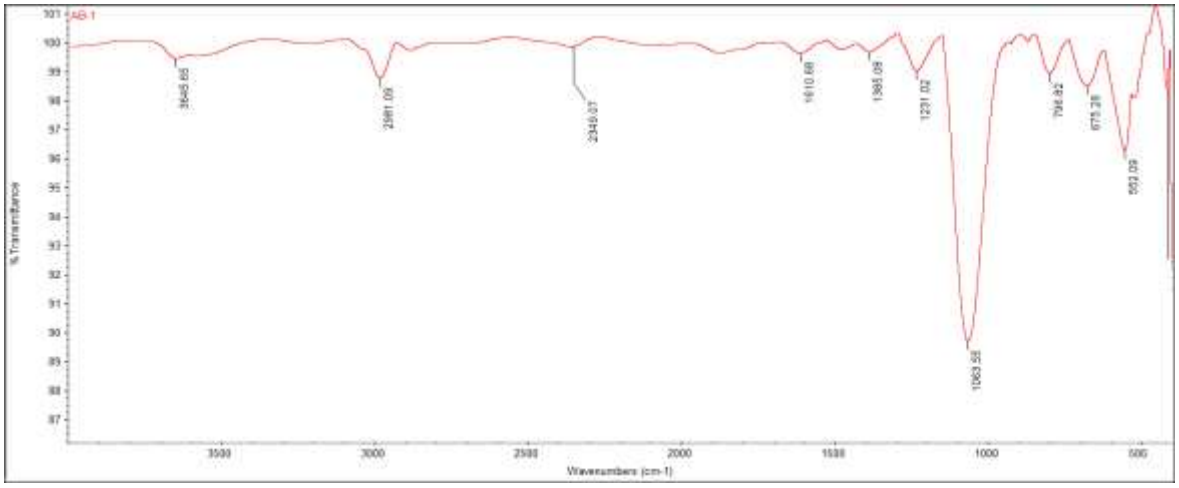

Figure 27: FTIR spectrum of nanocomposite material

XRD analysis of clay-biochar nanocomposites showed the existence of mineral crystals. In the spectrum, the three strong peaks at 19.9^0, 25^0, and 35^0 shown were identified as expansible phyllosilicates (Yao *et al.*, 2011) as was seen in Figure 28. These XRD results agreed well with EDX results that the pyrolysis method had effectively inserted silicates on top of the surfaces of carbon of the biochar to form a clay-biochar nanocomposite

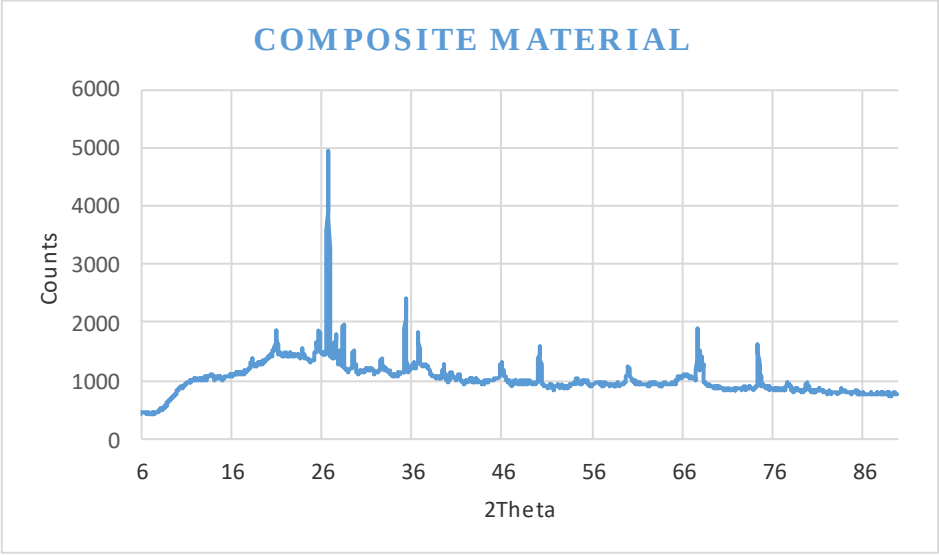

Figure 28: XRD pattern of clay-biochar nanocomposite

The SEM images of the clay biochar composites revealed that the sample surface was mainly covered by thin-film structures as shown in Figure 29 (A). At a higher magnification of times

five (X5), the films showed layered surfaces as seen in Figure 29 (B). Structural morphology of clay gave the description as shown in Figure 29 (C) (Wang *et al.,* 2004). The coverage of clay nanomaterial on the biochar surface was additionally established by the EDX study as given in Figure 30. Both the EDX pattern and the SEM image of the surface revealed high peaks for silicon, aluminum, titanium and iron, all those are all characteristics of clay's elemental form.

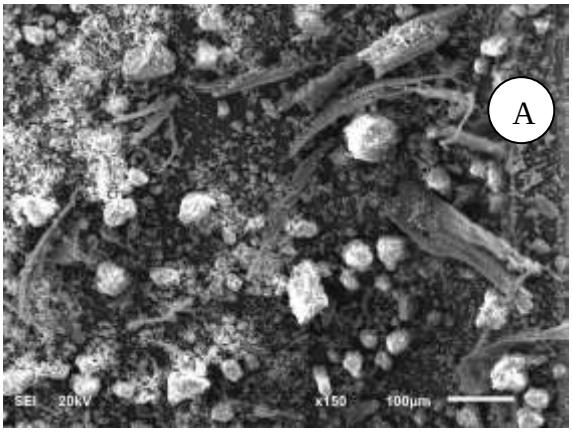

Figure 29 (A): SEM images of nanocomposite at 100 µm

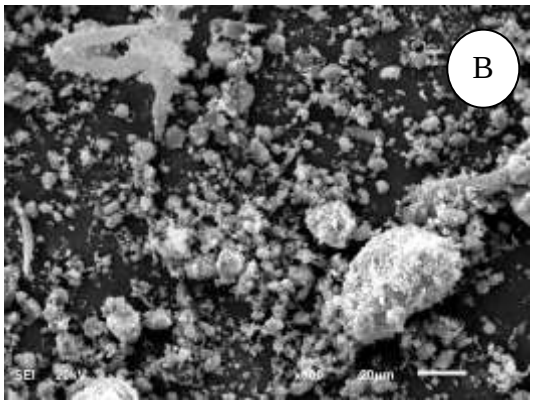

Figure 29 (B): SEM images of nanocomposite X5 at 20 µm

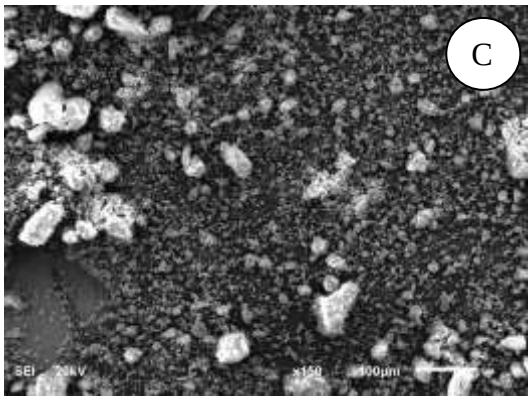

Figure 29 (C): SEM images of clay material

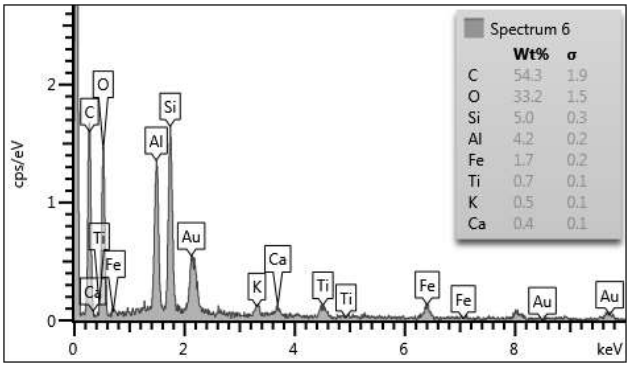

Figure 30: EDX spectrum of the nanocomposite

4.5 Adsorption and efficacy of the synthesized materials

Batch adsorption procedure was used as stated in section 3.9. Basic quality control and assurance, sample duplicates, sample blanks, and calibration standards protocols were followed.

Based on reducing concentrations of heavy metal in each sample, equation 13 was used to determine the removal efficiency

Percent removal efficiency = $\frac{C_i - C_f}{C_i} \times 100$ ---------- (13)

Where C_i is the original concentration of the metal (mg/L) and C_f is the final concentration of the heavy metal in water after the adsorption process (mg/L).

4.5.1 Effect of contact time

During the batch adsorption analysis, the following parameters were taken into account: pH, contact time, speed of the shaker, and dosage of the material. Until equilibrium distributions is attained, time plays a significant role in the adsorption of metals from water. According to research, the fibers begin to adsorb the majority of within the first few hours of contact. (Larson, 2013; Rediske, 2014). The data from the adsorption results was not varying for the four heavy metals and the maximum removal was realized after 60 mins of contact time for all the metals which agreed with Rediske, (2014). The heavy metals (Zn, Cu, Cd and Pb) showed maximum removal at 60 mins of contact time and beyond that time almost flatten or dropped as seen in Figures 31 (A-D). This is explained by the fact that there were enough open surface sites accessible for adsorption in the early stages but due to repelling forces between heavy metals in the solution and absorbent sites of exchange no more exchange was possible (Riskuwa-Shehu *et al*., 2019). Hence increase in duration of contact time does not have significant removal of the heavy metals, therefore 60 mins was selected as the optimum contact time for the rest of the adsorption experiments. The raw data for the effect of contact time on the selected heavy metals are attached in appendix A

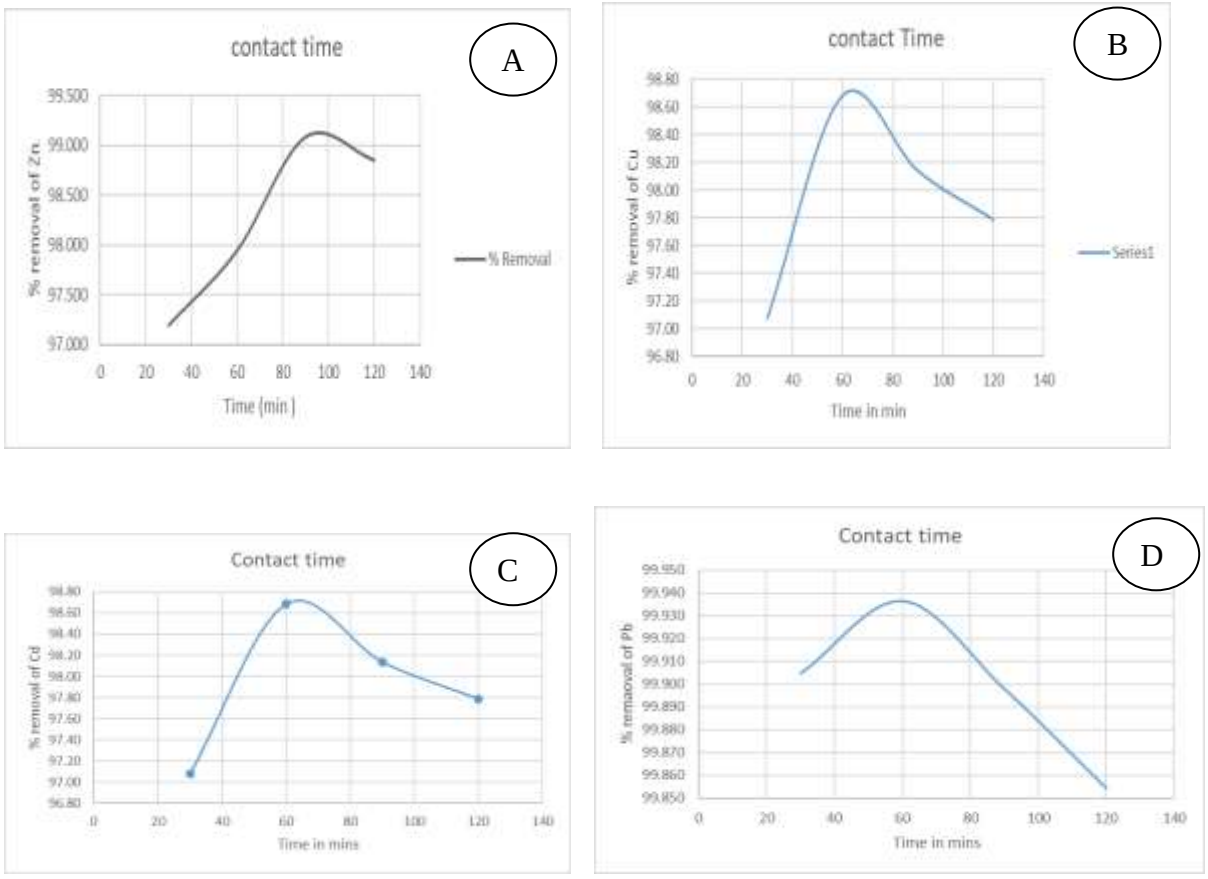

Figure 31: Effect of contact time on heavy metals (A): Zn (B): Cu (C): Cd and (D): Pb adsorption

4.5.2 Effect of pH

In an effort to determine the optimal pH for heavy metal adsorption, the impact of pH on the adsorption of heavy metals by calcined clay was examined. When addressing the adsorption of heavy metals from the aqueous solution in order to manage the adsorption capacity, one of the key elements is the pH of the solution since it impacts the surface characteristics of the adsorbent (Emam, 2013). Rediske (2014) discovered that cadmium adsorption was largely unaffected by pH values between 3 and 9. At pH ranges between 3 and 9, it was noted that the adsorbent loading and fiber mass had the same ratio (Rediske, 2014). For the four heavy metals (Zn, Cu, Cd, and Pb) adsorption to ascertain the best pH for their removals was done as described in section 3.10.1. The pH range was between pH 4 – pH 9. The highest removal as seen from the adsorption results at pH 8 was 99.40%, 98.88%, 99.56%, and 99.95%

removal efficiency for Zn, Cu, Cd, and Pb respectively as seen in figures 32 and 33. For the remaining parts of the adsorption trials, pH 8 was chosen as the optimum pH for the removal of heavy metals. The raw data for effect of pH of the selected heavy metals removal are attached in appendix B.

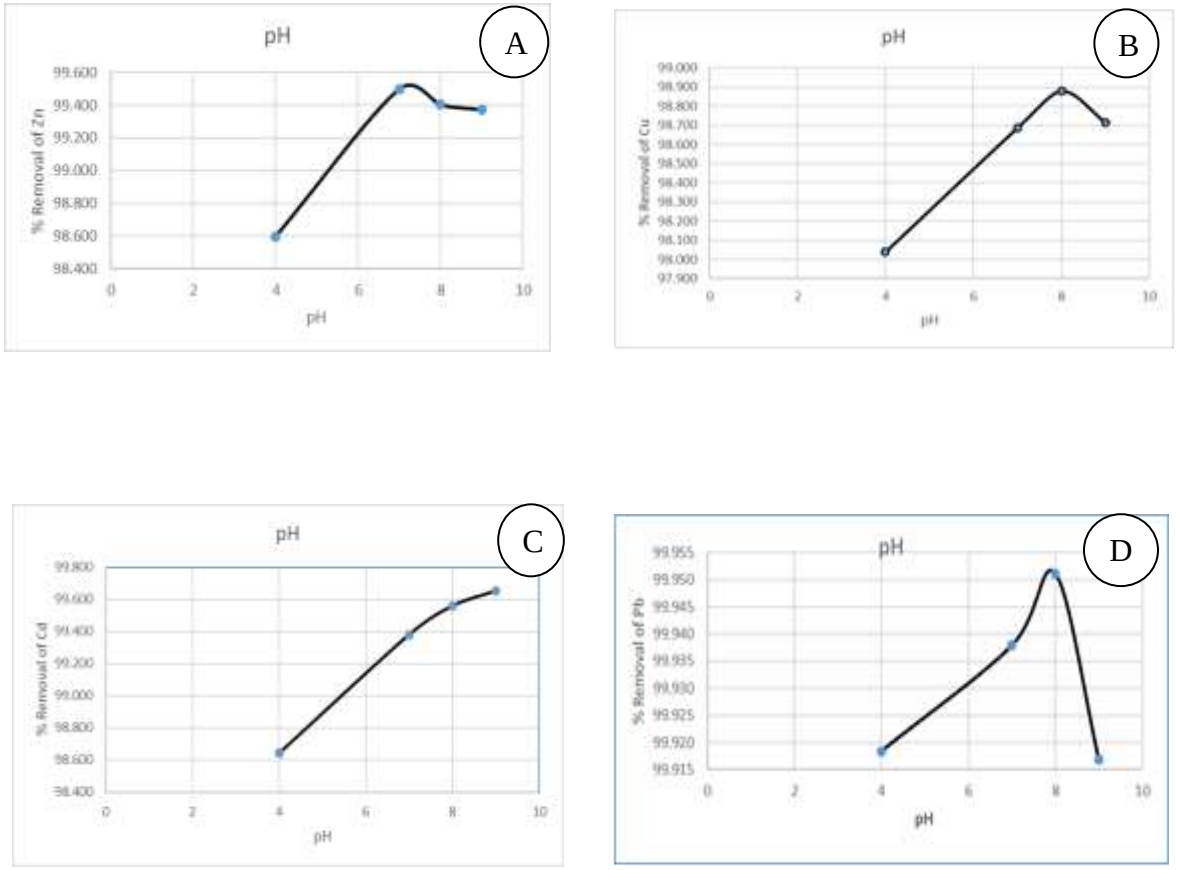

Figure 32: Effect of pH on adsorption of (A): Zn, (B): Cu, (C): Cd and (D): Pb metals

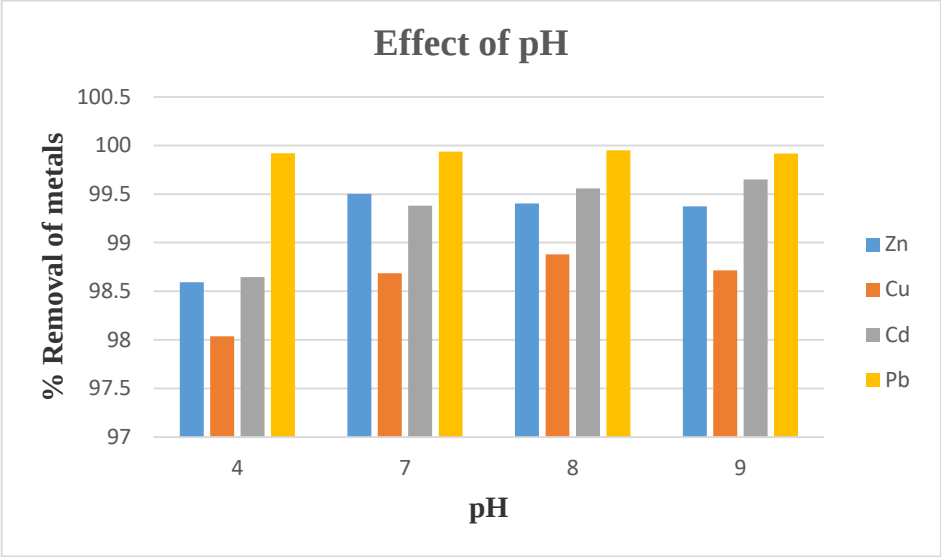

Figure 33: Effect of pH on adsorption of heavy metals

4.5.3 Effect of Agitation speed of the shaker

For the speed of the shaker, the results from the adsorption for the heavy metals were performed ranging from 50 rpm to 200 rpm using an orbital shaker. For Zn and Cu metals, the maximum removal efficiency was realized at 100 rpm while for Cd and Pb metals, it was at 150 rpm and 200 rpm respectively as shown in Figures 34 (A-D) and Figure 35. Since the efficiency was close the optimum selected agitation speed was 150 rpm for the remaining experiments. The raw data for the effect of agitation speed of the shaker on the selected heavy metals are attached in appendix C

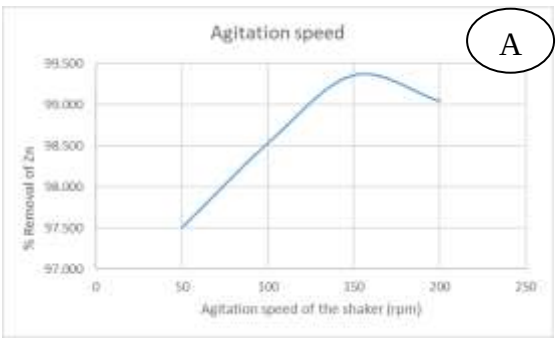

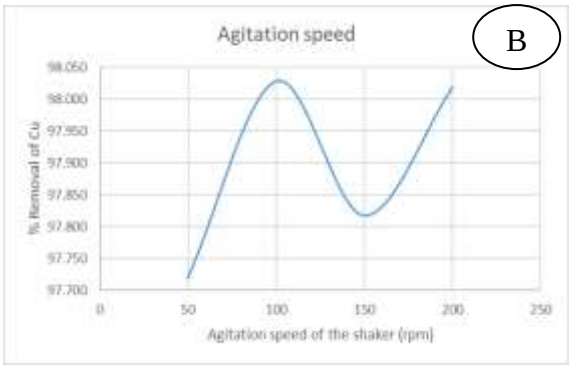

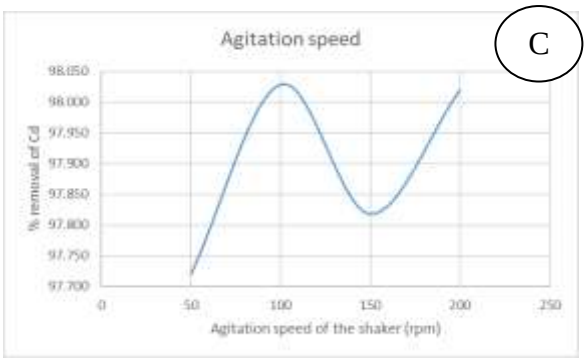

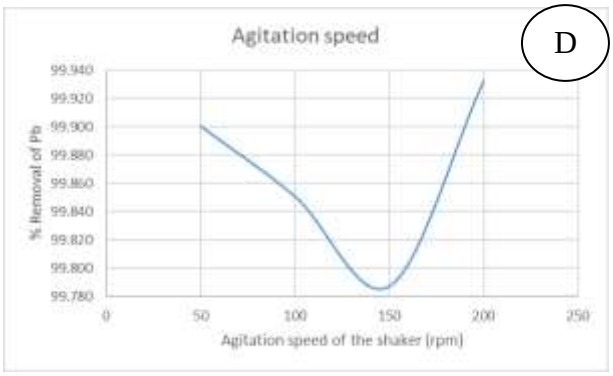

Figure 34: Effect of agitation speed of the shaker on adsorption of (A): Zn, (B): Cu, (C): Cd and (D): Pb metals

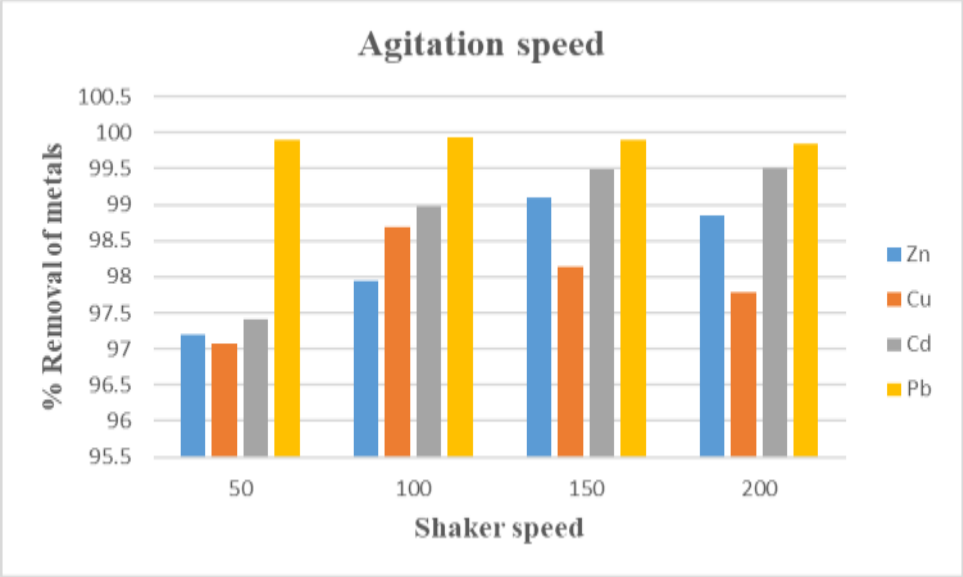

Figure 35: Effect of shaker speed on adsorption of heavy metals

4.5.4 Removal efficiencies of calcined clay silicates

Clay is a very important mineral due to its surface properties and reactivity and is very important for many industrial applications and environmental control. The removal of heavy metals using calcined clay produced an effective elimination from water. The calcined clay silicates removal of the selected heavy metals was increased in the order of Pb^{2+} > Cu^{2+} > Zn^{2+} > Cd^{2+} as can be seen in the Figures 36 (A-D) and Figure 37. For the adsorption of cations from solution, there is a general order of chemical affinity. Usually, the monovalent cations (such as Na^{+} and K^{+}) have a weaker affinity for adsorption than the divalent cations (such as Mg^{2+} and Ca^{2+}). The cations with the shortest hydrated ionic radii have, nonetheless, the strongest adsorption affinity among cations of the same charge (Huggett, 2004). This may be the cause of the various affinities of the heavy metals we chose in our scenario. This is consistent with the literature on the relative affinity of different clay minerals for the same divalent cations (Churchman *et al.*, 2006). The raw data for % elimination of the selected heavy metals using calcined clay dosage are attached in appendix D.

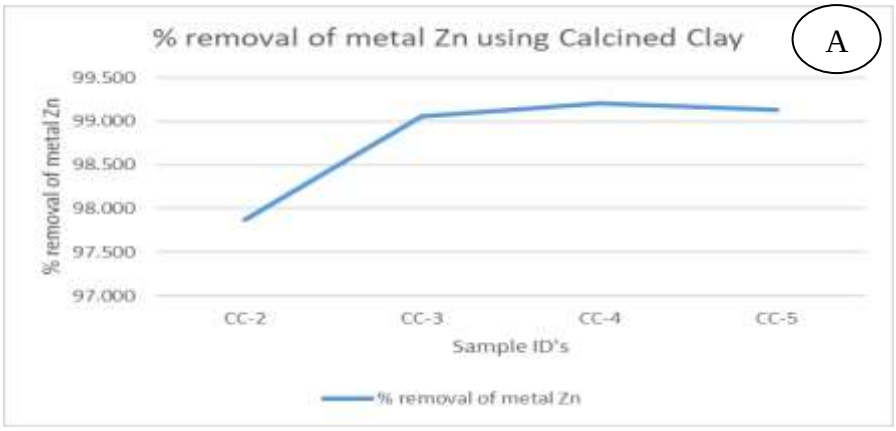
% removal of metal Zn using Calcined Clay
A
99.500
99.000
98.500
98.000
97.500
97.000
% removal of metal Zn
CC-2
CC-3
CC-4
CC-5
Sample ID's
% removal of metal Zn

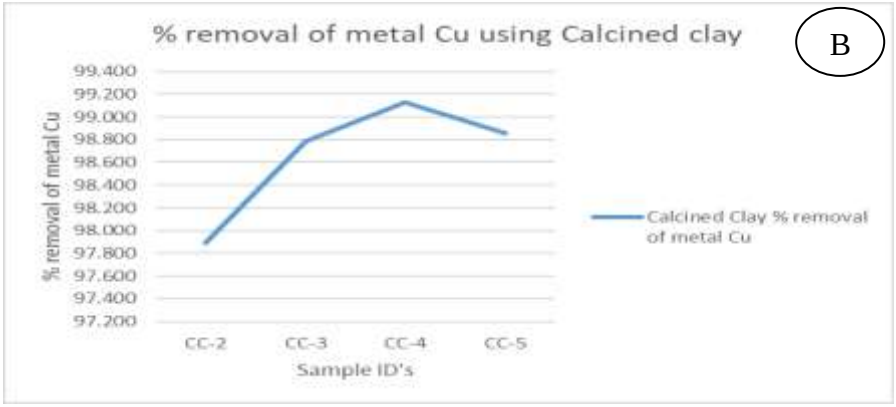
% removal of metal Cu using Calcined clay
B
99.400
99.200
99.000
98.800
98.600
98.400
98.200
98.000
97.800
97.600
97.400
97.200
% removal of metal Cu
CC-2
CC-3
CC-4
CC-5
Sample ID's
Calcined Clay % removal of metal Cu

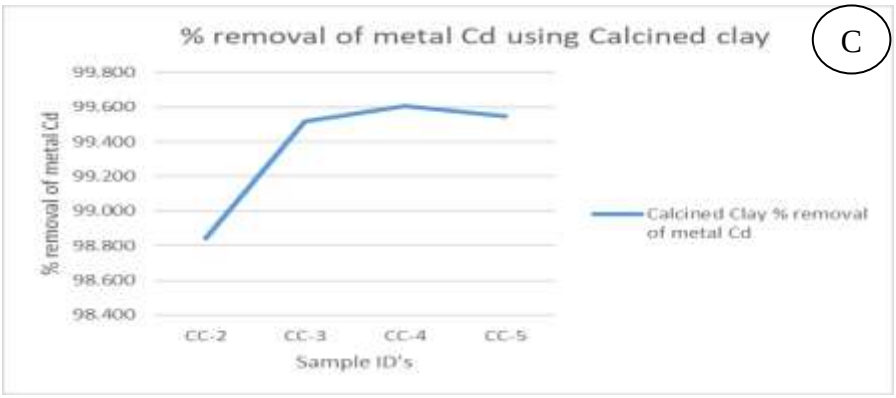
% removal of metal Cd using Calcined clay
C
99.800
99.600
99.400
99.200
99.000
98.800
98.600
98.400
% removal of metal Cd
CC-2
CC-3
CC-4
CC-5
Sample ID's
Calcined Clay % removal of metal Cd

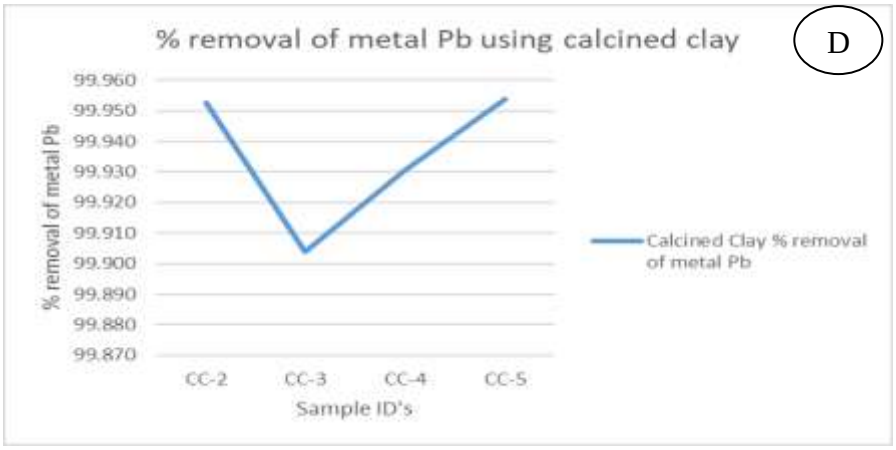

Figure 36: Removal efficacy of calcined clay on: (A): Zn, (B): Cu, (C): Cd, and (D): Pb metals

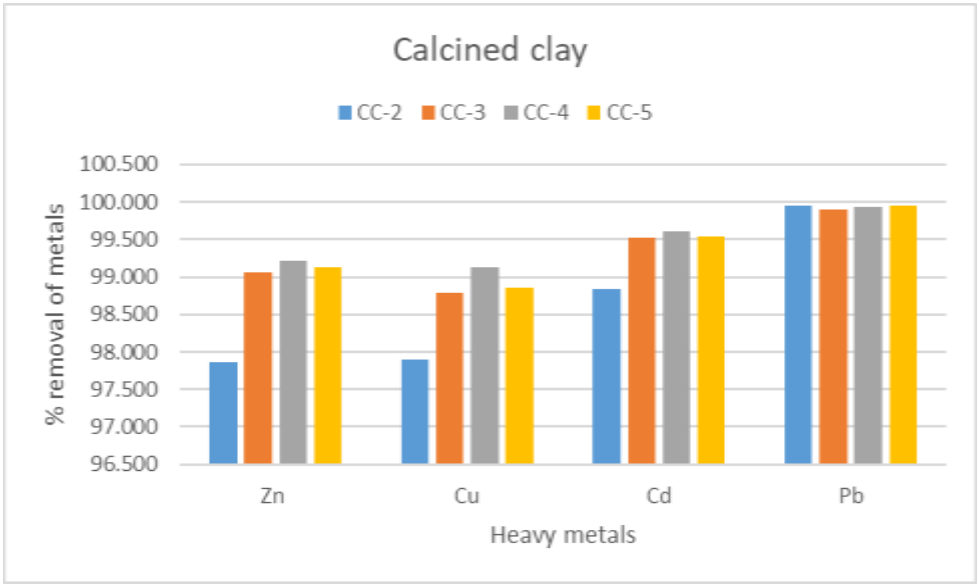

Figure 37: Removal efficiency of calcined clay for selected heavy metals

4.5.5 Removal efficiencies of biochar material

The thermal breakdown of organic compounds at temperatures between 350 and 700 ^{o} C in the absence of oxygen (O_2) results in biochar, which has potential as an adsorption material. Activated carbon, complexing agents, as well as ion-exchange membranes, all of which are costly materials used for the removal of heavy metals from polluted water, will be utilized less often if biochar is used as a substitute. The *Prosopis* biochar material produced the best

removal efficiency as compared with the other synthesized materials with the removal of the selected heavy metals in the order of Pb > Cd > Zn > and Cu as shown in Figures 38 (A-D) and Figure 39. Biochar are have mesoporous structure, which results in a high surface area, the presence of several functional groups, and a low ash content make them excellent and effective adsorbents. Raw data for percentage elimination of the particular heavy metals by different biochar dosage are attached in appendix E.

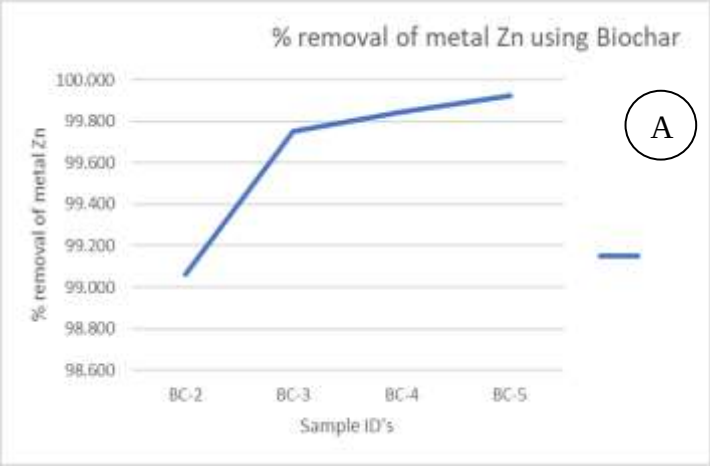

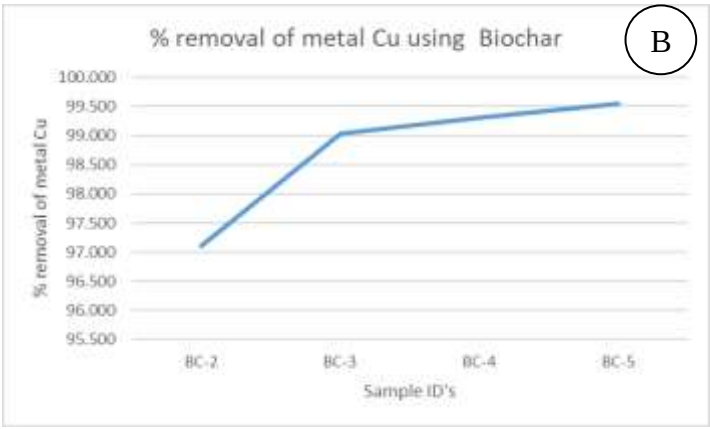

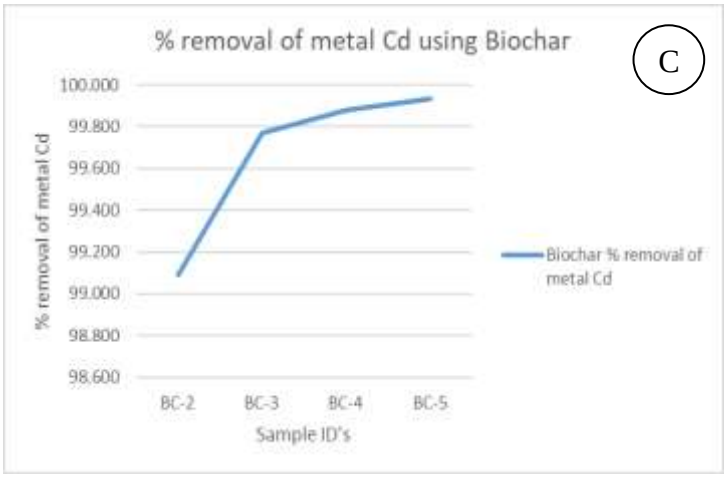

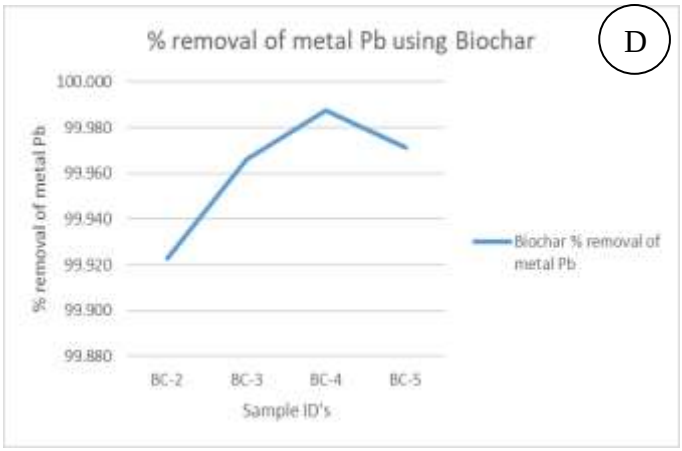

Figure 38: Removal efficacy of biochar clay on: (A): Zn, (B): Cu, (C): Cd, and (D): Pb metals

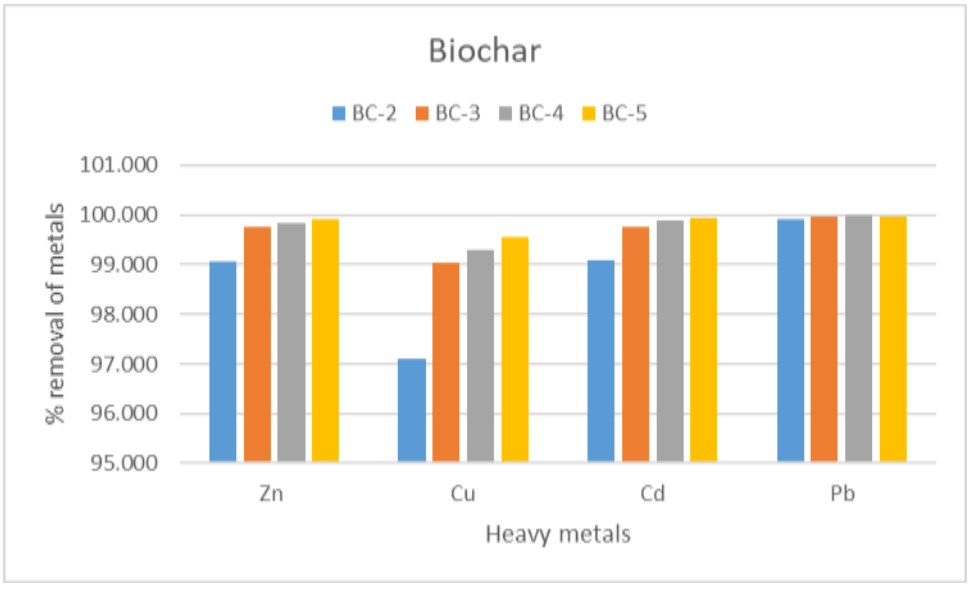

Figure 39: Removal efficiency of biochar for selected Heavy metals

4.5.6 Removal efficiencies of the nanocomposite material

Composite materials are materials that are made of modified material surfaces by either coating or re-engineering the material to increase the adsorption capacity. Modified biochar-clay composite had been used to remove methylene blue (MB) from aqueous solution and produced good results as reported by Yao *et al.,* (2014). The removal effectiveness of the nanocomposite material increased in the order of Pb^{2+} > Cd^{2+} > Zn^{2+} and Cu^{2+} for selected heavy metals as shown in Figures 40 (A-D) and Figure 41. The raw data for % removal of composite material dosage of the selected heavy metals are attached in appendix F.

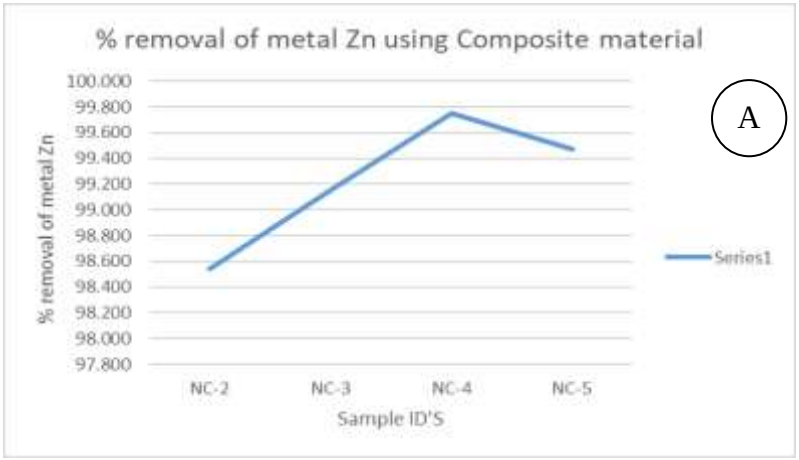

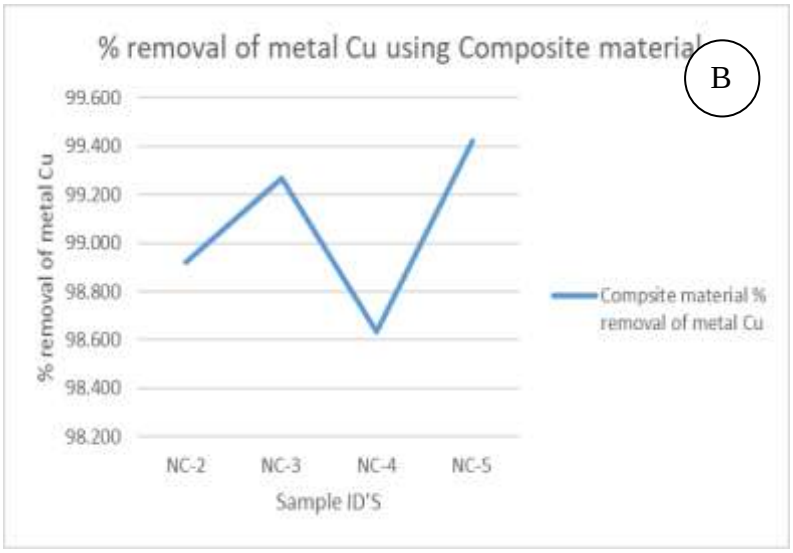

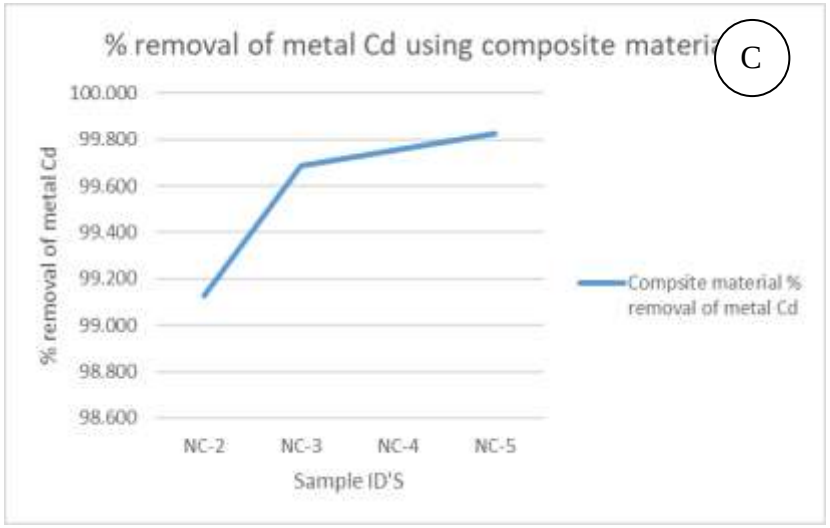

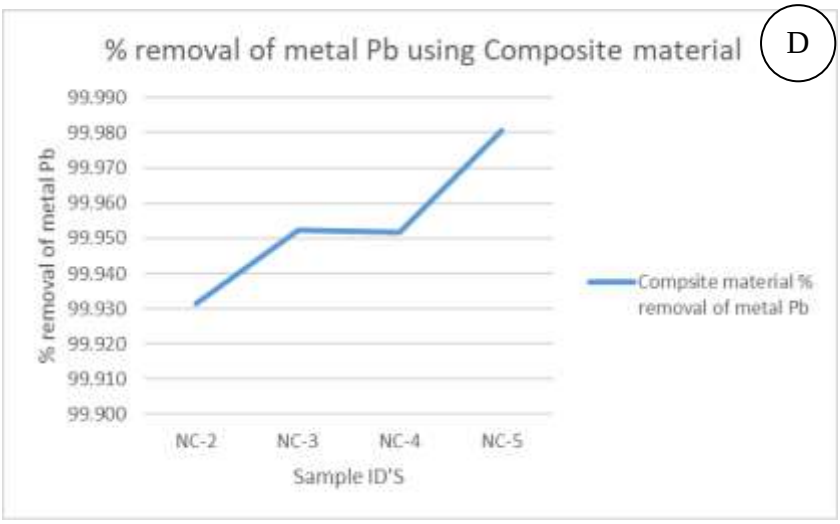

Figure 40: Removal efficacy of composite material on: (A): Zn, (B): Cu, (C): Cd, and (D): Pb metals

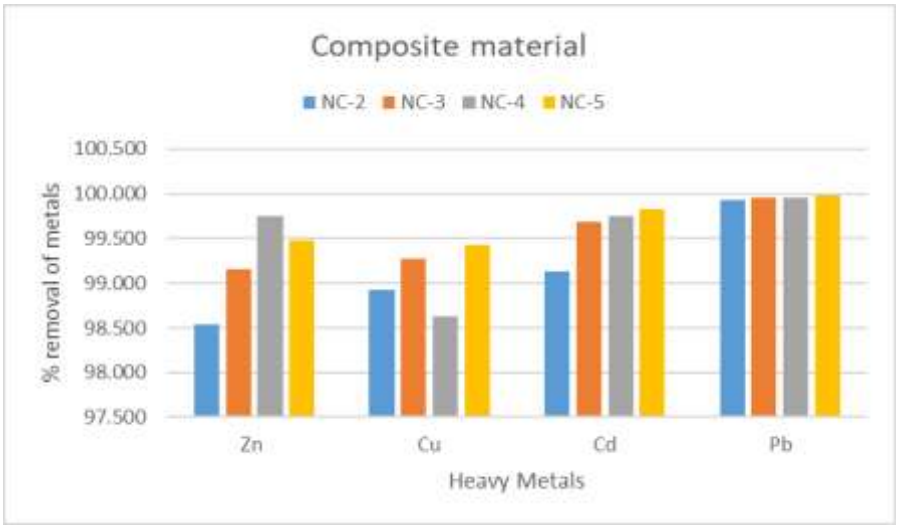

Figure 41: Removal efficiency of composite material for selected heavy metals

The material used in the adsorption batch experiments were three namely: calcined clay, biochar, and nanocomposite of biochar and clay silicates. All the materials produced high efficiencies of greater than 99 % but biochar material had the highest efficacy removal of all the heavy metals. However, it was evident from the results that the dosage increase of the materials increased the percentage removal efficiency of heavy metals in water. The dosage load reached saturation and in all the materials it was seen that removal of further metal from the water was constant and the curve gave a straight line. Figure 42 shows the summarized results of removal efficiency of different synthesized materials and illustrates that biochar material has on average revealed a better removal of the selected heavy metals.

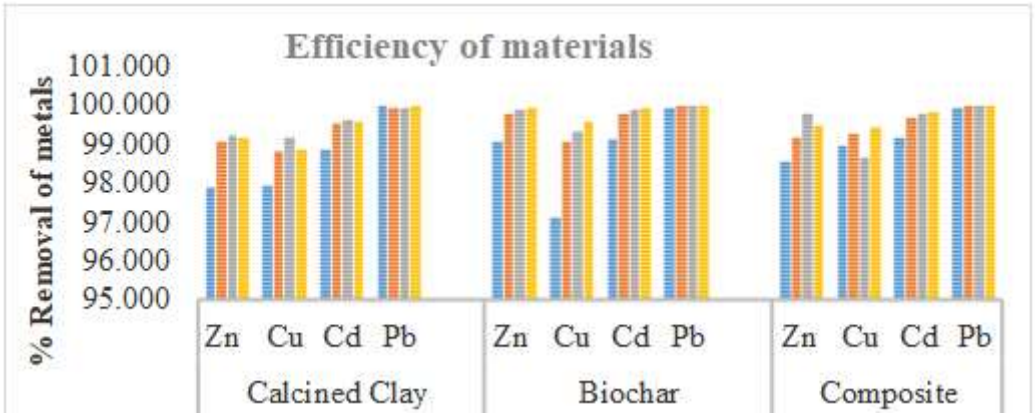

Figure 42: Removal efficiency of the synthesized materials for heavy metals

4.6 Freundlich and Langmuir isotherms

Adsorption isotherms are a methodology that can be employed to investigate adsorption. The explanations for how the adsorbate materials disperse in the liquid and solid phases are based on mathematical models (Crittenden, 2012). In studies on the adsorption of metals, the Freundlich and Langmuir isotherms are the two models that are most frequently utilized..

With the use of the synthesized materials and the experimental methodology and adsorption analysis techniques described in section 3.10, Freundlich and Langmuir isotherms for each metal solution were generated (Calcined clay, biochar, and composite material of clay

silicates and biochar). Chen *et.al*, (2015), had established that every metal is distinctive and that different types of synthesized materials follow different isotherms.

Figures 43–45 show the best-fit isotherm models for each metal in comparison to the synthesized materials. The best-fit model was created using the least-squares method, and the simulation with the greatest R2 value was selected. In order to show a relationship in the data, results above 0.500 were deemed sufficient, while values above 0.800 were more desirable.

4.6.1 Freundlich isotherms for calcined clay, biochar, and composite material for Zn, Cu, Cd and Pb

For calcined clay, removal of zinc, cadmium, and copper fit in the Freundlich isotherm with R^2 of 0.66, 0.6325, and 0.5655 respectively. Lead metal produced a poor fit with R^2 of 0.0233. Lead removal with biochar material had the best fit of 0.9978 while cadmium, copper, and zinc had 0.6908, 0.6727, and 0.6251 respectively. The removal of heavy metal ions using composite material gave the best fit with all the four metals in decreasing order of zinc > copper > cadmium > lead with R^2 of 0.9525, 0.9299, 0.9239, and 0.7236 respectively. Figures 43-46 is for Freundlich isotherm for calcined clay, Figures 47-50 is for Freundlich isotherm for biochar, while Figures 51-54 is for Freundlich isotherm for composite material for the selected heavy metal adsorptions. The raw data of Freundlich isotherms for calcined clay, biochar, and composite material for the selected heavy metals are attached in appendices G, H and I respectively.

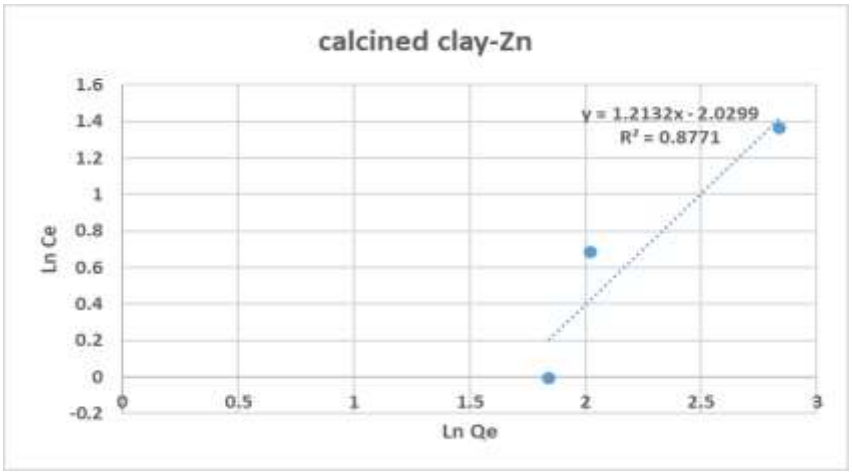

Figure 43: Freundlich isotherms for calcined clay demonstrating trends in zinc adsorption

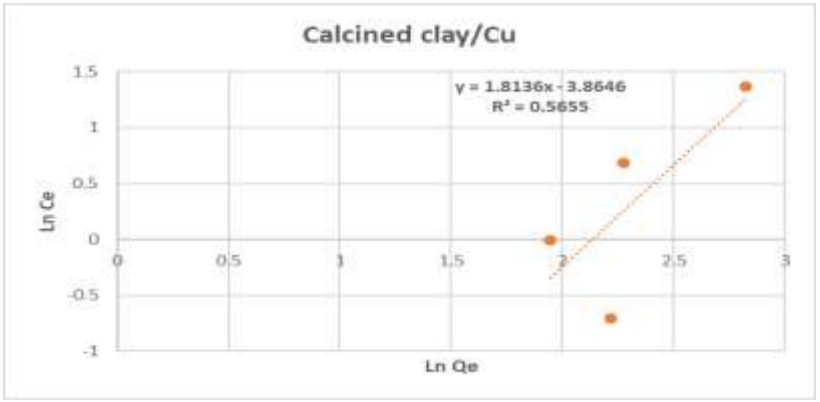

Figure 44: Freundlich isotherms for calcined clay demonstrating trends in copper adsorption

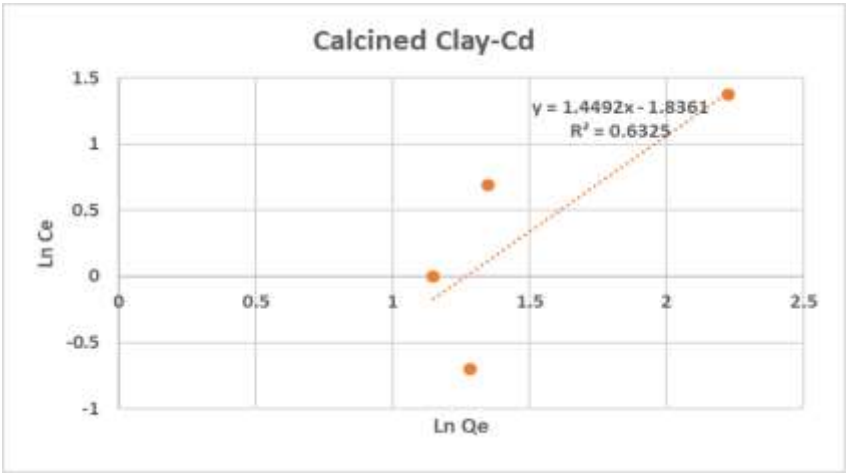

Figure 45: Freundlich isotherms for calcined clay demonstrating trends in cadmium adsorption

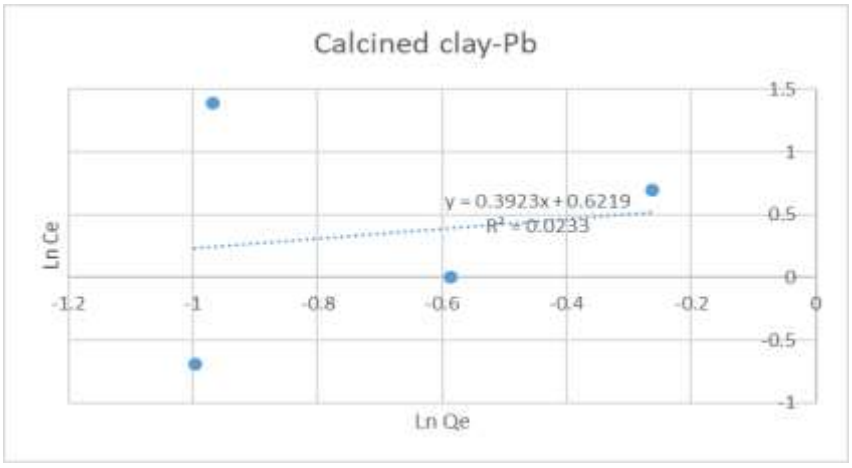

Figure 46: Freundlich isotherms for calcined clay demonstrating trends in lead adsorption

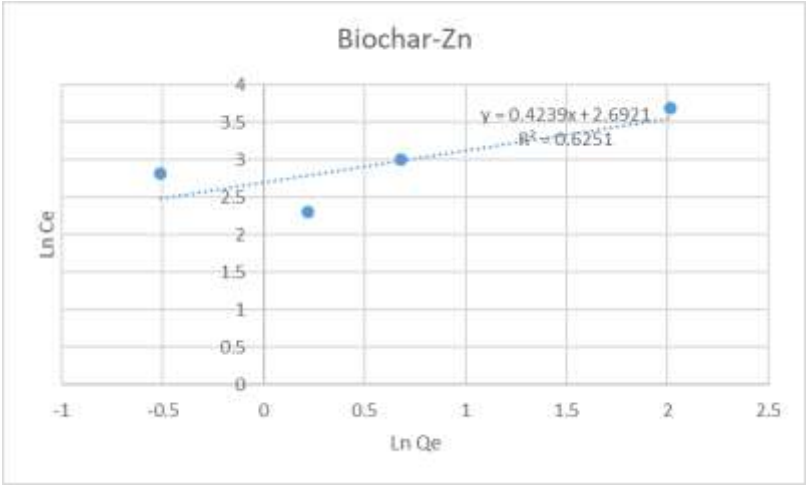

Figure 47: Freundlich isotherms for biochar demonstrating trends in zinc adsorption

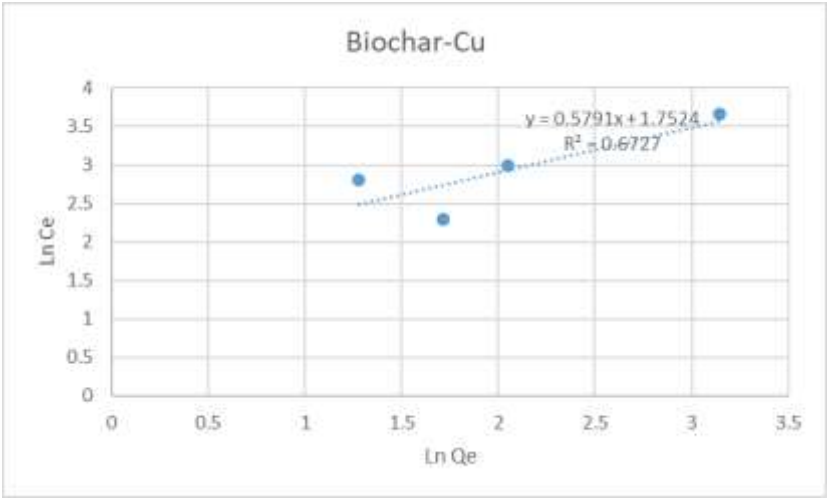

Figure 48: Freundlich isotherms for biochar demonstrating trends in copper adsorption

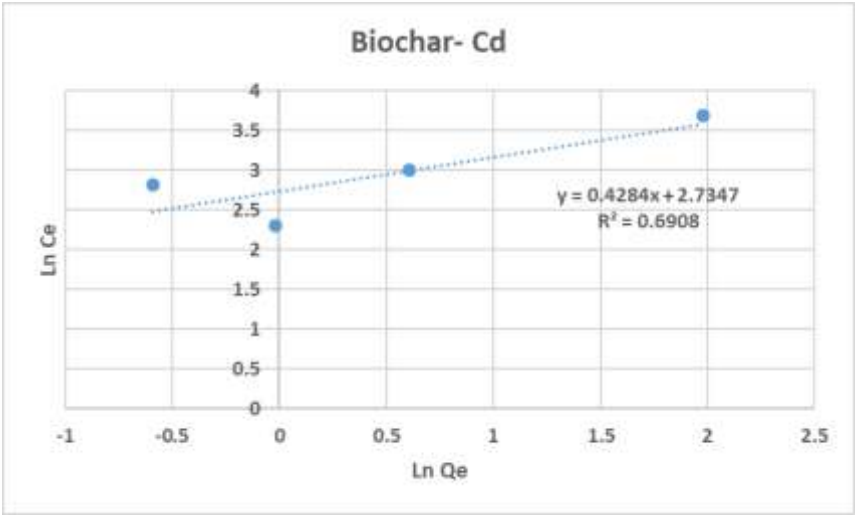

Figure 49: Freundlich isotherms for biochar demonstrating trends in cadmium adsorption

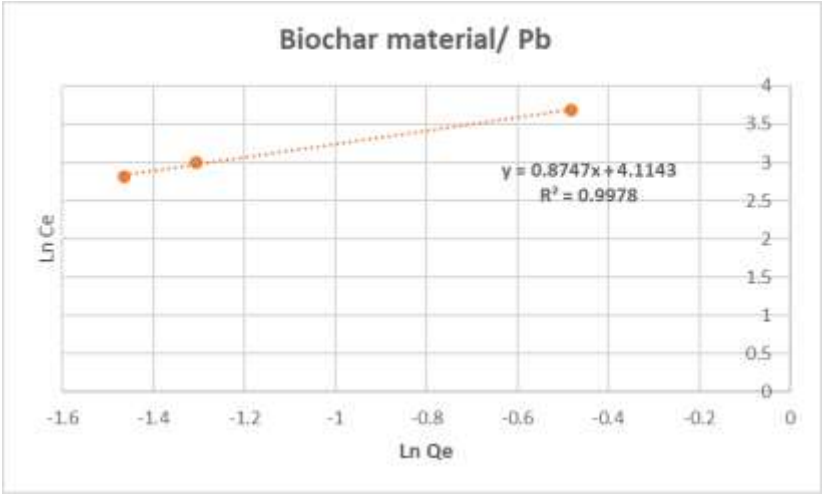

Figure 50: Freundlich isotherms for biochar demonstrating trends in lead adsorption

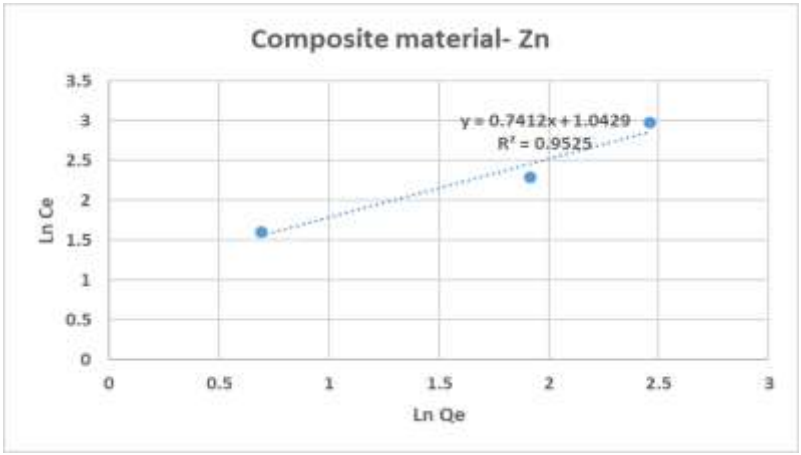

Figure 51: Composite material's Freundlich isotherm showing zinc adsorption trends

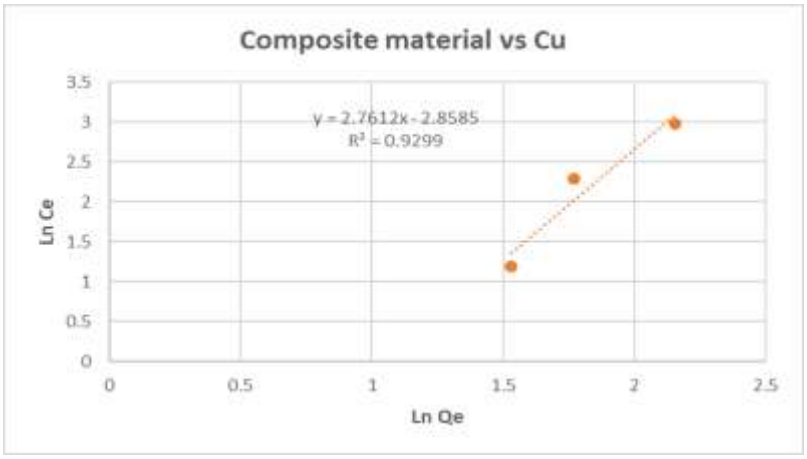

Figure 52: Composite material's Freundlich isotherm showing copper adsorption trends

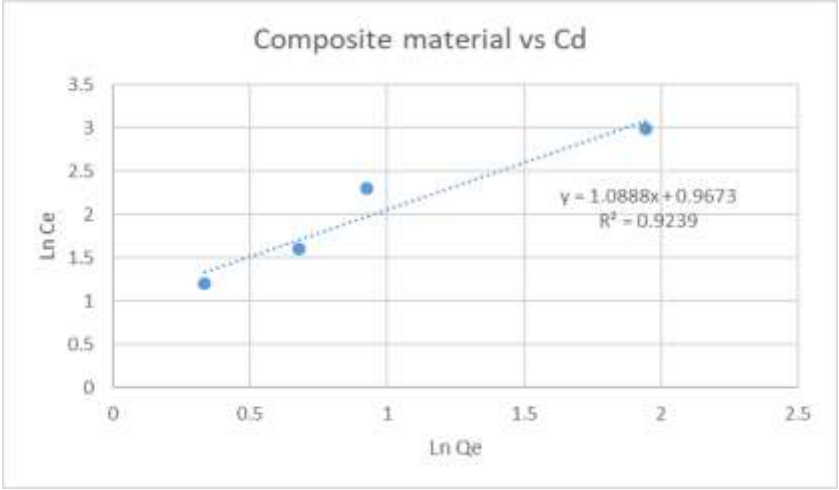

Figure 53: Composite material's Freundlich isotherm showing cadmium adsorption trends

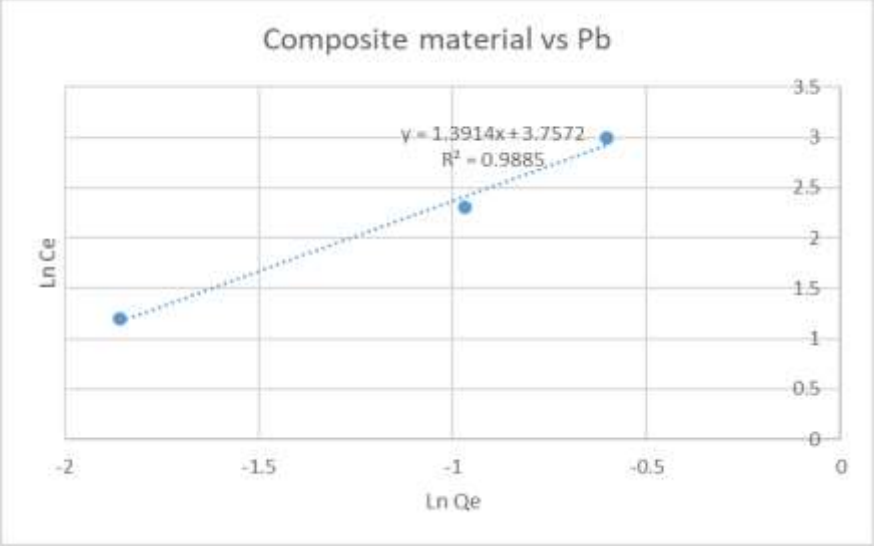

Figure 54: Composite material's Freundlich isotherm showing lead adsorption trends

The constants of n and K of Freundlich isotherms calculated from both slopes and intercept of the graphs above for calcined clay, biochar and composite material are summarised in tables 11 and 12.

K indicates the adsorption capacity of the material while n indicates the intensity of adsorption. For n values biochar gave the highest intensity of adsorption on average for the selected heavy metals while for K values also biochar had the highest values on average for the selected heavy metals followed by composite material and then calcined clay. As reported for copper removal using limestone adsorbents, n values of 2-10 were described as good adsorption, and n values of copper adsorption were 1.58, and copper efficiency of removal was high (Khayyun & Mseer, 2019).

Table 11: Freundlich isotherms constant (n) for calcined clay, biochar and composite materials for selected heavy metals

	Zn	**Cu**	**Cd**	**Pb**
	n	**n**	**n**	**n**
Calcined Clay	0.824	0.551	0.690	2.549
Biochar	2.359	1.727	2.334	1.143
Composite	1.349	0.362	0.918	0.719

Table 12: Freundlich isotherms constant (K) for calcined clay, biochar and composite materials for selected heavy metals

	Zn	**Cu**	**Cd**	**Pb**
	K	**K**	**K**	**K**
Calcined Clay	0.131	0.021	0.159	1.862
Biochar	14.763	5.768	1.995	61.209
Composite	2.837	0.057	2.631	42.828

4.6.2 Langmuir isotherms for calcined clay, biochar, and composite material for Zn, Cu, Cd, and Pb

Calcined clay with Langmuir isotherm adsorption gave the best fit as seen with lead and copper with an R^2 of 0.9995 and 0.9534 respectively, followed closely by cadmium and zinc with R^2 of 0.8127 and 0.801 respectively. For biochar material, all the Langmuir adsorption isotherms that satisfied the criteria were preferred with R^2 greater than 0.500. Lead and zinc metals had R^2 of 0.9732, and 0.9356 while copper and cadmium had 0.8465 and 0.7435 respectively. In the composite material, the metals produced the best fit for Langmuir adsorption isotherm with lead, zinc, cadmium, and copper showing R^2 of 0.9994, 0.9616, 0.9318, and 0.8588 respectively. Figures 55-58 is for Langmuir isotherms for biochar, figures 59-62 is for Langmuir isotherms for calcined clay, while Figures 63-66 is for Langmuir isotherms for composite material for the selected heavy metal adsorptions. The raw data Langmuir isotherms for calcined clay, biochar, and composite material for the selected heavy metals are attached in appendices J, K and L respectively.

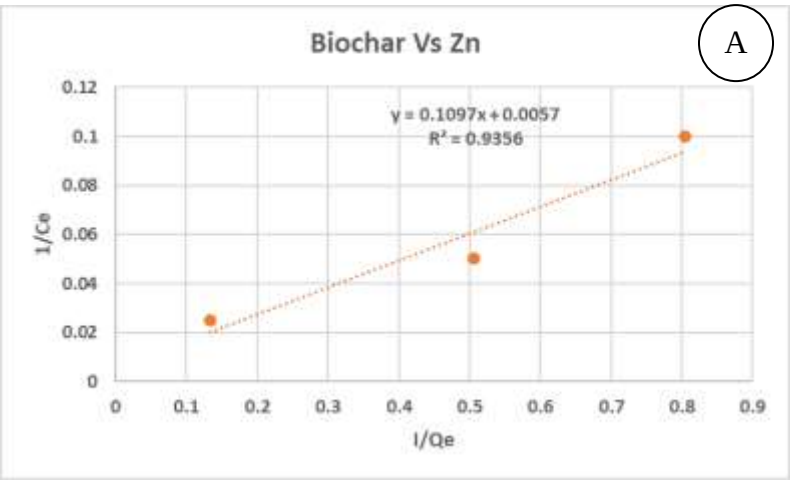

Figure 55: Langmuir isotherms for biochar demonstrating trends in zinc adsorption

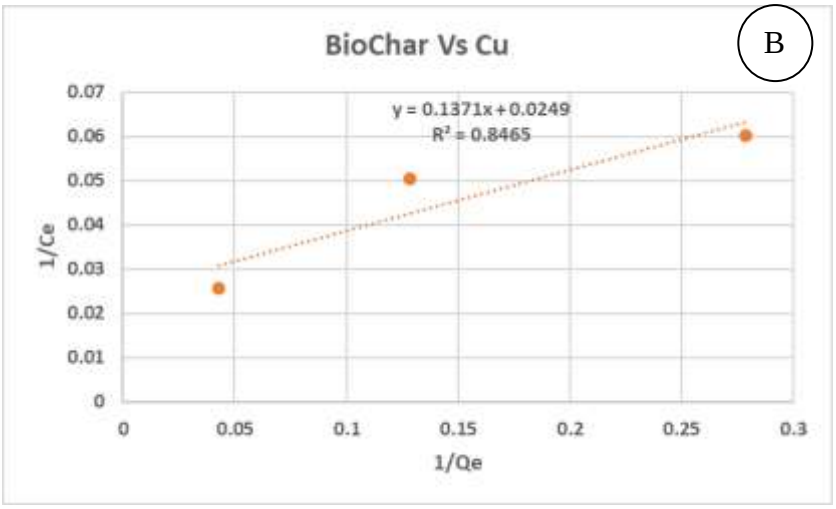

Figure 56: Langmuir isotherms for biochar demonstrating trends in copper adsorption

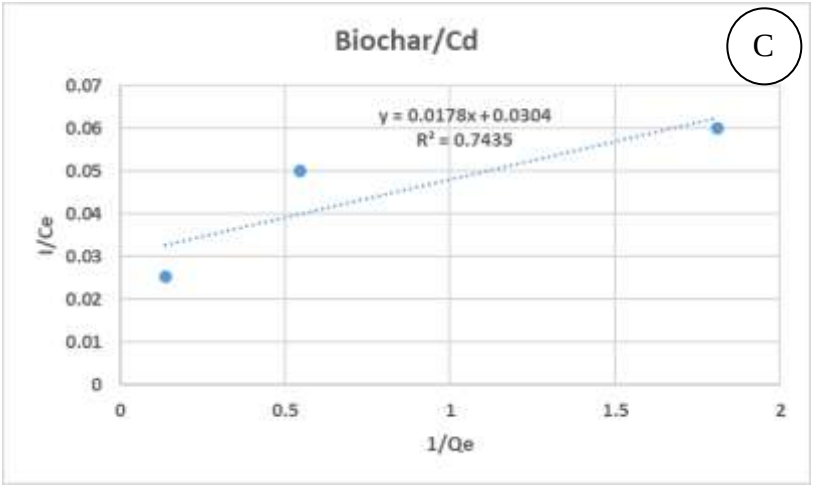

Figure 57: Langmuir isotherms for Biochar demonstrating trends in cadmium adsorption

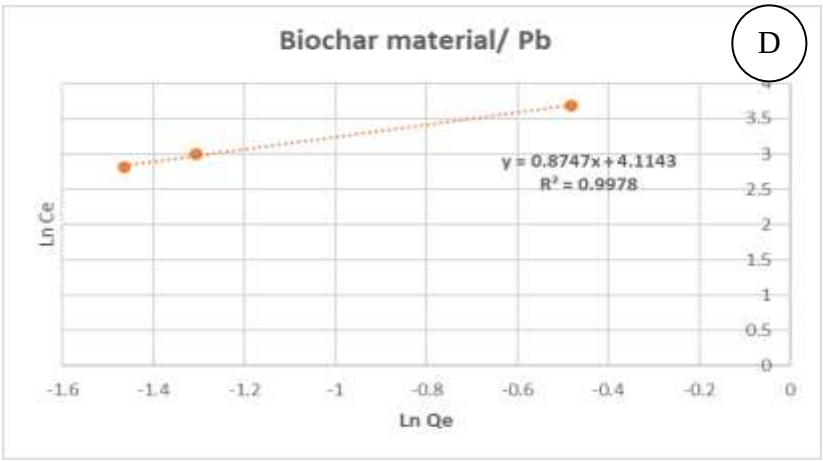

Figure 58: Langmuir isotherms for Biochar demonstrating trends in lead adsorption

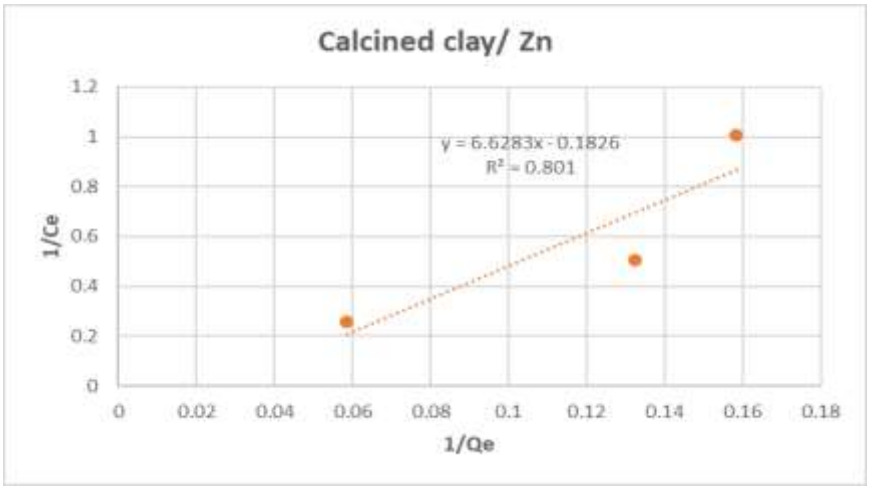

Figure 59: Langmuir isotherms for calcined clay demonstrating trends in zinc adsorption

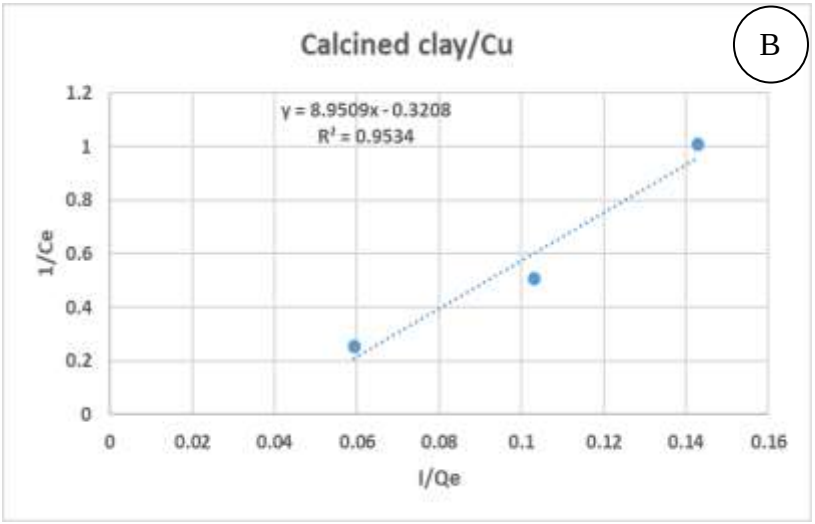

Figure 60: Langmuir isotherms for calcined clay demonstrating trends in copper adsorption

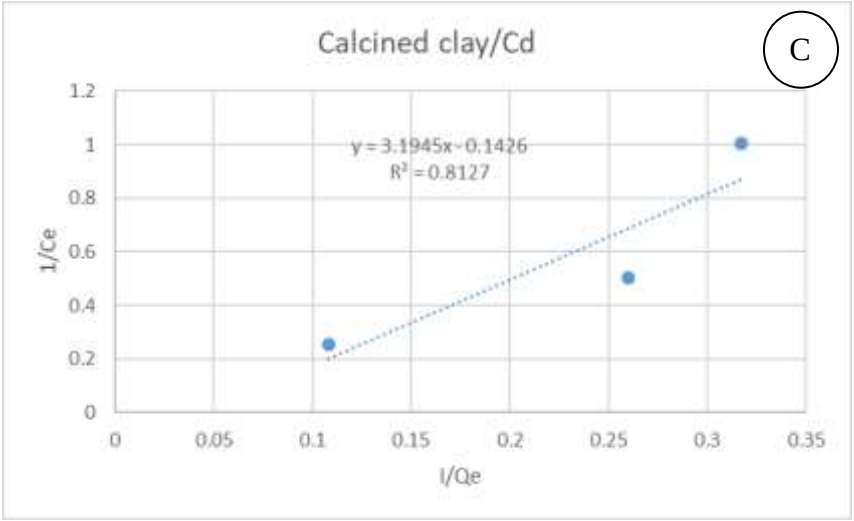

Figure 61: Langmuir isotherms for calcined clay demonstrating trends in cadmium adsorption

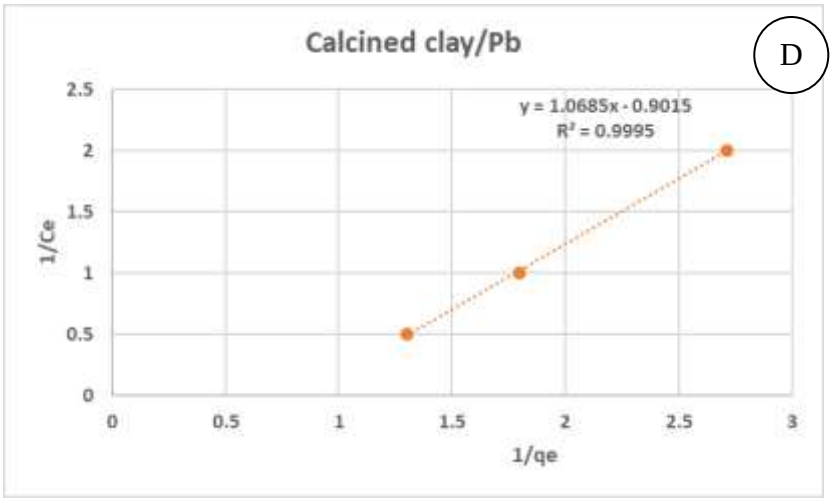

Figure 62: Langmuir isotherms for calcined clay demonstrating trends in lead adsorption

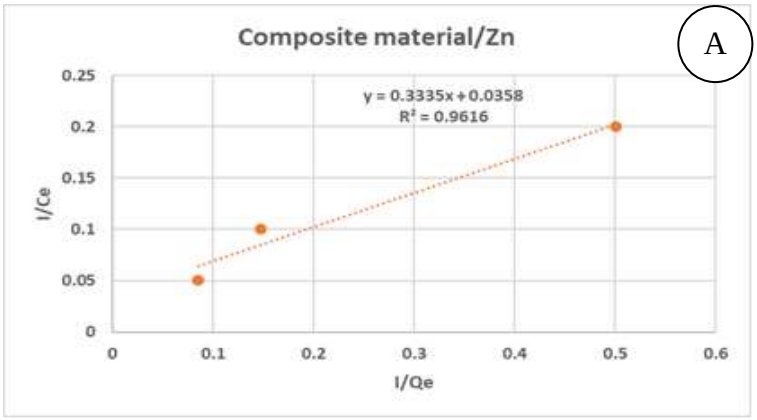

Figure 63: Composite material's Langmuir isotherm showing zinc adsorption trends

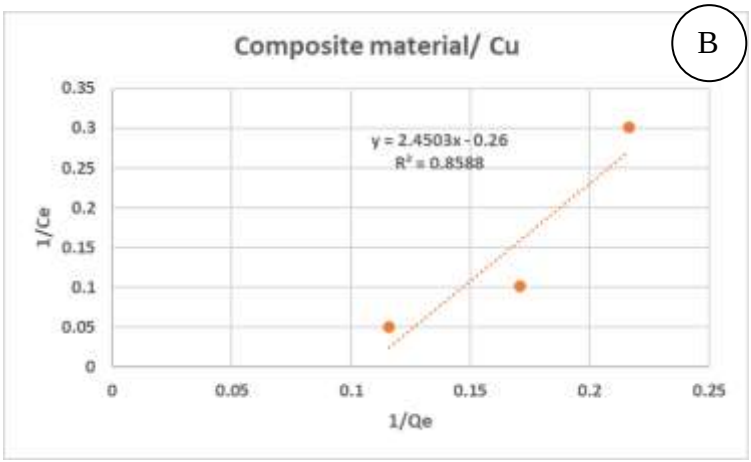

Figure 64: Composite material's Langmuir isotherm showing copper adsorption trends

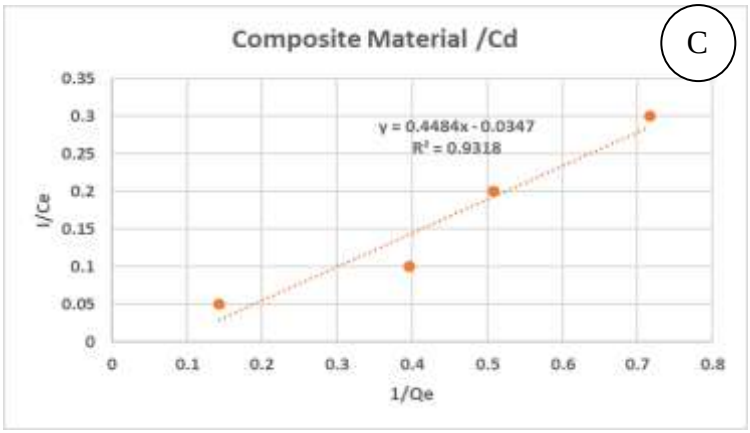

Figure 65: Composite material's Langmuir isotherm showing cadmium adsorption trends

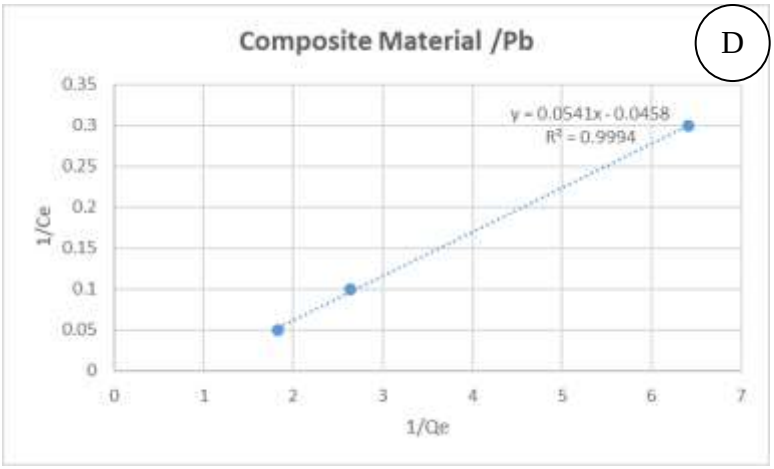

Figure 66: Composite material's Langmuir isotherm showing lead adsorption trends

The constants of q_m and K_L of Langmuir isotherms calculated from both slopes and intercept of the graphs above for calcined clay, biochar and composite material are summarised in tables 13 and 14. The Langmuir constant (K) describes the extent of interaction between the adsorbent and the surface of the material. A large K value shows a strong interaction between the adsorbent and material surface, and a small value indicates a weak interaction. While The q_m describes the maximum amount of material per unit mass of adsorbent to form a complete monomolecular layer on the surface (Khayyun & Mseer, 2019). Biochar produced better values of K_L and q_m as compared to calcined clay and composite material.

Table 13: Langmuir isotherm constant (q_m) for calcined clay, biochar and composite materials for selected heavy metals

	Zn	**Cu**	**Cd**	**Pb**
	q_m	**q_m**	**q_m**	**q_m**
Calcined Clay	0.151	0.112	0.313	0.936
Biochar	9.116	7.294	561.798	1.143
Composite	2.999	0.408	2.230	18.484

Table 14: Langmuir isotherm constant (K_L) for calcined clay, biochar and composite materials for selected heavy metals

	Zn	**Cu**	**Cd**	**Pb**
	K_L	**K_L**	**K_L**	**K_L**
Calcined Clay	-36.30	-27.90	-22.40	-1.19
Biochar	19.25	5.51	0.06	0.21
Bomposite	9.32	-9.42	-1.29	-1.18

4.7 Kinetic models and order of reactions

According to the kinetic experiments, the second-order kinetic pseudo-model better fits the data than the first-order pseudo-model. In contrast to the first-order pseudo model, the second-order pseudo provided straight-line fits. The rate constant for the second-order experiment was determined using the slope and y-intercept from the linear regression. A time vs. t/qt linear plot is used to demonstrate the pseudo-second-order kinetics model, and Figures 67 (A-D) provide a summary of the obtained parameters. From the correlation coefficient (R^2), which provides validation points for model comparisons, the value of R^2 is close to 1, making it the most suitable model to choose from.

Rate constants for zinc, copper, cadmium, and lead in a mixed solution are shown in tables 15-18. The raw data can be seen in appendix M

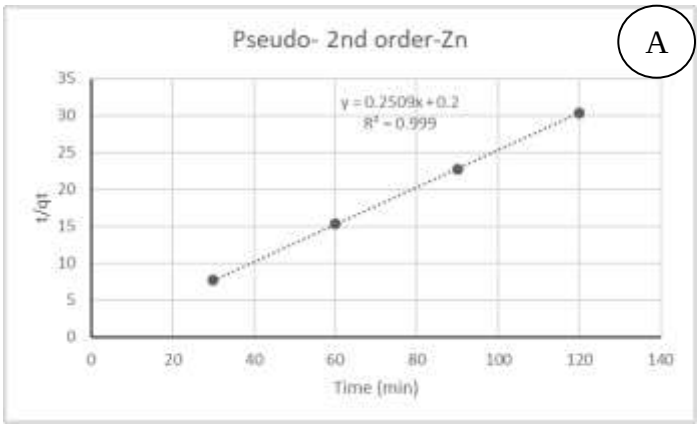

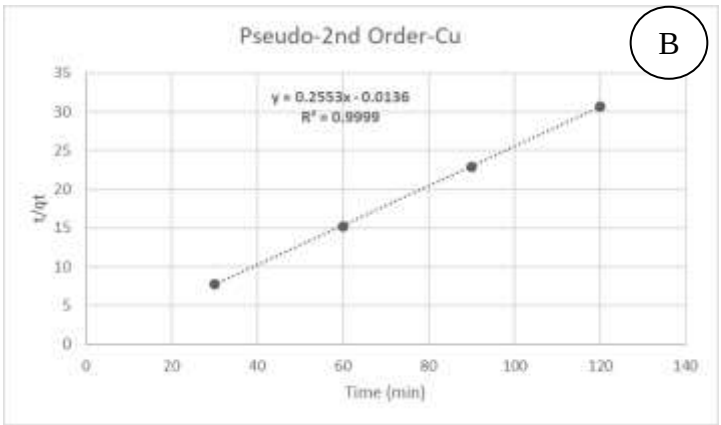

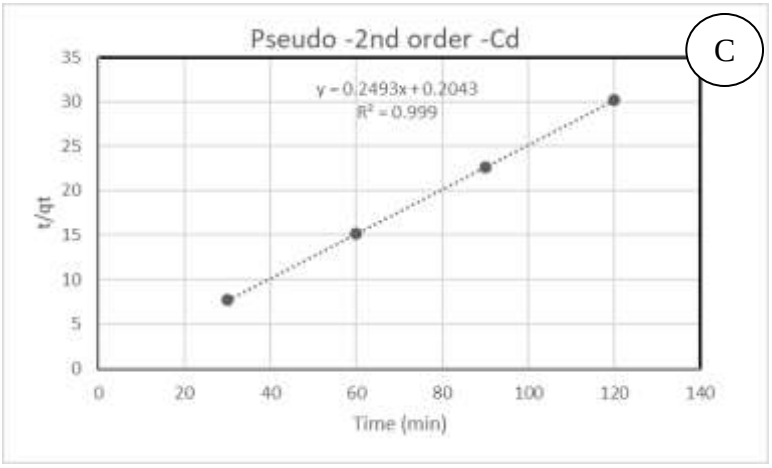

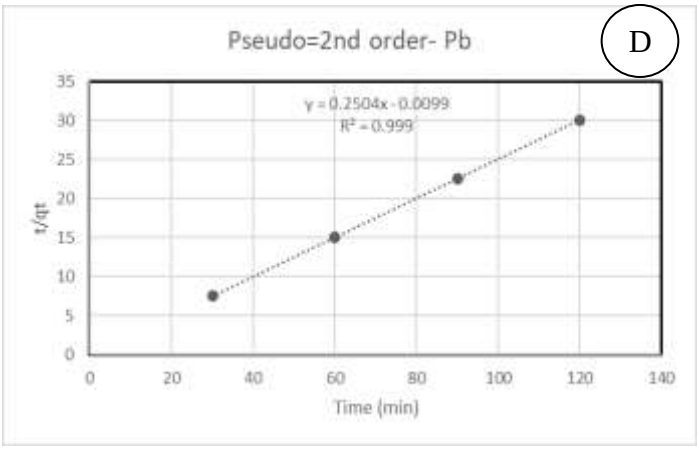

Figure 67 (A-D): Pseudo second order plot of Zinc (A), copper (B), cadmium (C), and lead(D) metals

Table 15: Pseudo second order rate constants for zinc removal using calcined clay

Intercept	Slope	q_e (mg/g)	q_e^2	K2	R^2
0.2	0.2509	3.990	15.92	0.3141	0.999

Table 16: Pseudo second order rate constants for copper removal using calcined clay

Intercept	Slope	q_e (mg/g)	q_e^2	K2	R^2
-0.01	0.2553	3.917	15.34	-6.518	0.999

Table 17: Pseudo second order rate constants for cadmium removal using calcined clay

Intercept	Slope	q_e (mg/g)	q_e^2	K2	R^2
0.2	0.2493	4.011	16.09	0.311	0.999

Table 18 : Pseudo second order rate constants for lead removal using calcined clay

Intercept	Slope	q_e (mg/g)	q_e^2	K2	R^2
-0.009	0.250	3.994	15.95	-6.967	0.999

CHAPTER FIVE

CONCLUSION AND RECOMMENDATIONS

5.1 Conclusions

Clay is an important material in the earth's crust, with vital minerals and elemental composition. The use of clay or modified clay for environmental pollution prevention and control has been there ever since humans have existed. Clays are valuable for this purpose because of their features, including charge, absorption capacity, big surface area, colloids, and swelling capacity, that give them an edge over other materials for pollution prevention and restoration. Its widespread availability also makes it attractive for mining and less costly.

Elemental analysis, surface morphology, and phase analysis were performed on clay silicate samples collected from Mukurweini in Nyeri County using XRF/EDX, FTIR, FESEM, FETEM, and XRD tools and techniques. For elemental analysis, calcined clay was found to be composed of 32.4 % Al_2O_3, 55.0 % SiO_2, 6 % Fe, and <3 % K_2O, CaO, and P_2O_5. Extracted clay silicates gave 5.1 % Al_2O_3, 83.6% $NaSiO_3$, 5% K_20 and < 3 % CaO, Fe, and P_2O_5. These results showed that there was a considerable increase in silicates yield synthesized after extraction with NaOH base as compared to original clay. The surface morphology of the synthesized clay silicates showed agglomerated spherical shape with an average diameter size of 80-90 nm using FESEM and FETEM techniques. Phase analysis using XRD depicted a $2\theta=30^o$ with sharp intense peaks which are usually related with sodium silicates. In general, 20% NaOH (w/v %) extraction yielded better results than 40% NaOH (w/v %) extraction, indicating that silica extraction percentage decreased as base concentration increased.

Elemental analysis of the biochar showed that it was mainly composed of 62.5% carbon, and 21.1% oxygen. In accordance with the majority of biochars reported in the literature, the

FTIR spectra revealed bands at 3500 cm^{-1} that were associated to O-H stretching, 2350 cm^{-1} bands ascribed to O=C=O absorption peak, and 1600 cm^{-1} bands attributed to carboxylate (-COO-) and primary(1^o) Amine (-N-H) bending. (Shahid, *et al.,* 2018). Phase characterization of biochar material depicted a large hump on the XRD spectrum between 11-13^o and is attributed to cellulose content in biochar. A narrow sharp peak at a $2\theta = 30^o$ is ascribed to carbon on the XRD spectrum which is what is reported in the literature.

Morphological surface characterization of the biochar the images revealed particles of different sizes with vascular features packed in rolls with comparatively flat surfaces as is reported in literature for biochar material. For the composite material elemental analysis revealed a high content of carbon, oxygen, silica, aluminium and iron. These contents are attributed to biochar and clay material that formed the composite material.

FTIR analysis further showed a broad peak at approximately 3645cm^{-1}, a peak at 2345cm^{-1} and a peak 1063 cm^{-1} attributed to O-H stretching, O=C=O absorption and –C-O stretching vibration respectively. This is a confirmation of a successful impregnation of clay silicates on the surfaces of the biochar material took place. XRD spectrum showed the existence of three strong peaks at 19.9^o, 25^o, and 35^o attributed to phyllosilicates from the clay and a small peak at 30^o ascribed to carbon which confirms the successful impregnation process to form the composite material. Using the FESEM-EDX technique to ascertain the morphology of the composite material, the surface analysis revealed high peaks for silica, aluminium, titanium, and iron which are elemental composition of clay. Also, presence of carbon revealed flat surfaces with vascular features packed in rolls attributed to the biochar material of the composite.

The materials used to assess the efficacy of the removal of the selected heavy metals were calcined clay, biochar and the composite material. All the synthesized materials produced

excellent adsorption efficiency of the selected heavy metals. However, biochar material had the highest efficiency removal of all the selected heavy metals. Adsorption isotherms Freundlich and Langmuir were used to assess the best fit for synthesized materials. Both isotherms gave composite material, the best fit for the experimental adsorption data. The kinetic experiments indicated pseudo-second-order reaction kinetics for of the selected heavy metals adsorption.

The community will gain from this research in a number of ways, among the benefit being the use of *Prosopis* biochar that will be a blessing to the communities it has long-term impacted as invasive species. A healthy and prosperous nation will result from the elimination of heavy metals and other contaminants from drinking water, which will also be an accomplishment for environmental rehabilitation.

5.2 Recommendations

The following are the recommendations from the research:

1. Work should be done on other clays from other counties
2. Research on biochar materials from other invasive species should be done.
3. Research on the use of other bases as extraction medium for the silicates should be undertaken.
4. Study the use of the nanocomposites synthesized for adsorption of other pollutants.
5. Investigation of alternative nanocomposite materials for removal of heavy metals should be done.

REFERENCES

Abadin, H., Ashizawa, A., Stevens, Y.-W., Llados, F., Diamond, G., Sage, G., Citra, M., Quinones, A., Bosch, S. J., & Swarts, S. G. (2020). Toxicological profile for lead. *ATSDR:Agency for Toxic Substances and Disease Registry*, *August*, 582. Http://arxiv.org/abs/1011.1669%0Ahttp://www.ncbi.nlm.nih.gov/pubmed/24049859%0Ahttps://stacks.cdc.gov/view/cdc/95222

Abdel-Raouf, N., Al-Homaidan, A. A., & Ibraheem, I. B. M. (2012). Microalgae and wastewater treatment. *Saudi Journal of Biological Sciences*, *19*(3), 257–275. Https://doi.org/10.1016/j.sjbs.2012.04.005

Abdullahi, Y., Ali, E. A., & Lawal, A. O. (2013). Roast-alkaline leaching of silica from kaolinitic clay. *ARPN Journal of Engineering and Applied Sciences*, *8*(10), 864–870.

Aditya, I. (2011). Impact of Population Growth on Environmental Degradation : Case of India Impact of Population Growth on Environmental Degradation : Case of India. *Journal of Economics and Sustainable Development*, *January 2011*.

Ahmed, F., Ali, I., Kousar, S., & Ahmed, S. (2022). The environmental impact of industrialization and foreign direct investment: empirical evidence from Asia-Pacific region. *Environmental Science and Pollution Research*, *29*(20), 29778–29792. Https://doi.org/10.1007/s11356-021-17560-w

Ahmed, R., Yamin, T., Ansari, M. S., & Hasany, S. M. (2006). Sorption behaviour of lead(II) ions from aqueous solution onto Haro river sand. *Adsorption Science and Technology*, *24*(6), 475–486. Https://doi.org/10.1260/026361706780154400

Appannagari, R. R. (2017). Environmental pollution causes and consequences: a study. North Asian International Research Journal of Social Science & Humanities, 3(8), 151-161.

Arruti, A., Fernández-Olmo, I., & Irabien, Á. (2010). Evaluation of the contribution of local sources to trace metals levels in urban PM2.5 and PM10 in the Cantabria region

(Northern Spain). *Journal of Environmental Monitoring*, *12*(7), 1451–1458. Https://doi.org/10.1039/b926740a

Barakat, M. A. (2011). New trends in removing heavy metals from industrial wastewater. *Arabian Journal of Chemistry*, *4*(4), 361–377. Https://doi.org/10.1016/j.arabjc.2010.07.019

Basta, N. T., Gradwohl, R., Snethen, K. L., & Schroder, J. L. (2001). Chemical Immobilization of Lead, Zinc, and Cadmium in Smelter-Contaminated Soils Using Biosolids and Rock Phosphate. *Journal of Environmental Quality*, *30*(4), 1222–1230. Https://doi.org/10.2134/jeq2001.3041222x

Beesley, L., & Marmiroli, M. (2011). The immobilisation and retention of soluble arsenic, cadmium and zinc by biochar. *Environmental Pollution*, *159*(2), 474–480. Https://doi.org/10.1016/j.envpol.2010.10.016

Beyersmann, D., & Hartwig, A. (2008). Carcinogenic metal compounds: Recent insight into molecular and cellular mechanisms. *Archives of Toxicology*, *82*(8), 493–512. Https://doi.org/10.1007/s00204-008-0313-y

Borchard, N., Wolf, A., Laabs, V., Aeckersberg, R., Scherer, H. W., Moeller, A., & Amelung, W. (2012). Physical activation of biochar and its meaning for soil fertility and nutrient leaching - a greenhouse experiment. *Soil Use and Management*, *28*(2), 177–184. Https://doi.org/10.1111/j.1475-2743.2012.00407.x

Briffa, J., Sinagra, E., & Blundell, R. (2020). Heavy metal pollution in the environment and their toxicological effects on humans. *Heliyon*, *6*(9), e04691. Https://doi.org/10.1016/j.heliyon.2020.e04691

Budambula, N. L. M., & Mwachiro, E. C. (2006). Metal status of Nairobi River waters and their bioaccumulation in Labeo cylindricus. *Water, Air, and Soil Pollution*, *169*(1–4), 275–291. Https://doi.org/10.1007/s11270-006-2294-x

Bunaciu, A. A., Udriştioiu, E. Gabriela, & Aboul-Enein, H. Y. (2015). X-Ray Diffraction: Instrumentation and Applications. *Critical Reviews in Analytical Chemistry*, *45*(4), 289–299. Https://doi.org/10.1080/10408347.2014.949616

Carter, D. B. W. C. B. (2009). Transmission Electron Microscopy A Textbook for Materials Science. springer publication.

Chakravarty, S., K., S., P., C., N., A., & Shukl, G. (2012). Deforestation: Causes, Effects and Control Strategies. *Global Perspectives on Sustainable Forest Management*. Https://doi.org/10.5772/33342

Charity, L. K., Wirnkor, V. A., Emeka, A. C., Isioma, A. A., Ebere, C. E., & Ngozi, V. E. (2018). Health risks of consuming untreated borehole water from Uzoubi Umuna Orlu, Imo State Nigeria. J Environ Anal Chem, 5(250), 2380-2391.

Chatterjee, R., Sajjadi, B., Chen, W. Y., Mattern, D. L., Hammer, N., Raman, V., & Dorris, A. (2020). Effect of pyrolysis temperature on physicochemical properties and acoustic-based amination of biochar for efficient CO2 adsorption. Frontiers in Energy Research, 8, 85.

Chen, G. (2004). Electrochemical technologies in wastewater treatment. *Separation and Purification Technology*, *38*(1), 11–41. Https://doi.org/10.1016/j.seppur.2003.10.006

Chen, X. (2015). Modeling of Experimental Adsorption Isotherm Data. *Information*, 14–22. Https://doi.org/10.3390/info6010014

Chen, Y., Chen, M., Li, Y., Wang, B., Chen, S., & Xu, Z. (2018). Impact of technological innovation and regulation development on e-waste toxicity: A case study of waste mobile phones. *Scientific Reports*, *8*(1), 1–9. Https://doi.org/10.1038/s41598-018-25400-0

Churchman, G. J., Gates, W. P., Theng, B. K. G., Yuan, G., Bergaya, F., & Lagaly, G. (2006). Handbook of clay science. In Clays and Clay Minerals for Pollution Control (pp.

630-633). Elsevier Ltd..

Coates, J. (2006). Interpretation of Infrared Spectra, A Practical Approach. *Encyclopedia of Analytical Chemistry*, 1–23. Https://doi.org/10.1002/9780470027318.a5606

Cumming, O., & Slaymaker, T. (Eds.). (2018). Equality in water and sanitation services. Routledge.

Duffus, J. H. (2002). "heavy metals" - A meaningless term? (IUPAC technical report). *Pure and Applied Chemistry*, *74*(5), 793–807. Https://doi.org/10.1351/pac200274050793

Elnour, A. Y., Alghyamah, A. A., Shaikh, H. M., Poulose, A. M., Al-Zahrani, S. M., Anis, A., & Al-Wabel, M. I. (2019). Effect of pyrolysis temperature on biochar microstructural evolution, physicochemical characteristics, and its influence on biochar/polypropylene composites. *Applied Sciences (Switzerland)*, *9*(6), 7–9. Https://doi.org/10.3390/app9061149

Emam, E. A. (2013). Modified Activated Carbon and Bentonite Used to Adsorb Petroleum Hydrocarbons Emulsified in Aqueous Solution. *American Journal of Environmental Protection*, *2*(6), 161. Https://doi.org/10.11648/j.ajep.20130206.17

Engwa, G. A., Ferdinand, P. U., Nwalo, F. N., & Unachukwu, M. N. (2019). Mechanism and health effects of heavy metal toxicity in humans. Poisoning in the modern world-new tricks for an old dog, 10, 70-90.

Fancello, D., Scalco, J., Medas, D., Rodeghero, E., Martucci, A., Meneghini, C., & De Giudici, G. (2019). XRD-thermal combined analyses: An approach to evaluate the potential of phytoremediation, phytomining, and biochar production. *International Journal of Environmental Research and Public Health*, *16*(11). Https://doi.org/10.3390/ijerph16111976

World Health Organization, International Atomic Energy Agency & Food and Agriculture Organization of the United Nations. (1996). Trace elements in human nutrition and

health. World Health Organization. https://apps.who.int/iris/handle/10665/37931

Fei, Y., & Hu, Y. H. (2022). Design, synthesis, and performance of adsorbents for heavy metal removal from wastewater: a review. *Journal of Materials Chemistry A*, *10*(3), 1047–1085. Https://doi.org/10.1039/d1ta06612a

Fernández-Luqueño, F., López-Valdez, F., Gamero-Melo, P., Luna-Suárez, S., Aguilera-González, E., Martínez, A., García-Guillermo, M., Hernández-Martínez, G., Herrera-Mendoza, R., Álvarez-Garza, M., & Pérez-Velázquez, I. (2013). Heavy metal pollution in drinking water - a global risk for human health: A review. *African Journal of Environmental Science and Technology*, *7*(7), 567–584. Https://doi.org/10.5897/AJEST12.197

Fu, R., Liu, Y., Lou, Z., Wang, Z., Baig, S. A., & Xu, X. (2016). Adsorptive removal of Pb(II) by magnetic activated carbon incorporated with amino groups from aqueous solutions. *Journal of the Taiwan Institute of Chemical Engineers*, *62*, 247–258. Https://doi.org/10.1016/j.jtice.2016.02.012

Gautam, P. K., Gautam, R. K., Banerjee, S., Chattopadhyaya, M. C., & Pandey, J. D. (2016). Heavy metals in the environment: fate, transport, toxicity and remediation technologies. Nova Sci Publishers, 60, 101-130.

Government of Kenya. (2006). The Environmental Management and Co- Ordination (Conservation of Biological Diversity and Resources , Access To Genetic Resources and Arrangement of Regulations Part I - Preliminary Part Ii – Conservation of Biological Part Iii – Access To Genetic Resour. *KENYA GAZETTE*, *160*, 1–18.

Government of Kenya. (2016). *Kenya gazette supplement the water act no.43 of 2016*. *164*(43), 1019.

Halim, M., Conte, P., & Piccolo, A. (2003). Potential availability of heavy metals to phytoextraction from contaminated soils induced by exogenous humic substances.

Chemosphere, *52*(1), 265–275. Https://doi.org/10.1016/S0045-6535(03)00185-1

Hans Wedepohl, K. (1995). The composition of the continental crust. *Geochimica et Cosmochimica Acta*, *59*(7), 1217–1232. Https://doi.org/10.1016/0016-7037(95)00038-2

Hodoroaba, V. D. (2019). Energy-dispersive X-ray spectroscopy (EDS). In Characterization of Nanoparticles (pp. 397-417). Elsevier.

Huggett, J. M. (2004). Clay Minerals. *Encyclopedia of Geology*, *i*, 358–365. Https://doi.org/10.1016/B0-12-369396-9/00273-2

Hughes, S. R., Kay, P., & Brown, L. E. (2013). Global synthesis and critical evaluation of pharmaceutical data sets collected from river systems. Environmental science & technology, 47(2), 661-677.

Ighalo, J. O., & Adeniyi, A. G. (2020). A mini-review of the morphological properties of biosorbents derived from plant leaves. *SN Applied Sciences*, *2*(3), 1–16. Https://doi.org/10.1007/s42452-020-2335-x

Jiang, M. Qin, Wang, Q. Ping, Jin, X. Ying, & Chen, Z. Liang. (2009). Removal of Pb(II) from aqueous solution using modified and unmodified kaolinite clay. *Journal of Hazardous Materials*, *170*(1), 332–339. Https://doi.org/10.1016/j.jhazmat.2009.04.092

Jones, D. G. (1999). Environmental impacts of technology. In *Wiley Encyclopedia of Electrical and Electronics Engineering* (Issue 65).

Jones, T. L., Brown, G. M., Raab, L. M., McVickar, J. L., Spaulding, W. G., Kennett, D. J., ... & Walker, P. L. (1999). Environmental imperatives reconsidered: demographic crises in western North America during the medieval climatic anomaly. Current anthropology, 40(2), 137-170.

Kaluli, W., Home, P. G., & Kenyatta, J. (2014). The heavy metal content of crops irrigated with untreated Wastewater: A case study of Nairobi, Kenya. *JAGST*, *16*(2), 123–140.

Kanchana, V., Gomathi, T., Geetha, V., & Sudha, P. N. (2012). Adsorption analysis of pb(II)

by nanocomposites of chitosan with methyl cellulose and clay. *Der Pharmacia Lettre*, *4*(4), 1071–1079.

Khan, S., Reid, B. J., Li, G., & Zhu, Y. G. (2014). Application of biochar to soil reduces cancer risk via rice consumption: A case study in Miaoqian village, Longyan, China. *Environment International*, *68*(2014), 154–161. Https://doi.org/10.1016/j.envint.2014.03.017

Khayyun, T. S., & Mseer, A. H. (2019). Comparison of the experimental results with the Langmuir and Freundlich models for copper removal on limestone adsorbent. *Applied Water Science*, *9*(8), 1–8. Https://doi.org/10.1007/s13201-019-1061-2

Kimani, N. G. (2007). Environmental Pollution and Impact. *UNEP-KENYA*, 1–40.

Kinuthia, G. K., Ngure, V., Beti, D., Lugalia, R., Wangila, A., & Kamau, L. (2020). Levels of heavy metals in wastewater and soil samples from open drainage channels in Nairobi, Kenya: community health implication. *Scientific Reports*, *10*(1), 1–13. Https://doi.org/10.1038/s41598-020-65359-5

Kolakowski, J. K. J. M. W. J. (1984). Stimulation of Lipid Peroxidation and Heme Oxygenase Activity with Inhibition of Cytochrome p-450 mono-oxygenase in the liver of rats repeatedly exposed to cadmium. *Toxicology*, *32*, 267–276.

Komkiene, J., & Baltrenaite, E. (2016). Biochar as adsorbent for removal of heavy metal ions [Cadmium(II), Copper(II), Lead(II), Zinc(II)] from aqueous phase. *International Journal of Environmental Science and Technology*, *13*(2), 471–482. Https://doi.org/10.1007/s13762-015-0873-3

Kumar, A., Rao, N. N., & Kaul, S. N. (2000). Alkali-treated straw and insoluble straw xanthate as low cost adsorbents for heavy metal removal–preparation, characterization and application. Bioresource Technology, 71(2), 133-142.

Kumari, N., & Mohan, C. (2021). Basics of clay minerals and their characteristic properties.

Clay Clay Miner, 24, 1-29.

Kurniawan, T. A., Chan, G. Y. S., Lo, W. H., & Babel, S. (2006). Physico-chemical treatment techniques for wastewater laden with heavy metals. *Chemical Engineering Journal*, *118*(1–2), 83–98. Https://doi.org/10.1016/j.cej.2006.01.015

Kwak, H. S., & Nguta, C. (1994). Report on the State of Water Pollution in Kenya, Publisher Korea Ocean Research and Development Institute (KORDI) and Kenya Marine and Fisheries Research Institute.

Laksmi Hendrati, R. (2019). Environmental and Social Sustainability: The role of Forest as the most influential ecosystem. *IOP Conference Series: Earth and Environmental Science*, *256*(1). Https://doi.org/10.1088/1755-1315/256/1/012052

Lalia, B. S., & Hashaikeh, R. (2021). Electrochemical precipitation to reduce waste brine salinity. *Desalination*, *498*(September 2020), 114796. Https://doi.org/10.1016/j.desal.2020.114796

Leaning, J. (2000). Environment and health: 5. Impact of war. Canadian Medical Association Journal,, 163(9), 1157-1161.

Lehmann, J., & Joseph, S. (2012). Biochar for environmental management: An introduction. *Biochar for Environmental Management: Science and Technology*, *1*, 1–12. Https://doi.org/10.4324/9781849770552

Liao, H. J., Chen, Y. H., & Jeng, S. S. (2006). Association of zinc with connective tissue in the digestive tract of common carp. *Fisheries Science*, *72*(4), 893–902. Https://doi.org/10.1111/j.1444-2906.2006.01233.x

Liu, Y., He, Z., & Uchimiya, M. (2015). Comparison of Biochar Formation from Various Agricultural By-Products Using FTIR Spectroscopy. *Modern Applied Science*, *9*(4), 246–253. Https://doi.org/10.5539/mas.v9n4p246

Loganathan, P., Hedley, M. J., & Grace, N. D. (2008). Pasture soils contaminated with

fertilizer-derived cadmium and fluorine: Livestock effects. *Reviews of Environmental Contamination and Toxicology, 192,* 29–66. Https://doi.org/10.1007/978-0-387-71724-1_2

Valko, M. M. H. C. M., Morris, H., & Cronin, M. T. D. (2005). Metals, toxicity and oxidative stress. Current medicinal chemistry, 12(10), 1161-1208.

Mateo-Sagasta, J., Marjani, S., Turral, H., & Burke, J. (2017). Water pollution from agriculture: a global review. *FAO and IWMI*, 35. Http://www.fao.org/3/a-i7754e.pdf

Matos, G. D., & Arruda, M. A. Z. (2003). Vermicompost as natural adsorbent for removing metal ions from laboratory effluents. *Process Biochemistry*, *39*(1), 81–88. Https://doi.org/10.1016/S0032-9592(02)00315-1

Maundu, P., Kibet, S., Morimoto, Y., Imbumi, M., & Adeka, R. (2009). Impact of Prosopis juliflora on Kenya's semi-arid and arid ecosystems and local livelihoods. Biodiversity, 10(2-3), 33-50.

Mcbride, M. B., Pitiranggon, M., & Kim, B. (2009). A comparison of tests for extractable copper and zinc in metal-spiked and field-contaminated soil. *Soil Science*, *174*(8), 439–444. Https://doi.org/10.1097/SS.0b013e3181b66856

Mittal, R., & Mittal, C. G. (2013). Impact of Population Explosion on Environment. *Modern Rohini Education Society (Regd.)*, *1*(1), 1–5. Http://weschool.rtmonline.in

Mohan, D., & Pittman, C. U. (2007). Arsenic removal from water/wastewater using adsorbents-A critical review. *Journal of Hazardous Materials*, *142*(1–2), 1–53. Https://doi.org/10.1016/j.jhazmat.2007.01.006

Kithiia, S. M. (2012). Water quality degradation trends in Kenya over the last decade. Water quality monitoring and assessment, 509.

Mungai, T. M., & Wang, J. (2019). Heavy metal pollution in suburban topsoil of Nyeri, Kapsabet, Voi, Ngong and Juja towns, in Kenya. SN Applied Sciences, 1, 1-11.

Nair, P. K. R. (1994). An Introduction to Agroforestry. In *Outlook on Agriculture* (Vol. 23, Issue 4). Klgwer Academic Publishers. Https://doi.org/10.1177/003072709402300413

Namgay, T., Singh, B., & Singh, B. P. (2010). Influence of biochar application to soil on the availability of As, Cd, Cu, Pb, and Zn to maize (Zea mays L.). *Australian Journal of Soil Research*, *48*(6–7), 638–647. Https://doi.org/10.1071/SR10049

Ndeda, L. A. , Manohar, S. 1. (2014). Determination of Heavy Metals in Nairobi Dam Water , (Kenya). *IOSR Journal of Environmental Science, Toxicology and Food Technology (IOSR-JESTFT)*, *8*(5), 68–73.

Obinnaa, I. B., & Ebere, E. C. (2019). A Review: Water pollution by heavy metal and organic pollutants: Brief review of sources, effects and progress on remediation with aquatic plants. *Analytical Methods in Environmental Chemistry Journal*, *2*(3), 5–38. Https://doi.org/10.24200/amecj.v2.i03.66

Osman, A. D., Lin, V., Robinson, P., & Jackson, D. (2011). Policy and governance issues in Kenya's border towns: The case of Wajir groundwater management. Australasian Review of African Studies, The, 32(1), 32-58.

Osman, A. I., Ahmed, A. T., Johnston, C. R., & Rooney, D. W. (2018). Physicochemical characterization of miscanthus and its application in heavy metals removal from wastewaters. *Environmental Progress and Sustainable Energy*, *37*(3), 1058–1067. Https://doi.org/10.1002/ep.12783

Owa, F. W. (2014). Water pollution: sources, effects, control and management. *International Letters of Natural Sciences*, *3*, 1–6. Www.ilns.pl

Owens, S. (1989). Integrated pollution-control in the United Kingdom: prospects and problems. *Environment & Planning C: Government & Policy*, *7*(1), 81–91. Https://doi.org/10.1068/c070081

Palm, R., & Bolsen, T. (2020). Climate change and sea level rise in South Florida (Vol. 34).

Cham, Switzerland: Springer International Publishing.

Patnaik, R. (2018). Impact of Industrialization on Environment and Sustainable Solutions - Reflections from a South Indian Region. *IOP Conference Series: Earth and Environmental Science*, *120*(1), 0–8. Https://doi.org/10.1088/1755-1315/120/1/012016

Pragst, F., Stieglitz, K., Runge, H., Runow, K. D., Quig, D., Osborne, R., Runge, C., & Ariki, J. (2017). High concentrations of lead and barium in hair of the rural population caused by water pollution in the Thar Jath oilfields in South Sudan. *Forensic Science International*, *274*, 99–106. Https://doi.org/10.1016/j.forsciint.2016.12.022

Prüss-Üstün, A., & Corvalän, C. (2007). Towards an estimate of the environmental burden of disease. *WHO*, *12*(2), 115–116.

Raikwar, M. K., Kumar, P., Singh, M., & Singh, A. (2008). Toxic effect of heavy metals in livestock health. *Veterinary World*, *1*(1), 28–30. Https://doi.org/10.5455/vetworld.2008.28-30

Rallet, D., Paltahe, A., Tsamo, C., & Loura, B. (2022). Synthesis of clay-biochar composite for glyphosate removal from aqueous solution. *Heliyon*, *8*(3), e09112. Https://doi.org/10.1016/j.heliyon.2022.e09112

Rayzman, V. L., Pevzner, I. Z., Sizyakov, V. M., Ni, L. P., Filipovich, I. K., & Aturin, A. V. (2003). Extracting Silica and Alumina from Low-Grade Bauxite. *Jom*, *55*(8), 47–50. Https://doi.org/10.1007/s11837-003-0105-z

Riskuwa-Shehu, M. L., Ismail, H. Y., & Sulaiman, M. (2019). Biosorption of Heavy Metals by Oscillatoria Species. *Microbiology Research Journal International*, *June*, 1–8. Https://doi.org/10.9734/mrji/2019/v27i630114

Robinson, W. C. . (1964). The Development of Modern Population Theory. *The American Journal of Economics and Sociology*, *23*(4), 375–392.

Sazali, N., Harun, Z., & Sazali, N. (2020). A Review on Batch and Column Adsorption of

Various Adsorbent Towards the Removal of Heavy Metal. *Journal of Advanced Research in Fluid Mechanics and Thermal Sciences*, *2*(2), 66–88.

Schindler, D. W. (2006). Recent advances in the understanding and management of eutrophication. Limnology and oceanography, 51(1part2), 356-363.

Selinus, O., Alloway, B., Centeno, J. A., Finkelman, R. B., Fuge, R., Lindh, U., & Smedley, P. (2013). *Essentials of Medical Geology: Revised Edition*, 1–805. Https://doi.org/10.1007/978-94-007-4375-5

Khan, S. A., Khan, S. B., Khan, L. U., Farooq, A., Akhtar, K., & Asiri, A. M. (2018). Fourier transform infrared spectroscopy: fundamentals and application in functional groups and nanomaterials characterization. Handbook of materials characterization, 317-344.

Sharma, R., Agrawal, P. R., Kumar, R., Gupta, G., & Ittishree. (2021). Current scenario of heavy metal contamination in water. *Contamination of Water*, *November*, 49–64. Https://doi.org/10.1016/b978-0-12-824058-8.00010-4

Sharma, V. K., & Sohn, M. (2009). Aquatic arsenic: Toxicity, speciation, transformations, and remediation. *Environment International*, *35*(4), 743–759. Https://doi.org/10.1016/j.envint.2009.01.005

Shiferaw, H., Alamirew, T., Dzikiti, S., Bewket, W., & Zeleke, G. (2021). Water use of Prosopis juliflora and its impacts on catchment water budget and rural livelihoods in Afar Region , Ethiopia. *Scientific Reports*, 1–14. Https://doi.org/10.1038/s41598-021-81776-6

Shrivastava, A. K. (2009). A review on copper pollution and its removal from water bodies by pollution control technologies. Indian Journal of Environmental Protection, 29(6), 552-560.

Singh, G., & Singh, B. (2017). Deforestation and Its Impact on Environment. *International Journal of Advanced Research in Science and Engineering (IJARSE)*, *6*(3), 262–268.

Sivakumar, K. K., & Dheenadayalan, M. S. (2012). Utilization of environmental waste materials (coal fly ash and Prosopis juliflora carbon) in the removal of chromium, Lead, zinc and copper from industrial effluents. European Chemical Bulletin, 1, 161-167.

Srinivasan, R. (2011). Advances in application of natural clay and its composites in removal of biological, organic, and inorganic contaminants from drinking water. Advances in Materials Science and Engineering, Vol 2011, Hindawi Publishing Corporation.

Stahl, R. S., & James, B. R. (1991). Zinc Sorption by B Horizon Soils as a Function of ph. *Soil Science Society of America Journal*, *55*(6), 1592–1597. Https://doi.org/10.2136/sssaj1991.03615995005500060015x

Szegedi, Á., Kónya, Z., Méhn, D. Óra, Solymár, E., Pál-Borbély, G., Horváth, Z. E., Biró, L. P., & Kiricsi, I. (2004). Spherical mesoporous MCM-41 materials containing transition metals: Synthesis and characterization. *Applied Catalysis A: General*, *272*(1–2), 257–266. Https://doi.org/10.1016/j.apcata.2004.05.057

Tarzia, M., De Vivo, B., Somma, R., Ayuso, R. A., mcgill, R. A. R., & Parrish, R. R. (2002). Anthropogenic vs. Natural pollution: An environmental study of an industrial site under remediation (Naples, Italy). *Geochemistry: Exploration, Environment, Analysis*, *2*(1), 45–56. Https://doi.org/10.1144/1467-787302-006

Tchounwou, P. B., Yedjou, C. G., Patlolla, A. K., & Sutton, D. J. (2012). Heavy metal toxicity and the environment. Molecular, clinical and environmental toxicology. Experientia Supplementum, 101, 133-64.

Teixeira, M. Do C., Santini, A., & Souto, E. B. (2017). Delivery of Antimicrobials by Chitosan-Composed Therapeutic Nanostructures. *Nanostructures for Antimicrobial Therapy: Nanostructures in Therapeutic Medicine Series*, 203–222. Https://doi.org/10.1016/B978-0-323-46152-8.00008-1

Parmar, M., & Thakur, L. S. (2013). Heavy metal Cu, Ni and Zn: toxicity, health hazards and

their removal techniques by low cost adsorbents: a short overview. International Journal of plant, animal and environmental sciences, 3(3), 143-157.

Tomno, R. M., Nzeve, J. K., Mailu, S. N., Shitanda, D., & Waswa, F. (2020). Heavy metal contamination of water, soil and vegetables in urban streams in Machakos municipality, Kenya. *Scientific African*, *9*. Https://doi.org/10.1016/j.sciaf.2020.e00539

UNCHS. (2002). Global Environment Outlook 3. In *United Nations Environment Programme*. Http://www.unep.org/geo/GEO3/english/pdf.htm

UNEP, ILO, and W. (2005). Bentonite, kaolin, and selected clay minerals. *WHO Library Cataloguing-in-Publication Data*, *231*.

Vasanthy, M., Sangeetha, M., & Kalaiselvi, R. (2004). A comparative study on the chromium removal efficiency of flyash and commercial activated carbon. *Journal of Industrial Pollution Control*, *20*(1), 37–44.

Verma, R., & Dwivedi, P. (2013). Heavy metal water pollution- A case study. *Recent Research in Science and Technology*, *5*(5), 98–99. Http://recent-science.com/

Voellkopf, U., Paul, M., & Denoyer, E. R. (1992). Analysis of solid samples by ICP-mass spectrometry. *Fresenius' Journal of Analytical Chemistry*, *342*(12), 917–923. Https://doi.org/10.1007/BF00322827

Wakie, T. T., Laituri, M., & Evangelista, P. H. (2016). Assessing the distribution and impacts of Prosopis juliflora through participatory approaches. *Applied Geography*, *66*, 132–143. Https://doi.org/10.1016/j.apgeog.2015.11.017

Walker, R. J. (2016). Population Growth and its Implications for Global Security. *The American Journal of Economics and Sociology*, *75*(4), 980–1004.

Wang, S., Hu, Y., Zong, R., Tang, Y., Chen, Z., & Fan, W. (2004). Preparation and characterization of flame retardant ABS/montmorillonite nanocomposite. *Applied Clay Science*, *25*(1–2), 49–55. Https://doi.org/10.1016/j.clay.2003.08.003

Wang, S., Xu, Y., Norbu, N., & Wang, Z. (2018). Remediation of biochar on heavy metal polluted soils. *IOP Conference Series: Earth and Environmental Science*, *108*(4). Https://doi.org/10.1088/1755-1315/108/4/042113

WHO. (2011). Guidelines for Drinking-water Quality. *WHO Library Cataloguing-in-Publication Data*, *4th Edition*, 1–541.

Yaashikaa, P. R., Kumar, P. S., Varjani, S., & Saravanan, A. (2020). A critical review on the biochar production techniques, characterization, stability and applications for circular bioeconomy. *Biotechnology Reports*, *28*, e00570. Https://doi.org/10.1016/j.btre.2020.e00570

Yabe, J., Ishizuka, M., & Umemura, T. (2010). Current levels of heavy metal pollution in Africa. *Journal of Veterinary Medical Science*, *72*(10), 1257–1263. Https://doi.org/10.1292/jvms.10-0058

Yang, X., Roonasi, P., & Holmgren, A. (2008). A study of sodium silicate in aqueous solution and sorbed by synthetic magnetite using in situ ATR-FTIR spectroscopy. *Journal of Colloid and Interface Science*, *328*(1), 41–47. Https://doi.org/10.1016/j.jcis.2008.08.061

Yang, X. Y., & Al-Duri, B. (2001). Application of branched pore diffusion model in the adsorption of reactive dyes on activated carbon. *Chemical Engineering Journal*, *83*(1), 15–23. Https://doi.org/10.1016/S1385-8947(00)00233-3

Yao, Y., Gao, B., Fang, J., Zhang, M., Chen, H., Zhou, Y., Creamer, A. E., Sun, Y., & Yang, L. (2014). Characterization and environmental applications of clay-biochar composites. *Chemical Engineering Journal*, *242*, 136–143. Https://doi.org/10.1016/j.cej.2013.12.062

Yao, Y., Gao, B., Inyang, M., Zimmerman, A. R., Cao, X., Pullammanappallil, P., & Yang, L. (2011). Biochar derived from anaerobically digested sugar beet tailings: Characterization and phosphate removal potential. *Bioresource Technology*, *102*(10),

6273–6278. Https://doi.org/10.1016/j.biortech.2011.03.006

Zeraatpishe, M., Khaledian, Y., Ebrahimi, S., Sheikhpouri, H., & Behtarinejad, B. (2013). The Effect of Deforestation on Soil Erosion , Sediment and Some Water Quality Indicates. *1St International Conference on Environmental Crisis and Its Solutions; 13-14 Feb 2013, Kish Island-Iran, Scientifiic and Research Branch, Khouzestan, Islamic Azad University, July 2015*, 602–607.

Zhao, S. X., Ta, N., & Wang, X. D. (2017). Effect of temperature on the structural and physicochemical properties of biochar with apple tree branches as feedstock material. Energies, 10(9), 1293.

APPENDICES

Appendix A: Raw data of the effect of contact time on selected heavy metals adsorption

The variation of contact time from 30 -120 min was conducted while keeping the rest of the parameters constant (dosage of calcined clay, agitation speed, and pH) as 5 g/25ml, 150 rpm, and pH-8 respectively.

Sample ID	**Zn (μg/L)**	**Cu (μg/L)**	**Cd (μg/L)**	**Pb (μg/L)**	**Time (min)**
C-1	1000 (Ci)	1000	1000	1000	
C-2	22.44825 (C_f)	23.368	20.753	0.763	**30**
C-3	16.424	10.5255	8.1615	0.50925	**60**
C-4	7.27175	14.89525	4.10725	0.817	**90**
C-5	9.15775	17.69375	3.86075	1.16475	**120**

	% Removal $\frac{Ci - Cf}{Ci} \times 100$			
Time (min)	**Zn**	**Cu**	**Cd**	**Pb**
30	97.755	97.663	97.925	99.924
60	98.358	98.947	99.184	99.949
90	99.273	98.510	99.589	99.918
120	99.084	98.231	99.614	99.884

Appendix B: Raw data of the effect of pH on the selected heavy metals adsorption

The study of effect of pH was performed by adjusting the pH from 4-9 and keeping the rest of the parameters constant (dosage of calcined clay, agitation speed, and time) as. 10g/50ml, 150 rpm, and 120 min respectively.

Sample ID	**Zn (μg/L)**	**Cu (μg/L)**	**Cd (μg/L)**	**Pb (μg/L)**	**pH**
P-1	1000 (C_i)	1000	1000	1000	
P-2	12.65575 (C_f)	17.6715	12.19775	0.73475	4
P-3	4.49625	11.82425	5.58775	0.55925	7
P-4	5.371	10.089	3.98475	0.44025	8
P-5	5.635	11.55925	3.14575	0.74875	9

	% Removal $\frac{Ci - Cf}{Ci} \times 100$			
pH	**Zn**	**Cu**	**Cd**	**Pb**
4	98.734	98.233	98.780	99.927
7	99.550	98.818	99.441	99.944
8	99.463	98.991	99.602	99.956
9	99.437	98.844	99.685	99.925

Appendix C: Raw data of the effect of agitation speed of shaker on the selected heavy metal adsorption

The study of the effect of agitation speed was performed by changing the shaker's speed from 50 to 200 rpm and keeping the rest of the parameters constant (dosage of calcined clay, contact time, and pH) as 5 g/50ml, 120min, and pH-8 respectively.

Sample ID	**Zn (**μg/L**)**	**Cu (**μg/L**)**	**Cd (**μg/L**)**	**Pb (**μg/L**)**	**Agitation speed of shaker (rpm)**
AS-1	1000	1000	1000	1000	
AS-2	19.915	18.241	16.453	0.797	50 rpm
AS-3	11.728	15.769	8.451	1.1939	100 rpm
AS-4	5.157	17.458	4.38	1.701	150 rpm
AS-5	7.675	15.843	5.032	0.54	200 rpm

Agitation speed of shaker (rpm)	% Removal ($\frac{Ci - Cf}{Ci} \times 100$			
	Zn	**Cu**	**Cd**	**Pb**
50 rpm	98.009	98.176	98.355	99.920
100 rpm	98.827	98.423	99.155	99.881
150 rpm	99.484	98.254	99.562	99.830
200 rpm	99.233	98.416	99.497	99.946

Appendix D: Raw data of the Removal efficiency of calcined clay dosage on selected heavy metal adsorption

The batch procedure was carried out by changing the amounts of the calcined clay of 5, 10, 20, and 40 mg while keeping the rest of the parameters constant (contact time, agitation speed, and pH) as 120 min, 150 rpm, and pH-8 respectively

Sample ID	**Dosage of calcined clay (g)**	**Zn (μg/L)**	**Cu (μg/L)**	**Cd (μg/L)**	**Pb (μg/L)**
CC-1		1000	1000	1000	1000
CC-2	5	17.06	16.869	9.258	0.38
CC-3	10	7.552	9.703	3.849	0.769
CC-4	20	6.314	6.995	3.156	0.556
CC-5	40	6.908	9.163	3.613	0.369

Sample ID	**Dosage of calcined clay (g)**	% Removal ($\frac{Ci - Cf}{Ci} \times 100$)			
		Zn	**Cu**	**Cd**	**Pb**
CC-2	5	97.868	97.891	98.843	99.953
CC-3	10	99.056	98.787	99.519	99.904
CC-4	20	99.211	99.126	99.606	99.931
CC-5	40	99.137	98.855	99.548	99.954

Appendix E: Raw data of the Removal efficiency of biochar dosage on selected heavy metal adsorption

The batch procedure was carried out by changing the amounts of the biochar to 0.5, 1, 2, and 1.2 mg while keeping the rest of the parameters constant (contact time, agitation speed, and pH) as 120 min, 150 rpm, and pH-8 respectively

Sample ID	**Dosage of biochar (g)**	**Zn (**µg/L**)**	**Cu (**µg/L**)**	**Cd (**µg/L**)**	**Pb (**µg/L**)**
BC-1		1000	1000	1000	1000
BC-2	0.5	7.5	23.217	7.255	0.617
BC-3	1	1.973	7.777	1.836	0.271
BC-4	1.2	1.243	5.547	0.984	0.1
BC-5	2	0.6	3.585	0.553	0.231

Sample ID	**Dosage of biochar (g)**	% Removal ($\frac{Ci - Cf}{Ci} \times 100$)			
		Zn	**Cu**	**Cd**	**Pb**
BC-2	0.5	99.063	97.098	99.093	99.923
BC-3	1	99.753	99.028	99.771	99.966
BC-4	1.2	99.845	99.307	99.877	99.988
BC-5	2	99.925	99.552	99.931	99.971

Appendix F: Raw data of the Removal efficiency of composite dosage on selected heavy metal adsorption

The batch procedure was performed by changing the amounts of the synthesized nanocomposite material of 1, 2, 4, and 6 mg while keeping the rest of the parameters constant (contact time, agitation speed, and pH) as 120 min, 150 rpm, and pH-8 respectively

Sample ID	**composite material dosage (g)**	**Zn (**μg/L**)**	**Cu (**μg/L**)**	**Cd (**μg/L**)**	**Pb (**μg/L**)**
NC-1		1000	1000	1000	1000
NC-2	1	11.67	8.618	6.995	0.547
NC-3	2	6.791	5.857	2.523	0.38
NC-4	4	1.996	10.936	1.969	0.387
NC-5	6	4.207	4.62	1.396	0.156

Sample ID	**composite material dosage (g)**	**% Removal(** $\frac{Ci - Cf}{Ci} \times 100$ **)**			
		Zn	**Cu**	**Cd**	**Pb**
NC-2	1	98.5413	98.9228	99.1256	99.9316
NC-3	2	99.1511	99.2679	99.6846	99.9525
NC-4	4	99.7505	98.6330	99.7539	99.9516
NC-5	6	99.4741	99.4225	99.8255	99.9805

Appendix G-1: Raw data of Freundlich isotherm for calcined clay for zinc metal

Zn			
Dosage (g)	**C_i(µg/l)**	**C_e (µg/l)**	**q_e(µg/g)**
5	1000	17.06	4.9147
10	1000	7.552	2.48112
20	1000	6.314	1.2421075
40	1000	6.908	0.6206825

Ln C_e	**Ln Q_e**
2.836737	1.592231
2.021812	0.90871
1.842769	0.21681
1.93268	-0.47694

Appendix G-2: Raw data of Freundlich isotherm for calcined clay for copper metal

Cu			
Dosage (g)	**C_i(µg/l)**	**C_e (µg/l)**	**q_e(µg/g)**
5	1000	16.869	4.915655
10	1000	9.703	2.4757425
20	1000	6.995	1.24125625
40	1000	9.163	0.61927313

Ln C_e	**Ln Q_e**
2.825478	1.592425
2.272435	0.90654
1.945196	0.216124
2.215174	-0.47921

Appendix G-3: Raw data of Freundlich isotherm for calcined clay for cadmium metal

Cd			
Dosage (g)	**Ci(µg/l)**	**Ce (µg/l)**	**qe(µg/g)**
5	1000	9.258	4.95371
10	1000	3.849	2.4903775
20	1000	3.156	1.246055
40	1000	3.613	0.62274188

Ln C_e	**Ln Q_e**
2.225488	1.600137
1.347813	0.912434
1.149305	0.219983
1.284538	-0.47362

Appendix G-4: Raw data of Freundlich isotherms for calcined clay for lead metal

Pb			
Dosage (g)	**Ci(µg/l)**	**Ce (µg/l)**	**qe(µg/g)**
5	1000	0.38	4.9981
10	1000	0.769	2.4980775
20	1000	0.556	1.249305
40	1000	0.369	0.62476938

Ln C_e	**Ln Q_e**
-0.96758	1.609058
-0.26266	0.915521
-0.58699	0.222587
-0.99696	-0.47037

Appendix H-1: Raw data of Freundlich isotherm for biochar for zinc metal

Zn			
Dosage (g)	**C_i(µg/l)**	**C_e (µg/l)**	**q_e (µg/g)**
0.5	1000	7.5	49.625
1	1000	1.973	24.950675
1.2	1000	0.6	20.82083333
2	1000	1.243	12.4844625

Ln Ce	Ln Qe
2.014903	3.904495
0.679555	3.216901
0.217528	2.524485
-0.51083	3.035954

Appendix H-2: Raw data of Freundlich isotherm for biochar for copper metal

Cu			
Dosage (g)	**C_i (µg/l)**	**C_e (µg/l)**	**q_e (µg/g)**
0.5	1000	23.217	48.83915
1	1000	7.777	24.805575
2	1000	5.547	12.4306625
1.2	1000	3.585	20.75864583

Ln C	Ln Q
3.144885	3.888532
2.051171	3.211068
1.713257	2.520166
1.276758	3.032963

Appendix H-3: Raw data of Freundlich isotherm for biochar for cadmium metal

Cd			
Dosage (g)	**Ci(µg/l)**	**Ce (µg/l)**	**qe(µg/g)**
0.5	1000	7.255	49.63725
1	1000	1.836	24.9541
2	1000	0.984	12.4877
1.2	1000	0.553	20.8218125

Ln Ce	Ln Qe
1.981691	3.904742
0.607589	3.217038
-0.01613	2.524744
-0.5924	3.036001

Appendix H-4: Raw data of Freundlich isotherm for biochar for lead metal

Pb			
Dosage (g)	**Ci(µg/l)**	**Ce (µg/l)**	**qe(µg/g)**
0.5	1000	0.617	49.96915
1	1000	0.271	24.993225
2	1000	0.1	12.49875
1.2	1000	0.231	20.82852083

Ln Ce	Ln Qe
-0.48289	3.911406
-1.30564	3.218605
-1.46534	3.036323
-2.30259	2.525629

Appendix I-1: Raw data of Freundlich isotherm for composite material for zinc metal

Zn			
Dosage (g)	**C_i(µg/l)**	**C_e (µg/l)**	**q_e(µg/g)**
1	1000	11.67	24.70825
2	1000	6.791	12.4151125
4	1000	1.996	6.237525
6	1000	4.207	4.1491375

Ln Ce	Ln Qe
2.457021	3.207137
1.915598	2.518914
0.691145	1.830583
1.43675	1.4229

Appendix I-2: Raw data of Freundlich isotherm for composite material for copper metal

Cu			
Dosage (g)	**C_i(µg/l)**	**C_e (µg/l)**	**q_e(µg/g)**
1	1000	8.618	24.78455
2	1000	5.857	12.4267875
4	1000	10.936	6.18165
6	1000	4.62	4.147416667

Ln Ce	Ln Qe
2.15385	3.21022
1.76764	2.51985
1.53039	1.42249
2.39206	1.82159

Appendix I-3: Raw data of Freundlich isotherm for composite material for cadmium metal

Cd			
Dosage (g)	**Ci(µg/l)**	**Ce (µg/l)**	**qe(µg/g)**
1	1000	6.995	24.825125
2	1000	2.523	12.4684625
4	1000	1.969	6.23769375
6	1000	1.396	4.16085

Ln Ce	Ln Qe
1.9452	3.21186
0.92545	2.5232
0.67753	1.83061
0.33361	1.42572

Appendix I-4: Raw data of Freundlich isotherm for composite material for lead metal

Pb			
Dosage (g)	**Ci(µg/l)**	**Ce (µg/l)**	**qe(µg/g)**
1	1000	0.547	24.986325
2	1000	0.38	12.49525
4	1000	0.387	6.24758125
6	1000	0.156	4.166016667

Ln Ce	Ln Qe
-0.60331	3.218329
-0.96758	2.525349
-1.8579	1.42696
-0.94933	1.832194

Appendix J-1: Raw data of Langmuir isotherm for calcined clay for zinc metal

Zn			
Dosage (g)	C_i(µg/l)	C_e (µg/l)	q_e(µg/g)
5	1000	17.06	4.9147
10	1000	7.552	2.48112
20	1000	6.314	1.2421075
40	1000	6.908	0.6206825

$1/C_e$	$1/q_e$
0.058616647	0.203471
0.132415254	0.403044
0.158378207	0.805083
0.144759699	1.61113

Appendix J-2: Raw data of Langmuir isotherm for calcined clay for copper metal

Cu			
Dosage (g)	C_i(µg/l)	C_e (µg/l)	q_e(µg/g)
5	1000	16.869	3.915655
10	1000	9.703	2.4757425
20	1000	6.995	1.24125625
40	1000	9.163	0.61927313

$1/C_e$	$1/q_e$
0.059280337	0.255385
0.103060909	0.403919
0.142959257	0.805635
0.109134563	1.614796

Appendix J-3: Raw data of Langmuir isotherm for calcined clay for cadmium metal

Cd			
Dosage (g)	Ci(µg/l)	Ce (µg/l)	qe(µg/g)
5	1000	9.258	4.95371
10	1000	3.849	2.4903775
20	1000	3.156	1.246055
40	1000	3.613	0.62274188

$1/C_e$	$1/q_e$
0.108015	0.201869
0.259808	0.401546
0.316857	0.802533
0.276778	1.605802

Appendix J-4: Raw data of Langmuir isotherm for calcined clay for lead metal

Pb			
Dosage (g)	Ci(µg/l)	Ce (µg/l)	qe(µg/g)
5	1000	0.38	4.9981
10	1000	0.769	2.4980775
20	1000	0.556	1.249305
40	1000	0.369	0.62476938

$1/C_e$	$1/q_e$
2.631579	0.200076
1.30039	0.400308
1.798561	0.800445
2.710027	1.600591

Appendix K-1: Raw data of Langmuir isotherm for biochar for zinc metal

Zn			
Dosage (g)	C_i(µg/l)	C_e (µg/l)	q_e(µg/g)
0.5	1000	7.5	49.625
1	1000	1.973	24.950675
2	1000	1.243	12.4844625
1.2	1000	0.6	20.82083333

$1/C_e$	$1/q_e$
0.13333	0.02015
0.50684	0.04008
0.80451	0.0801
1.66667	0.04803

Appendix K-2: Raw data of Langmuir isotherm for biochar for copper metal

Cu			
Dosage (g)	C_i(µg/l)	C_e (µg/l)	q_e(µg/g)
0.5	1000	23.217	48.83915
1	1000	7.777	24.805575
1.2	1000	3.585	20.7586458
2	1000	5.547	12.4306625

$1/C_e$	$1/q_e$
0.04307	0.02048
0.12858	0.04031
0.27894	0.04817
0.18028	0.08045

Appendix K-3: Raw data of Langmuir isotherm for biochar for cadmium metal

Cd			
Dosage (g)	Ci(µg/l)	Ce (µg/l)	qe(µg/g)
0.5	1000	7.255	49.6373
1	1000	1.836	24.9541
1.2	1000	0.553	20.822
2	1000	0.984	12.4877

$1/C_e$	$1/q_e$
0.137836	0.020146
0.544662	0.040074
1.808318	0.048027
1.01626	0.080079

Appendix K-4: Raw data of Langmuir isotherm for biochar for lead metal

Pb			
Dosage (g)	Ci(µg/l)	Ce (µg/l)	qe(µg/g)
0.5	1000	0.617	49.9692
1	1000	0.271	24.9932
2	1000	0.1	12.4988
1.2	1000	0.231	20.8285

$1/C_e$	$1/q_e$
1.62075	0.02001
3.69004	0.04001
10.00000	0.08001
4.32900	0.04801

Appendix L-1: Raw data of Langmuir isotherm for composite material for zinc metal

Zn			
Dosage (g)	C_i(µg/l)	C_e (µg/l)	q_e(µg/g)
1	1000	11.67	24.70825
2	1000	6.791	12.4151125
4	1000	1.996	6.237525
6	1000	4.207	4.1491375

$1/C_e$	$1/q_e$
0.08569	0.040472
0.147254	0.080547
0.501002	0.16032
0.237699	0.241014

Appendix L-2: Raw data of Langmuir isotherm for composite material for copper metal

Cu			
Dosage (g)	C_i(µg/l)	C_e (µg/l)	q_e(µg/g)
1	1000	8.618	24.7846
2	1000	5.857	12.4268
6	1000	4.620	4.1474
4	1000	10.936	6.1817

1/Ce	1/qe
0.116036	0.040348
0.170736	0.080471
0.21645	0.241114
0.091441	0.161769

Appendix L-3: Raw data of Langmuir isotherm for composite material for cadmium metal

Cd			
Dosage (g)	Ci(µg/l)	Ce (µg/l)	qe(µg/g)
1	1000	6.995	24.8251
2	1000	2.523	12.4685
4	1000	1.969	6.2377
6	1000	1.396	4.1609

$1/C_e$	$1/q_e$
0.14296	0.04028
0.39635	0.0802
0.50787	0.16032
0.71633	0.24034

Appendix L-4: Raw data of Langmuir isotherm for composite material for lead metal

Pb			
Dosage (g)	Ci(µg/l)	Ce (µg/l)	qe(µg/g)
1	1000	0.547	24.9863
2	1000	0.38	12.4953
6	1000	0.156	4.1660
4	1000	0.387	6.2476

$1/C_e$	$1/q_e$
1.82815	0.04002
2.63158	0.08003
6.41026	0.24004
2.58398	0.16006

Appendix M-1: Kinetic model of pseudo second-order raw data of zinc metal adsorption.

Zn				
Time (t)	**C_i**	**C_e**	**q_t**	**t/q_t**
30	1000	22.448	4.888	6.138
60	1000	16.424	4.918	12.200
90	1000	7.272	4.964	18.132
120	1000	9.158	4.954	24.222

Appendix M-2: Kinetic model of pseudo second-order raw data of copper metal adsorption

Cu				
Time (t)	**C_i**	**C_e**	**q_t**	**t/q_t**
30	1000	23.368	4.883	6.1436
60	1000	10.526	4.947	12.1276
90	1000	14.895	4.926	18.2722
120	1000	17.694	4.912	24.4323

Appendix M-2: Kinetic model of pseudo second-order raw data of cadmium metal adsorption

Cd				
Time (t)	**C_i**	**C_e**	**q_t**	**t/q_t**
30	1000	20.753	4.8962	6.1272
60	1000	8.162	4.9592	12.0987
90	1000	4.107	4.9795	18.0742
120	1000	3.861	4.9807	24.0930

Appendix M-4: Kinetic model of pseudo second-order raw data of lead metal adsorption

Pb				
Time (t)	**C_i**	**C_e**	**q_t**	**t/q_t**
30	1000	0.763	4.996	6.005
60	1000	0.509	4.997	12.006
90	1000	0.817	4.996	18.015
120	1000	1.165	4.994	24.028

Appendix N: Raw Data for the Calibration of the Heavy Metals on ICP-MS

Standard -1 (200 ppb)

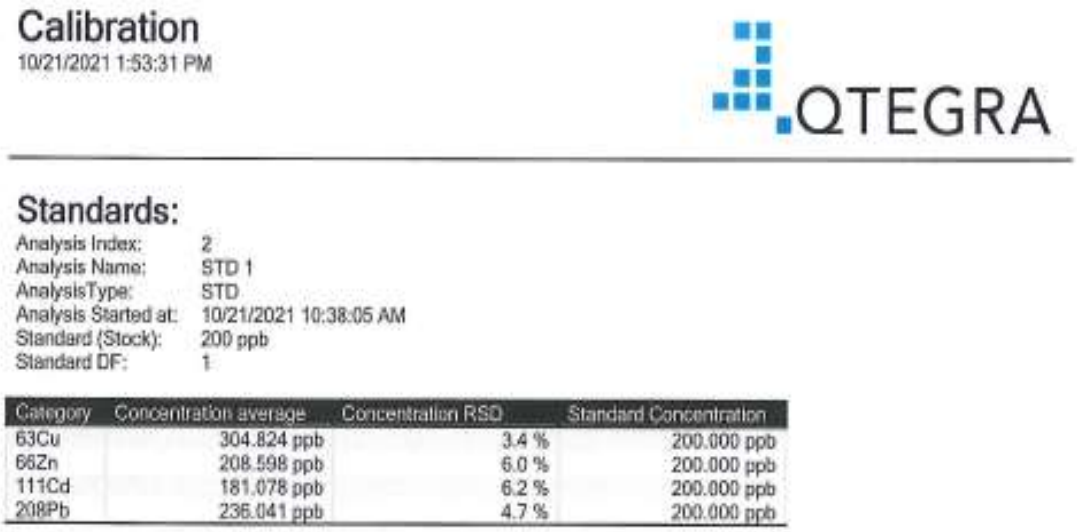

Calibration
10/21/2021 1:53:31 PM

QTEGRA

Standards:

Analysis Index: 2
Analysis Name: STD 1
AnalysisType: STD
Analysis Started at: 10/21/2021 10:38:05 AM
Standard (Stock): 200 ppb
Standard DF: 1

Category	Concentration average	Concentration RSD	Standard Concentration
63Cu	304.824 ppb	3.4 %	200.000 ppb
66Zn	208.598 ppb	6.0 %	200.000 ppb
111Cd	181.078 ppb	6.2 %	200.000 ppb
208Pb	236.041 ppb	4.7 %	200.000 ppb

Standard -2 (400 ppb)

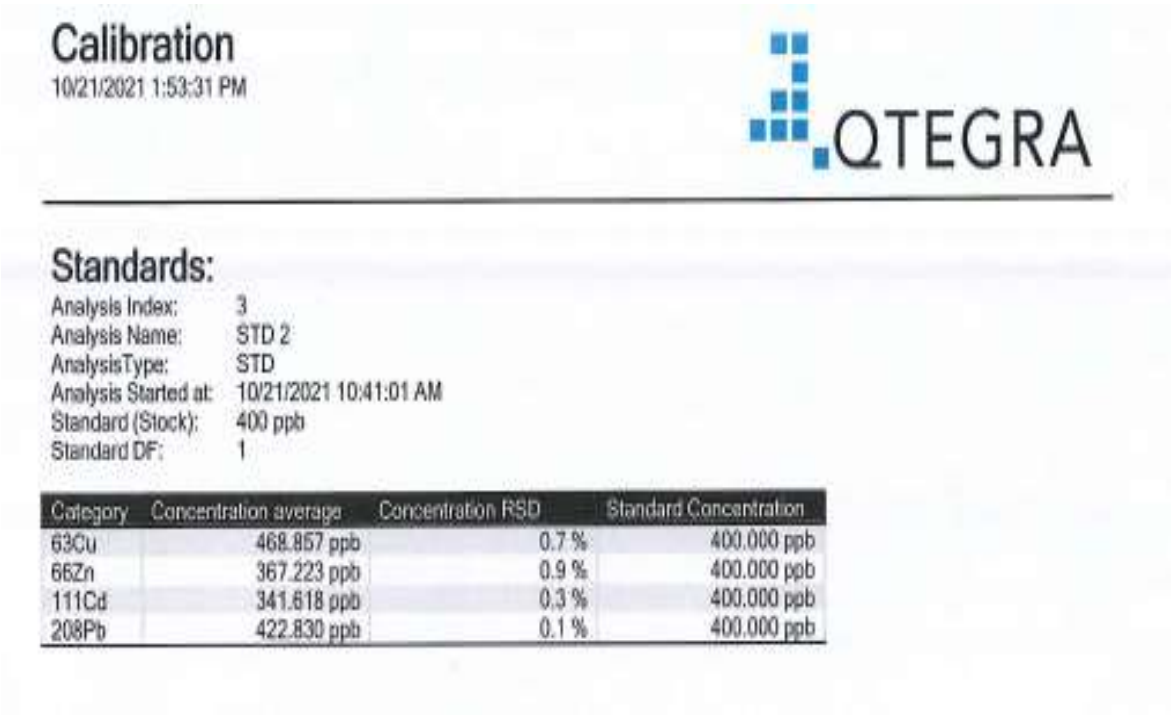

Calibration
10/21/2021 1:53:31 PM

QTEGRA

Standards:

Analysis Index: 3
Analysis Name: STD 2
AnalysisType: STD
Analysis Started at: 10/21/2021 10:41:01 AM
Standard (Stock): 400 ppb
Standard DF: 1

Category	Concentration average	Concentration RSD	Standard Concentration
63Cu	468.857 ppb	0.7 %	400.000 ppb
66Zn	367.223 ppb	0.9 %	400.000 ppb
111Cd	341.618 ppb	0.3 %	400.000 ppb
208Pb	422.830 ppb	0.1 %	400.000 ppb

Standard -3 (600 ppb)

Calibration

10/21/2021 1:53:31 PM

QTEGRA

Standards:

Analysis Index: 4
Analysis Name: STD 3
AnalysisType: STD
Analysis Started at: 10/21/2021 10:43:57 AM
Standard (Stock): 600 ppb
Standard DF: 1

Category	Concentration average	Concentration RSD	Standard Concentration
63Cu	628.912 ppb	0.8 %	600.000 ppb
66Zn	675.508 ppb	1.2 %	600.000 ppb
111Cd	677.216 ppb	1.1 %	600.000 ppb
208Pb	608.658 ppb	1.0 %	600.000 ppb

Standard -4 (800 ppb)

Calibration

10/21/2021 1:53:31 PM

QTEGRA

Standards:

Analysis Index: 5
Analysis Name: STD 4
AnalysisType: STD
Analysis Started at: 10/21/2021 10:46:54 AM
Standard (Stock): 800 ppb
Standard DF: 1

Category	Concentration average	Concentration RSD	Standard Concentration
63Cu	786.382 ppb	0.7 %	800.000 ppb
66Zn	815.839 ppb	0.6 %	800.000 ppb
111Cd	823.727 ppb	0.5 %	800.000 ppb
208Pb	796.181 ppb	0.6 %	800.000 ppb

Standard -5 (1000 ppb)

Calibration

10/21/2021 1:53:31 PM

QTEGRA

Standards:

Analysis Index: 6
Analysis Name: STD 5
AnalysisType: STD
Analysis Started at: 10/21/2021 10:49:51 AM
Standard (Stock): 1000 ppb
Standard DF: 1

Category	Concentration average	Concentration RSD	Standard Concentration
63Cu	945.039 ppb	0.7 %	1,000.000 ppb
66Zn	953.415 ppb	0.9 %	1,000.000 ppb
111Cd	961.826 ppb	0.6 %	1,000.000 ppb
208Pb	981.520 ppb	0.8 %	1,000.000 ppb

Appendix O: Calibration Curve of heavy metals

Calibration

10/21/2021 1:53:31 PM

QTEGRA

Calibration Curves:

Instrument Name	Serial Number
ICAP RQ	Undefined

LabBook	LabBook Path
20211021001 -2.imexp	Application Data\Workspace\LabBooks

63Cu

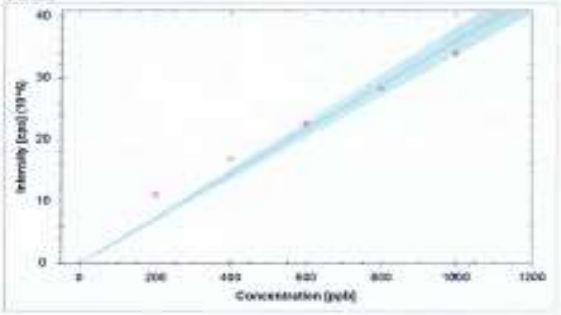

f(x) = 35982.7291*x + 1636.7802
R² = 0.9661
BEC = 0.045 ppb
LoD = 0.0198 ppb

66Zn

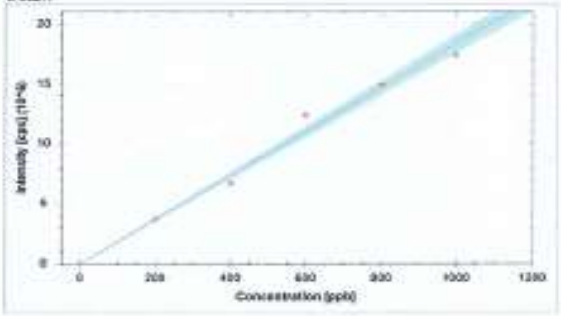

f(x) = 18411.8420*x + 2206.8710
R² = 0.9865
BEC = 0.120 ppb
LoD = 0.0146 ppb

111Cd

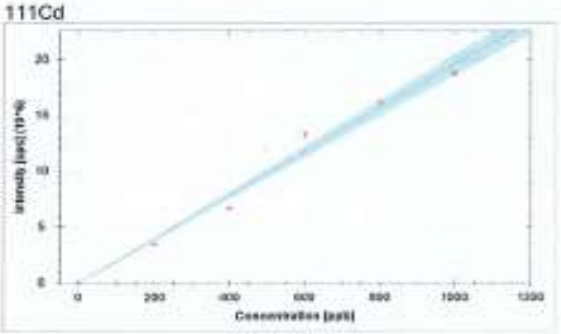

f(x) = 19625.8293*x + 1466.7579
R² = 0.9838
BEC = 0.075 ppb
LoD = 0.0165 ppb

208Pb

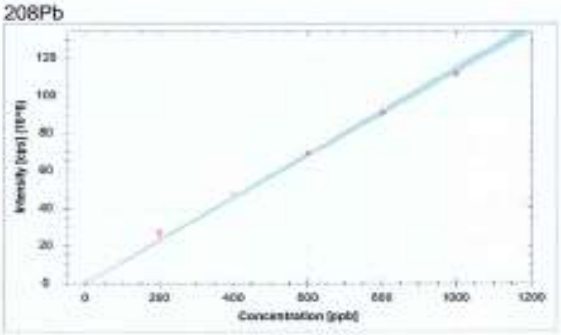

f(x) = 114203.0503*x + 186.6692
R² = 0.9966
BEC = 0.002 ppb
LoD = 0.0010 ppb